PROBING THE MOLECULAR REQUIREMENTS FOR

BREAST CANCER CELL MOTILITY

APPROVED BY SUPERVISORY COMMITTEE

_____

Gray W. Pearson, Ph.D (mentor)

_____

Rolf Brekken, Ph.D (chair)

_____

Melanie Cobb, Ph.D

_____

Angelique Whitehurst, Ph.D

ACKNOWLEDGEMENTS

I would like to express my gratitude to my mentor, Dr. Gray Pearson for his patience and advice in my time at UT Southwestern Medical Center. In addition, I thank my committee members, Drs. Kathlynn Brown, Melanie Cobb, Angelique Whitehurst, and Rolf Brekken for their insight and guidance in my thesis. I am very grateful for all the assistance from the faculty and personnel of the Live Cell Imaging, High Throughput Screening, and Histology Core facilities and people at UT Southwestern Medical Center.

I want to give thanks to all of the Pearson lab members, Amanda Prechtl, Jill Westcott, Erin Pineda, and Matthew Esparza for their help, their camaraderie, and their encouragement. Lab would not be as hilarious without each and every one of you. I would like to recognize all my friends: old and new, academic and non-academic for their generosity, patience, and fun times. I want to give appreciation to my family for their everlasting support and love, especially during the three-day drive from Oregon to Texas and moving all of my possessions up three flights of stairs in the Texas summer heat. Lastly, I would like to thank my fiancé, Dr. Julio Morales, for keeping my head above water and giving counsel during this and future endeavors.

PROBING THE MOLECULAR REQUIREMENTS FOR BREAST CANCER CELL MOTILITY

BY

TUYEN THI THANH DANG

DISSERTATION

Presented to the Faculty of the Graduate School of Biomedical Sciences

The University of Texas Southwestern Medical Center at Dallas

In Partial Fulfillment of the Requirements

For the Degree of

DOCTOR OF PHILOSOPHY

The University of Texas Southwestern Medical Center

Dallas, Texas

December, 2014

PROBING THE MOLECULAR REQUIREMENTS FOR

BREAST CANCER CELL MOTILITY

Publication No. _____

TUYEN THI THANH DANG, Ph.D.

The University of Texas Southwestern Medical Center at Dallas, 2014

GRAY W. PEARSON, Ph.D.

Invasion of breast cancer cells into the stroma is an early step in metastasis. How invasive ability is conferred in breast cancer cells is poorly understood. It has been shown that the tumor microenvironment can assist in the progression of cancer. The mechanism by which the microenvironment, specifically the mammary fibroblast, contributes to the invasion of breast cancer cells is unknown. To elucidate the function of mammary fibroblasts in breast cancer invasion, we co-cultured and co-injected breast cancer cells with mammary fibroblasts. We have found that mammary fibroblasts can induce invasion of motile basal-subtype breast cancer cells better than non-motile luminal subtype breast cancer cells. Based on these observations, the intrinsic motility of breast cancer cells was the determinate for invasion. To discover novel

regulators of motility, we screened 879 distinct miRNAs using a wounding assay as a readout for migration. To prioritize, we determined which of the miRNAs inhibited migration and were expressed in non-motile breast cancer cells. This approach led us to focus on miR203a. We discovered that miR203a inhibits the expression of the transcription factor deltaNp63alpha, which leads to a decrease in cell migration. To determine how deltaNp63alpha controlled migration, we next determined which genes and miRNAs require deltaNp63alpha for expression. From these analyses, we discovered that deltaNp63alpha is required for the expression of miR205, the transcription factor Slug and the tyrosine kinase Axl. Additional functional analyses revealed that Slug, Axl and miR205 contributed to migration through their actions within parallel signaling pathways. Furthermore, using, an orthotropic xenograft model, we determined that deltaNp63alpha and Slug functionally contribute to the induction of collective invasion in vivo. Together, our results suggest a deltaNp63alpha dependent signaling through miR205, Axl, and Slug can lead to the induction of breast cancer invasion.

Table of Contents

Publications

Dang TT, Prechtl AM, Pearson GW. Breast cancer subtype-specific interactions with the microenvironment dictate mechanisms of invasion. Cancer research. 2011;71(21):6857-66. Epub 2011/09/13. doi: 10.1158/0008-5472.can-11-1818. PubMed PMID: 21908556; PubMed Central PMCID: PMCPmc3206184

Yang C, Sudderth J, Dang T, Bachoo RM, McDonald JG, DeBerardinis RJ. Glioblastoma cells require glutamate dehydrogenase to survive impairments of glucose metabolism or Akt signaling. Cancer research. 2009;69(20):7986-93. Epub 2009/10/15. doi: 10.1158/0008-5472.can-09-2266. PubMed PMID: 19826036; PubMed Central PMCID: PMCPmc2764330.

List of Figures

List of Appendices

List of Abbreviations

Axl: Axl receptor tyrosine kinase

BSA: bovine serum albumin

CAFs: cancer associated fibroblasts

ChIP: chromatin immuno precipitation

ChIP-Seq: chromatin immunoprecipitation sequencing

CML: chronic myeloid leukemia

DAB: 3,3'-diaminobenzidine

DCIS: ductal carcinoma in situ

DME/F-12: Dulbecco's Modified Eagle Medium/Nutrient mixture F-12

DNA: deoxyribonucleic acid

DOC: sodium deoxycholate

ECM: extracellular matrix

EDTA: Ethylenediaminetetraacetic acid

EGF: epidermal growth factor

ER: estrogen receptor

ERK1/2: mitogen-activated protein kinase 3/1

FBS: fetal bovine serum

FITC: fluorescein

H&E: hematoxylin and eosin staining

Her2: human epidermal growth factor receptor 2

HGF: hepatocyte growth factor

HS: horse serum

IP: immunoprecipitation

MCFDCIS: MCF10A-DCIS.com

miRNA: microRNA

mRNA: messenger RNA

MMPs: matrix metalloproteinase

p63: tumor protein p63

PBS: phosphate buffered saline

PCR: polymerase chain reaction

Pen/Strep: penicillin/streptomycin

PR: progesterone receptor

RNA: ribonucleic acid

RPMI: Roswell Park Memorial Institute medium

RT-PCR: real-time polymerase chain reaction

SDS: sodium dodecyl sulfate

siRNA: small interfering RNA

SMA: smooth muscle actin

SDF-1: stromal cell derived factor 1

SDPP: Stroma-derived Prognostic Predictor

Slug: SNAI2, snail family zinc finger 2

TAMs: Tumor associated macrophages

TBS: Tris buffered saline

TCGA: The Cancer Genome Atlas

TGFbeta: transforming growth factor beta

Twist: twist family bHLH transcription factor 1

UTR: un-translated region

UTSW: University of Texas Southwestern Medical Center

Zeb1/2: zinc finger E-box binding homeobox 1/2

Chapter One: Breast Cancer

Introduction

Overview:

Breast cancer kills approximately 40,000 women each year in the United States (1). The main cause of death in these patients is not the primary tumor itself, but rather the metastasis of breast cancer cells to vital organs such as the brain, bone, and lungs. Invasion of breast cancer cells into the mammary stroma is an early and necessary step in the metastatic cascade. However, how breast cancer cells gain invasive properties is unknown. The goal of my project is to elucidate a mechanism by which breast cancer cells invade.

Breast cancer progression: From normal to invasive breast cancer:

In a cross-sectional view of a normal mammary duct, the luminal epithelial cells form a hollow tube. The myoepithelial cells, which secrete the basement membrane, surround the luminal epithelial cells. The basement membrane forms a barrier between the mammary epithelium and the mammary stroma, which consists of extracellular matrix (ECM), fibroblasts, immune cells and adipocytes (2). Under normal conditions epithelial cells that detach from the basement membrane and invade into the hollow lumen undergo anoikis (3).

During breast cancer progression, neoplastic cells invade into the hollow lumen, where they can survive and proliferate. To circumvent anoikis, up regulation of ERK1/2 signaling can decrease the induction of Bmf function. Bmf function is required for anoikis (4). At this stage, the breast cancer cells have not punctured through the basement membrane and this lesion is considered non-invasive. This non-invasive lesion is called ductal carcinoma in situ (DCIS) (5). If treated at this stage, the survival rate of the patient is approximately 99% over 5 years (6).

However, when the breast cancer cells invade through the basement membrane and into the surrounding stroma, the patient's survival rate drastically decreases. The survival rate drops because the invasive breast cancer cells have access to the lymphatic and vascular systems for which they can use to metastasize to distant vital organs. It is the metastatic growth that ultimately kills the patient. The signaling differences between DCIS and invasive breast cancer are unknown. In addition, the changes necessary for cells to gain invasive properties are also unknown (Fig 1-1).

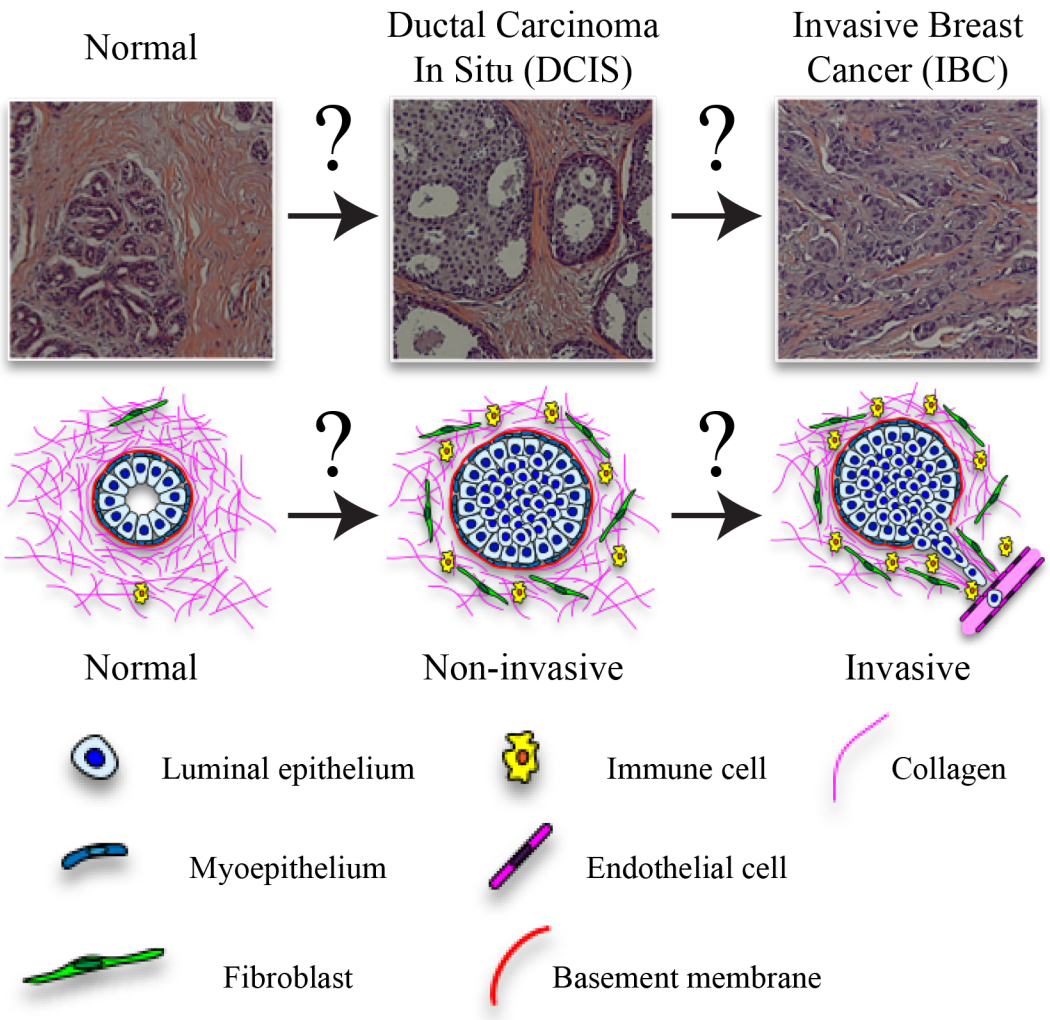

Figure 1-1: Schematic of Breast cancer progression from normal to invasive breast cancer. Top panel is Hematoxylin and Eosin (H&E) images of human breast tissue at normal, ductal carcinoma in situ (DCIS), and invasive breast cancer stages. Lower panel is a cartoon cross-section of the mammary duct at each corresponding stage.

Metastasis Progression:

There are six steps in the metastasis: 1) invasion of cancer cells into the microenvironment, 2) intravastation of the cancer cells into the lymphatic and/or vascular systems, 3) survival of the cancer cells in circulation, 4) extravasation of the cancer cells into secondary/foreign tissues/organs location, 5) seeding of cancer cells in the secondary location and 6) colonization of the foreign tissue (7, 8). Though colonization of cancer cells into the secondary site is the ultimate cause of death, invasion of the breast cancer cells into the breast stroma is necessary for colonization. The focus of this thesis is to elucidate the mechanism by which cancer cells gain the ability to invade into the local microenvironment.

Methods of invasion: Single-cell versus collective-cell invasion:

There is much debate on how breast cancer cells invade into the surrounding stroma. There are two major mechanisms, single-cell and collective-cell invasion. Both share the common trait that the invading cells are motile cells. However, how these methods of cell invasion are regulated is still unknown.

Single-cell invasion can be categorized into two groups: 1) mesenchymal and 2) amoeboid (9, 10). Mesenchymal single-cell invasion occurs when epithelial cells transition to mesenchymal-like cells, or EMT to gain the ability to migrate. Cells undergoing EMT, lose their epithelial traits such as E-cadherin, EpCAM, polarity, and static motility and gain N-cadherin, Twist, Slug, Vimentin and motility to name a few. The classical regulator of EMT is TGFbeta signaling (11). Mesenchymal cells can invade into the surrounding stroma through the secretion of proteases and remodeling of the microenvironment (12). The reorganization of the microenvironment is the hallmark difference between amoeboid versus mesenchymal-single cell invasion.

In amoeboid-single cell invasion, cells may have undergone EMT, but secretion of proteases and reorganization of the microenvironment is not necessary for the cells to migrate away from the primary mass. The amoeboid cells migrate by squeezing and navigate around the surrounding ECM rather than making de novo paths; an example of amoeboid migration is MDA-MB-231 (13). It is unknown how the amoeboid single-cell invasion program is regulated.

Though single-cell migration has been well studied, in breast cancer patient samples, it is uncommon to see single cells breaking off from the primary tumor (Fig 1-1). In actuality, it is more common to see streams/chords of breast cancer cells invading into the surrounding stroma. Suggesting that collective cell migration is the more frequent mechanism of breast cancer cell invasion. Collective-cell migration can be categorized into 2 groups: 1) sprouting and 2) branching migration (9). Sprouting migration is seen in vascular development. In sprouting migration, there is a leader/tip cell that makes the way for the follower/stalk cells to migrate in behind (14). In branching migration, cells migrate collectively into the stroma and unlike sprouting migration, there is no obvious tip/leader cell that drives the migration forward (15). The hallmark characteristic that connects these 2 types of collective cell migration is that the migrating cells still maintain some epithelial characteristics and cell-to-cell contacts. However, the signaling pathway(s) that regulate the collective cell migration program is unknown. This thesis will be focusing on the collective-cell migration as a means of invasion (Fig 1-2).

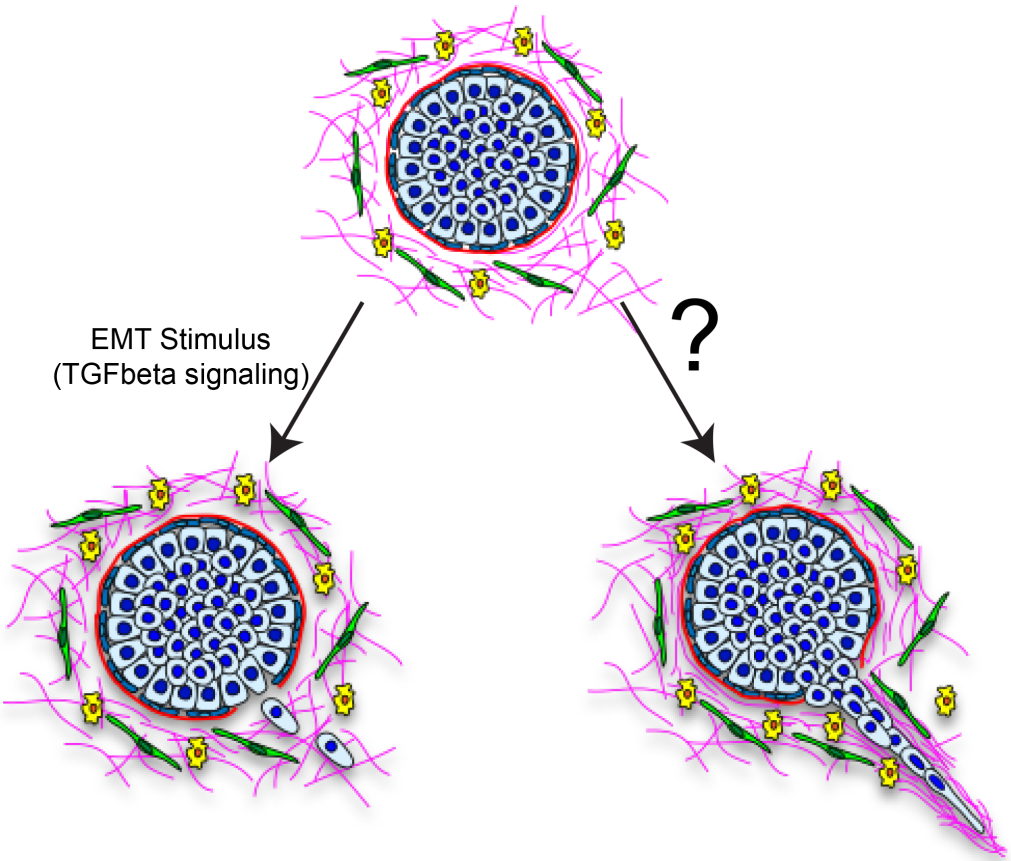

Figure 1-2: Modes of cell migration.

Tumor microenvironment:

During breast cancer progression, the neoplastic cells are not the only cell type undergoing a change in expression to confer disease; the stroma around the cancer also transform to a more conducive environment to support the advancement of the disease. In breast cancer, Finak et al have shown that gene expression microarrays of matched normal and tumor stroma have very different transcriptional patterns. The differences in gene expression pattern termed Stroma-derived Prognostic Predictor, SDPP can predict clinical outcome of patients independent of breast cancer receptor status. The SDPP's 26-gene set includes genes that are involved in immune, wounding, and developmental responses (16). The SDPP signature was developed from a mixture of stromal components such as fibroblasts, immune cells, and adipocytes to name a few. These components can assist in the growth, invasion and metastasis of breast cancer cells.

Tumor associated macrophages, TAMs, have been shown to promote metastasis through angiogenesis, invasion, and metastasis. TAMs can promote angiogenesis through the secretion of vascular endothelial growth factor, VEGF. The neo-vasculature provides the tumor with nutrients and a potential route of metastasis. Frequently tumor-associated vessels are poorly constructed leading to "leaky" vasculature (17). Cancer cells can take advantage of these leaky vessels and intravastize away from the primary mass. TAMs can also secrete chemo-attractants such as epidermal growth factor, EGF, which can stimulate migration of the cancer cells (17). For macrophages to become TAMs, the cancer cells must provide a stimulus such as CSF-1. Ablation of CSF-1 in the microenvironment leads to decrease tumor aggression (18). Thus, macrophages, a component in the tumor microenvironment can contribute to a permissive situation for breast cancer cell invasion.

Another component of the tumor microenvironment is cancer-associated fibroblasts, CAFs. CAFs, which have also been known as myofibroblasts, are characterized by smooth muscle actin, stress fibers, and high secretion of matrix metalloproteinase, MMPs and collagen-I (19, 20). The most well known stimulus to convert fibroblasts to CAFs is TGFbeta signaling perpetuated by the tumor cells (21, 22). In response to TGFbeta signaling, CAFs can secrete pro-growth ligands, such as epidermal growth factor, EGF and hepatocyte growth factor, HGF, chemoattractants, and remodel the collagen in the in the microenvironment (21, 23, 24). These actions by the CAFs can allow cancer cells to metastasize from the primary site of disease.

Changes in the ECM around the neoplastic lesion have been shown to correlate to disease progression. Dense mammographic densities have been associated with increased risk of breast cancer (25) and the disposition of collagen can contribute to the density (26). However, it is not only the increase amount but also the linearization of the collagen fibers around the tumor that can promote breast cancer cell invasion (27). In our studies, we find that when there is no invasion, the collagen-I is organized in a mesh-like network and form a ring around the lesion. However, during invasion, the collagen-I becomes linearized and run parallel to the invasive structure (28).

Correlation between collagen-I organization and cancer progression have been seen in breast cancer, how the changes in collagen-I architecture affect cancer progression is still an undergoing feat. Stromal and cancer cells can sense fibrillar collagen through collagen receptors such as integrins and DDRs (29). Integrins are transmembrane proteins that form heterodimers composed of alpha and beta subunits. There are 18 alpha and 8 beta subunits (30). The integrin configurations where collagen-I is a ligand are alpha1, -2, -10 or -11 and beta1 (30, 31). Upon ligand binding the integrins undergo an intracellular conformational change that induces

downstream signaling. These changes may produce a docking site/scaffolding for intracellular proteins, which can further transduce signaling (30). Discoidin Domain Receptors (DDRs) are tyrosine kinase receptors. There are two DDRs, DDR1 and DDR2 (32). Upon ligand binding, the DDR receptors autophosporylates and transduce downstream signaling pathways such as PI3K and ERK1/2 signaling (29, 32).

Under normal conditions, collagen-I is secreted in a procollagen form (33). It is processed by the cleavage of its N- and C-terminus by procollagen N-proteinase and procollagen C-proteinase (34). Collagen is then arranged into fibers through the crosslinking of collagen units by lysyl oxidase. Lysyl oxidase was discovered in 1968 (35). This enzyme is secreted as a proenzyme of about 50 kDa and once in the extracellular matrix can be cleaved by metalloproteinase resulting in a 32 kDa enzyme (36). It has been shown that lysyl oxidase contributes to the stiffness of the microenvironment through the cross-linking of collagen fibers and that loss of this enzyme decreased the progression of breast cancer in vivo (37). However, the mechanism by which lysyl oxidase expression and activity is induced during breast cancer progression is still unknown.

MicroRNAs mechanism of action:

MicroRNAs (miRNAs) were first discovered in 1993 in Caenorhabditis elegans (38, 39). MiRNAs are non-coding RNAs that are ~20 nucleotides in length after processing. The function of these RNA elements is to silence gene expression. MiRNAs are endogenous in normal cells and can exist as genes are within host genes. Most importantly when transcribed, the RNA strand forms a hairpin structure for which Drosha, cleaves into small 20-30 nucleotide fragments. Once exported out of the nucleus, these miRNAs are then furthered processed by Dicer to form the mature miRNA sequences. The mature miRNA is then loaded onto the RISC complex,

which consists of the Argonaute and other proteins (40). The miRNA-protein complex then binds to the 3' un-translated regions (UTR) of messenger RNAs (mRNA) to inhibit translation. MiRNAs can inhibit gene expression by either binding to the mRNA and prohibiting translation and/or degrade the mRNA before translation. The exact mechanism by which the miRNA induce the degradation of its target is unknown (41).

How the miRNAs target specific mRNAs is through base-pair sequence matching of the seed sequence of the miRNA. The seed sequence of a miRNA is the 2-7 nucleotide identities in the mature miRNA. However, targeting of mRNA by miRNAs does not have to be a perfect nucleotide sequence match between the 3' UTR of the mRNA and the seed sequence of the miRNA. The nucleotides in the seed sequence, most commonly nucleotide 5 and/or 6, can flip out/bulged out of alignment creating a new seed sequence for mRNA targeting (42, 43). Targeting of mRNA by miRNAs is not solely based on sequence paring but rather a combination of frequency of message, accessibility to the 3' UTR and conserved targeting sequence (44). Based on these parameters miRNAs can target multiple genes and thus can regulate multiple signaling pathways.

MicroRNAs in cancer:

It has been found that miRNAs can contribute to cancer progression. One of the most well studied miRNAs is miR21. MiR21 was found to be highly expressed in breast tumors than in normal tissue samples and was correlated to metastasis (45, 46). It has been shown that miR21 may mediate tumor growth by targeting the apoptosis program (47, 48); however the exact miR21 anti-apoptotic target(s) has not been identified. Studies inhibiting miR21 function through an anti-miR21 in MCF-7 and MDA-MB-231 found it to be growth, migration, and metastasis

inhibitory (46, 49). Therefore, miR21 acts as an oncomiR by regulating anti-apoptotic and pro-migratory programs.

MiR34c is a miRNA that suppresses tumor progression. It is regulated by p53 a known tumor suppressor and functions by inhibiting cell proliferation. Corney, et al found that in conditional knockdown of p53 expression in ovarian epithelium, miR34c was down regulated. Upon further investigations, they found a p53 response element upstream of miR34c host gene. Overexpression of miR34c in ovarian cancer cell lines resulted in inhibited cell growth in plastic and in soft agar (50). Achair, et al found that overexpression of miR34c in breast cancer cells promotes a G2/M cell cycle arrest and an increase in apoptosis (51). Therefore, miRNAs can act as oncomiRs or as tumor suppressors.

Chapter Two: mammary fibroblast induced collective invasion

Introduction

Studies presented in this chapter have been published as "Breast Cancer Subtype-Specific Interactions with the Microenvironment Dictate Mechanisms of Invasion" in Cancer Research, 2011.

Overview:

Elucidation of the transition between DCIS to invasive breast cancer is difficult because of the difficulties of in vitro modeling of the 3-dimensional architecture of non-invasive lesions and the time required for tumor progression in mouse models. Here we found that the addition of patient-derived mammary fibroblasts in organotypic cultures of breast cancer cells can induce a subset of breast cancer subtypes to invade. The propensity of mammary fibroblast to induce invasion correlated with the intrinsic motility of the breast cancer cells and the ability of the mammary fibroblasts to reorganize the microenvironment.

Breast cancer subtypes:

Breast cancer can be categorized into five different subtypes: luminal A, luminal B, Her2-postive, basal, and claudin-low (52). These subtypes greatly differ in gene expression as seen through multiple gene expression microarray studies. Most importantly the survival rates of patients with the different breast cancer subtypes greatly differ. The luminal A/B subtypes express many epithelial traits such as E-cadherin. These subtypes are characterized by the expression of progesterone, PR and estrogen, ER receptor, which have been utilized for targeted therapies such as tamoxifen. Since luminal subtypes are heavily reliant on ER signaling for growth and the development of efficient endocrine-targeted therapies, the 5-year survival rate of

patients is approximately 72% for stage III patients. Stage III breast cancer patients have invasive breast cancer with metastasis to nearby lymph nodes and muscle tissue (6).

The Her2-postive subtype is characterized by the amplification and heavy reliance on the Her2 receptor. Increase Her2 signaling results in uncontrolled proliferation. The Her2+ subtype also expresses many epithelial characteristics such as E-cadherin (53). The 5-year survival rate for Her2+ stage III patients is 85% and this high survival rate is due to the efficient endocrine therapy treatments such as trastuzumab, which targets the Her2 receptor (6).

Basal-subtype breast cancers are mostly triple-negative, meaning the cancer cells lack ER, PR, and Her2 receptors. The 5-year survival rate of patients with stage III triple-negative breast cancer is approximately 45%, which in part is due to the lack of targeted therapies as compared to the ER-positive or Her2-postive cancers (6). This breast cancer subtype still expresses epithelial characteristics such as E-cadherin, but also has elevated mesenchymal traits such as Slug expression.

Claudin-low breast cancer subtype was once grouped into the basal-subtype due to the lack of ER, PR, and Her2 receptors. However, they differ in the basal-subtype in that they have low expression of claudins, and high expression of mesenchymal genes such as Zeb1/2, Slug, Twist, etc. Claudins are tight junction proteins (52).

Mammary fibroblasts in the tumor microenvironment:

As previously discussed, during breast cancer progression, the cancer epithelium is not the only cell type that undergoes transformation to confer disease. Studies comparing the tumor microenvironment and the microenvironment of the normal breast showed significant differences in gene pattern (16, 54). One of the stromal cells in the tumor microenvironment that may assist in the progression of the disease is cancer-associated fibroblasts, CAFs, or also known as

myofibroblasts. These cells are characterized by stress fibers and smooth muscle actin, SMA (54, 55).

CAFs can promote the growth of tumors through the secretion of SDF-1. SDF-1 works with its receptor, CXCR4 located on the cancer cells to promote proliferation (23). The appearances of CAFs occur early in disease progression and are most likely derived from resident fibroblasts that have been transformed by the cancer cells (55, 56). One way cancer cells can promote the transformation of CAFs is through the secretion of TGFbeta1 (21). CAFs are often located near neoplasia especially near invasive structures (55). The presence of CAFs near cancer invasion is not a surprise since they secrete many ECM remodeling factors such as MMPs and chemoattractants such HGF (19, 21). Thus, CAFs are an important component to the tumor microenvironment in the cascade of disease progression.

ERK1/2 signaling in breast cancer:

ERK1/2 signaling has been implicated in cancer progression. It has been shown that ERK1/2 phosphorylation and therefore activation was elevated in tumors compared to normal matched breast samples (57). The increase in ERK1/2 signaling leads to increased proliferation through up regulation of pro-growth genes such as AP-1 and c-Myc (58). ERK1/2 signaling can also increase cell motility of cancer cells (59). Importantly, ERK1/2 signaling can induce the motility of mature non-motile normal-like MCF10A breast cells in organotypic cultures. However, even with the newfound ability to move within the spheroid, the ERK1/2 signaling could not induce the MCF10A cells to invade into the modeled ECM (60). Therefore, motility and ERK1/2 activation is not sufficient to induce breast cancer invasion and requires additional factors.

Methods and Materials

Cell culture and reagents:

MCFDCIS cells were purchased from Asterand. T47D and MCF-7 cells were from the American Type Culture Collection. HCC1143, HCC1806, HCC1954, HCC1569 and HCC1428 were gifts from Dr. John Minna's lab at University of Texas, Southwestern Medical Center (UTSW). MCFDCIS cells were cultured in 5% horse serum, 20 ng/ml EGF, 0.5 ug/ml hydrocortisone, 100 ng/ml cholera toxin, 10 ug/ml insulin, 1X pen/strep in DME-F12. All other breast cancer cells including MDA-MB-231 were cultured in 10% FBS in RPMI. T47D had 10 ug/ml of insulin and HCC1143 had 5 ng/ml EGF supplemented in their media. Mammary fibroblasts were isolated from normal and tumor patient samples treated at UTSW. Tissue samples were minced with a scalpel and digested with 0.25 mg/ml collagenase-I overnight in a rotary incubator. Mammary fibroblasts were separated from other stromal and cancer cells by differential centrifugation. The mammary fibroblasts were grown in 10% FBS in DME-F12 and used within 17 passages from initial isolation. Validation of mammary fibroblast isolation was done through immunofluorescence staining with SMA and E-cadherin. Patient-derived mammary fibroblasts were stained positive for SMA and negative for E-cadherin (data not shown).

Organotypic culture:

Single cells were plated on top of a mixture of Matrigel: collagen-I in either BD Falcon or Nunc eight-well chamber slides in an overlay media consisting of 2% Matrigel. For MCFDCIS, the overlay media had 2% horse serum, 0.5 ug/ml hydrocortisone, 100 ng/ml cholera toxin, 10 ug/ml insulin, 1X pen/strep, in DME-F12. On day 2 of organotypic culture, the MCFDCIS cultures' overlay media was switched to 5% horse serum in DME-F12 and supplemented with 2% Matrigel. For all other cancer cell lines, their overlay media was their growth media with 2%

Matrigel supplemented. Cultures were grown for 4 days before real-time imaging or 6 to 8 days before immunofluorescence. In co-cultures, mammary fibroblasts were pelleted then resuspended in the Matrigel: collagen-I mixture before plating into the 8-well chamber slides.

Quantification of invasion:

In all experiments, an invasive spheroid had to have at least 3 cells collectively invading away from the primary mass of 15 or more cells. Each quantification had at least 50 spheroids counted per condition in 3 independent experiments.

Fibroblast conditioned media:

Fibroblasts were plated on tissue culture plastic in 10% FBS in DME-F12. 24 hours later the cells were washed twice with PBS and then cultured in serum-free DME-F12. After 48 hours the conditioned media was harvested and supplemented with 2% Matrigel and 5% horse serum before adding onto day 2 organotypic cultures.

Transfection of Fibroblasts:

Mammary fibroblasts were plated at a density of 20,000 cells per well in a 96-well plate and were reverse transfected with RNAiMax (Life Technologies), using ON-TARGETplus SMART pools (Dharmacon). Non-targeting control (cat. no. 001810-10-05) or Cdc42 (J-005057-05: CGGAAUAUGUACCGACUGU; J-005057-06: GCAGUCACAGUUAUGAUUG; J-005057-07: GAUGACCCCUCUACUAUUG; and J-005057-08: CUGCAGGGCAGAGGAUUA) siRNAs were used at a final concentration of 100 nM. Mammary fibroblasts were harvested 24 hours after transfection and embedded in Matrigel: collagen-I at 2,500 cells per well for organotypic culture. Organotypic cultures were analyzed for collagen-I reorganization (day 5 post-transfection) or fibroblast-induced tumor cell invasion (day 7 post-transfection).

Immunofluorescence:

Cultures were fixed with 2% formaldehyde diluted in 1X phosphate-buffered saline, PBS for 20 minutes, permeabilized with 0.05% Triton X-100 diluted in 1X PBS for 10 minutes and then blocked in 10% goat serum, 0.1% bovine serum albumin, BSA, 0.2% Triton X-100, 0.05% Tween-20 in 1X PBS for 1 hour. Primary antibodies were incubated overnight with the cultures and then washed three times with 0.1% BSA, 0.2% Triton X-100, 0.05% Tween-20 in 1X PBS each for 10 minutes. Cultures were incubated with secondary antibodies for 1 hour and then washed 3 times with 0.1% BSA, 0.2% Triton X-100, 0.05% Tween-20 in 1X PBS each for 10 minutes then washed once with 1X PBS. Cultures were mounted with Prolong Gold (Life Technologies). Primary and secondary antibodies are listed in Appendix I. Hoechst (1:2,000, Life Technologies) was used as a counterstain.

Western blot:

Cells were washed with 1X PBS and lysed on ice with 50 mM Tris pH 7.4, 150 mM NaCl, 1% Triton X-100, 0.5% deoxycholic acid, 0.2 mM NaVO4, 100 mM NaF, and 50 mM beta-Glycerophosphate in water. Lysates were then vortexed for 10 seconds, incubated on ice for 10 minutes and then spun at 14,000 rpm for 15 minutes. Supernants were collected and Laemli buffer (40% glycerol, 6% SDS, 6% beta-mercaptoethanol, 20 mM EDTA, 0.1% bromophenol blue, in water) was added to a final concentration of 1X. Lysates were loaded on SDS-Page gels and ran for 45 minutes at 200 volts. Gels, membranes, and Whatman paper were equilibrated for 15 minutes in 1X transfer buffer (0.58% (w/v) Tris, 0.29% (w/v) glycine, 3.75% (w/v) SDS, 20% (v/v) methanol, in water) before loading into a semi-transfer apparatus and ran for 1 hour at 20 volts. Membranes were rinsed with 1X PBS before blocking for 1 hour in 10% Casein (BioRad), 1/10 PBS, in water. Primary antibodies were diluted in 1:1000 Tween-20, 10% Casein (BioRad),

1/10 PBS, in water and incubated with the membrane overnight at 4 degrees. Membranes were washed with 1X TBS, 0.15% Tween-20 for 3 times at 5 minutes per wash. Membranes were incubated with secondary antibodies in 0.01% SDS, 1:1000 Tween-20, 10% Casein (BioRad), 1/10 PBS in water for 1 hour in the dark at room temperature. Membranes were washed with 1X TBS, 0.15% Tween-20 for 3 times at 5 minutes per wash, 3 quick washes with 1X PBS, and then imaged on the Odyssey. Primary and secondary antibodies are listed in Appendix I.

Real-time imaging of organotypic cultures and immunofluorescence:

Cultures were imaged with a PerkinElmer Ultraview ERS spinning disk confocal microscope in a 37 degree Celsius chamber supplemented with humidified CO2 and a CCD camera (Orca AG, Hamamatsu). At least 10 xy points were imaged per condition per experiment with a z-span of 100 micron and 10 z-slices per xy point. Each time point was 30 minutes long. Immunofluorescence images were acquired on a Nikon Eclipse TE 2000-E confocal microscope.

Xenografts:

Severe combined immunodeficient female mice (UTSW Mouse Breeding Core Facility) between the ages of 6-8 weeks were injected in the number 4 fat pad with 50,000 MCFDCIS cells with or without 2,000,000 mammary fibroblasts in a 50:50 Matrigel: DME-F12 mixture. Xenografts grew for 2 weeks before daily treatment of vehicle or 25 mg/kg/dose of PD0325901 by oral gavage. Vehicle consists of 0.5% hydroxypropylmethylcellulose and 0.1% Tween-80 in water. Mice were sacrificed with CO2 in accordance to UTSW Institutional Animal Care and Use Committee guidelines. Tumors were removed, fixed in formalin at room temperature overnight, embedded in paraffin and sliced at five micron thickness for immunohistochemistry.

Immunohistochemistry:

Paraffin sections were incubated in xylene for 10 minutes 3 times, 100% ethanol for 3

minutes twice, 95% ethanol for 3 minutes twice, and distilled water for 3 minutes. Incubation in boiling sodium citrate bath for 20 minutes was used as an antigen retrieval method. Slides were allowed to cool in the sodium citrate solution for 20 minutes, blocked in 3% H2O2 for 30 minutes, incubated in distilled water for 1 minute and then blocked in 1% BSA in 1X PBS for 1 hour. Primary antibodies were diluted in Signal Stain (Cell Signaling) and incubated on the slides overnight at 4 degrees Celsius in a humidified chamber. Slides were washed 4 times in 1X TBS and 0.1% Tween-20 for 5 minutes per wash and then incubated in the dark at room temperature for 1 hour with HRP polymer secondary conjugate antibody (Vector ImmPress Reagent kit). Slides were washed 4 times in 1X TBS+ 0.1% Tween-20 for 5 minutes per wash, then DAB (Vector ImmPact DAB) was added to the slide and the reaction was stopped when the slides were dipped in water. Slides were counterstained with hematoxylin, rinsed until the excess stain was gone, dried, and then mounted with Permount.

Results

Mammary fibroblast-induced invasion is dependent on breast cancer intrinsic subtype:

MCFDCIS cells are unique in that when injected into the mammary fat pad of female mice, they form early stage breast cancer, DCIS-like lesions (Fig 2-1A) at 3 weeks post-injection. If the MCFDCIS tumors were allowed to grow to 6 weeks post-injection, the lesions spontaneously become invasive (61). The invasive stage was triggered at 3 weeks post-injection by co-injection with mammary fibroblasts (Fig 2-1A, (61)). Co-injected with mammary fibroblasts, the MCFDCIS cells form non-invasive lesions at 2 weeks post-injection (Fig 2-1A) as can be seen through the peri-tumoral staining of SMA. SMA is present in myoepithelial cells that are located in the perimeter of ducts and DCIS lesions. In addition to myoepithelial cells, cancer associated fibroblasts or myofibroblasts express SMA.

To elucidate how mammary fibroblasts can induce the invasion of MCFDCIS, we co-cultured the MCFDCIS with mammary fibroblasts in organotypic cultures. Organotypic culture was chosen because it allowed study of single and collective-cell invasion. MCF10A, a normal-like breast cancer cell line, can form non-invasive spheroids with an intact basement membrane as shown through the continuous staining of laminin-5. At day 8 of culture, MCF10A spheroids start to hollow out similar to the hollow lumens of mammary ducts (Fig 2-2). MDA-MB-231 cells can spontaneously collectively invade in organotypic culture (Fig 2-2). When cultured alone, MCFDCIS cells form 3-dimensional clonal spheroids, reminiscent of DCIS lesions and have an intact basement membrane as seen through laminin-5 staining (Fig 2-1B and 2-2). Co-culture with mammary fibroblasts was sufficient to induce the collective invasion of MCFDCIS cells from the primary mass. There is also a disruption of basement membrane at the point of invasion (Fig 2-1 B and C).

To determine if the mammary fibroblasts were sufficient to induce the invasion of patient-derived breast cancer cell lines, we conducted a small screen of single and co-culture organotypic cultures of HCC1806, HCC1143, HCC1954, HCC1569, HCC1428, T47D and MCF-7 (Fig 2-1 D and E). Surprisingly we found that mammary fibroblasts were able to induce collective cell invasion in the basal- but not luminal subtypes (Fig 2-1 D and E). The ability of mammary fibroblasts to induce the collective cell invasion in the basal- but not luminal-subtype may contribute to the poor clinical outcome of basal-subtype patients when compared to luminal-subtype patients.

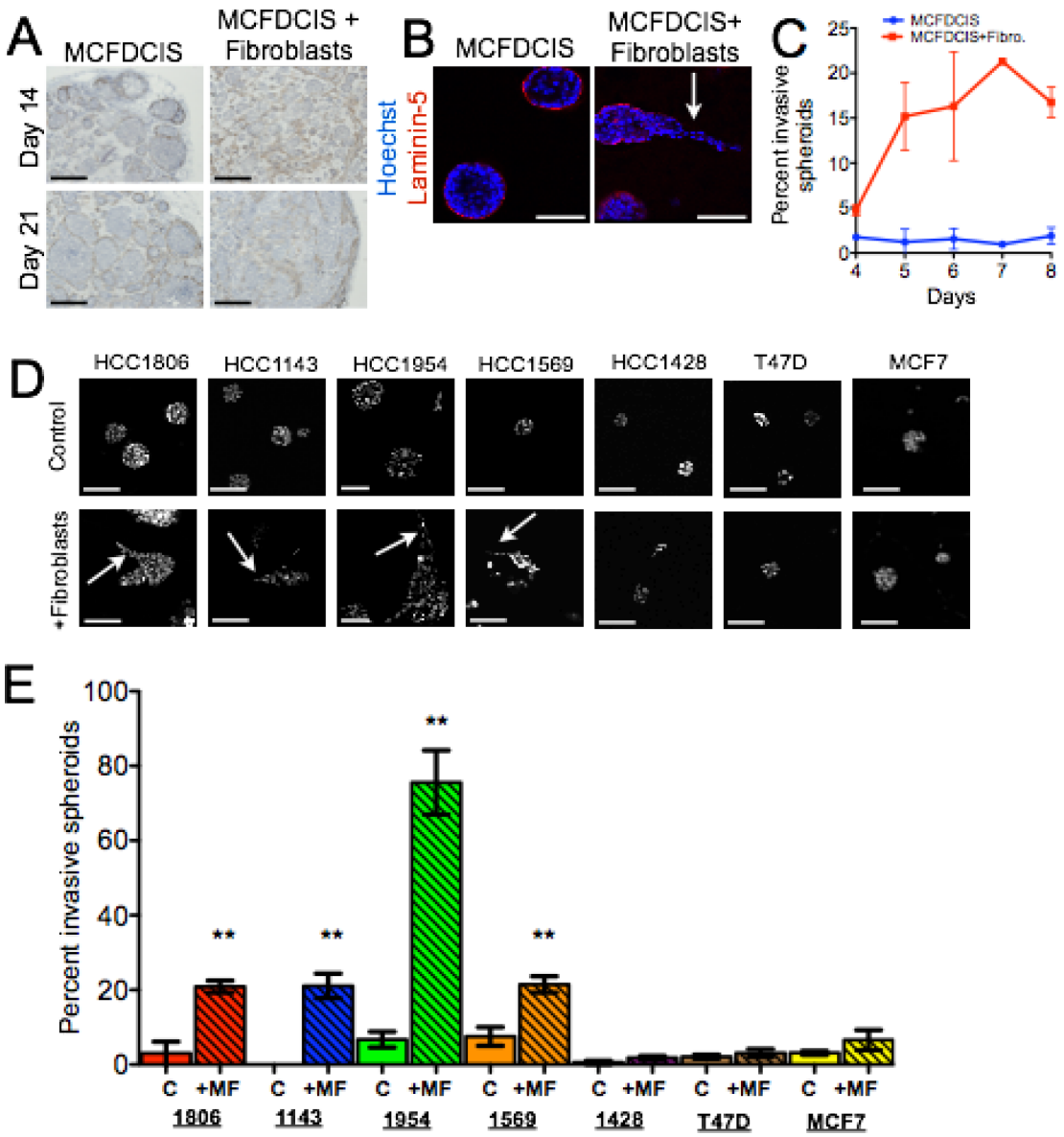

Figure 2-1: Mammary fibroblasts specifically induce basal-subtype breast cancer cells to invade in organotypic culture. **A.** MCFDCIS xenografts co-injected with or without mammary fibroblasts on day 14 and 21 post-injection. SMA (myoepithelial cells, brown), and counterstained with Hematoxylin (nuclei, blue). **B.** Immunofluorescence of MCFDCIS with and without mammary fibroblasts in organotypic culture. Laminin-5 (basement membrane, red) and counterstained with Hoechst (nuclei, blue). **C.** Percent of invasive spheroids overtime in single and co-cultures of MCFDCIS and mammary fibroblasts in organotypic cultures. **D.** Cell line organotypic culture panel of 4 basal-subtypes, HCC1806, HCC1143, HCC1954, HCC1569 and 3 luminal-subtypes, HCC1428, T47D, and MCF7 with and without mammary fibroblasts. Arrows point to invasive structures. **E.** Quantification of intrinsic and mammary fibroblast-induced invasion. Quantifications are t-test of sample versus control condition. Graphs show mean with standard deviation bars. **p-value = 0.01. Scale bar is 100 um.

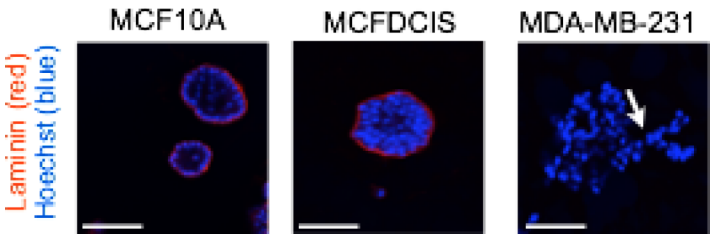

Figure 2-2: Organotypic cultures allow ductal carcinoma in situ-like growth and spontaneous collective cell invasion. Single cultures of MCF10A (normal, non-invasive), MCFDCIS (basal-subtype, non-invasive), and MDA-MB-231 (claudin-low subtype, invasive) in organotypic cultures. Arrow points to an invasive structure. Laminin-5 (basement membrane, red) and counterstained with Hoechst (nuclei, blue). Scale bars are 100 um.

Mammary fibroblasts induce sprouting invasion of motile breast cancer cells:

To understand how mammary fibroblasts induce collective cell invasion, we conducted real-time imaging of single and co-culture of MCFDCIS with and without mammary fibroblasts. We found that single cultures of MCFDCIS cells with mCherry-CAAX labeling, which highlight the plasma membrane, form non-invasive DCIS-like lesions. Movement was detected within the spheroid and each cell maintains at least one cell-to-cell contact with another. Most importantly, there were no plasma membrane protrusions into the modeled ECM (Fig 2-3A). In organotypic cultures, mammary fibroblasts can move towards MCFDCIS spheroids and induce the cells within the spheroid to sprout out toward the mammary fibroblast as seen by the protrusion of the plasma membrane (Fig 2-3A). Mammary fibroblasts not only induced the plasma membrane protrusions but also the displacement of the cells from the main mass. This displacement can be seen through the movement of the cells expressing the nuclear labeling, H2B-mcherry (Fig 2-3 B). Once invaded, MCFDCIS cells continue to invade towards mammary fibroblasts and maintain cell-to-cell contacts with each other (Fig 2-3C and Fig 2-4). Since the induction of invasion in MCFDCIS cells occur in less than one population doubling, these cells are motile not proliferating invasive cells.

To determine if the intrinsic motility of the breast cancer cells is the determining factor of mammary fibroblast induced invasion, we conducted real-time imaging of single and co-cultures of at least two basal- and two luminal-subtype breast cancer cell lines. In single cultures, we found that the luminal-subtypes, HCC1428 and T47D were not as motile as basal-subtypes HCC1954 and HCC1806 as seen through the track displacement and speed of cells over time (Fig 2-5 and Fig 2-6A). When we co-culture the breast cancer cells with mammary fibroblasts only the basal-subtype breast cancer spheroids could be induced to invade. The luminal-subtype

spheroids were not induced to invade even though there were nearby mammary fibroblasts (Fig 2-6 B). Based on these data, the intrinsic motility of the breast cancer cells was the determining factor of mammary fibroblast induced invasion.

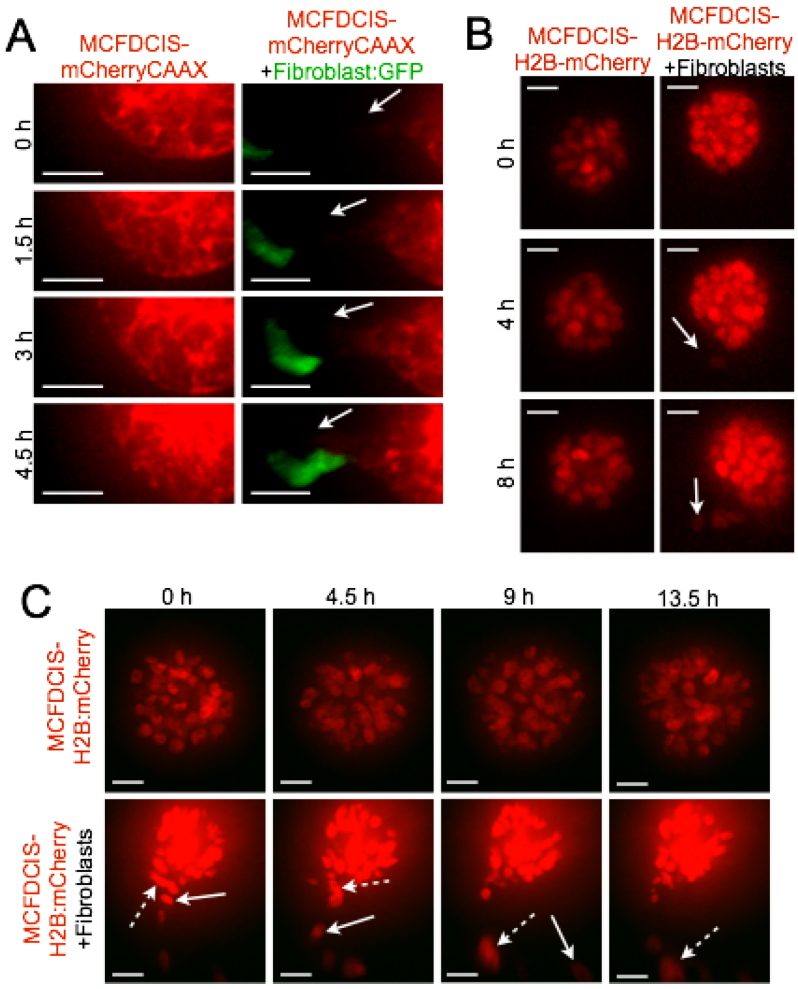

Figure 2-3: Mammary fibroblasts induce sprouting invasion of the MCFDCIS cells. A. Time-lapse images of MCFDCIS:mCherry-CAAX cells cultured with or without mammary fibroblasts:GFP. Arrow points to the sprouting MCFDCIS cells. **B.** Time-lapse images of single and co-culture organotypic cultures of MCFDCIS:H2B-mcherry and mammary fibroblasts (unlabeled). Arrow points to nuclei of sprouting MCFDCIS cells. **C.** Time-lapse images of single and co-culture organotypic cultures of MCFDCIS:H2B-mcherry and mammary-fibroblasts (unlabeled). Arrows point to nuclei of sprouting MCFDCIS cells invading away from the main mass. Scale bar is 20 um.

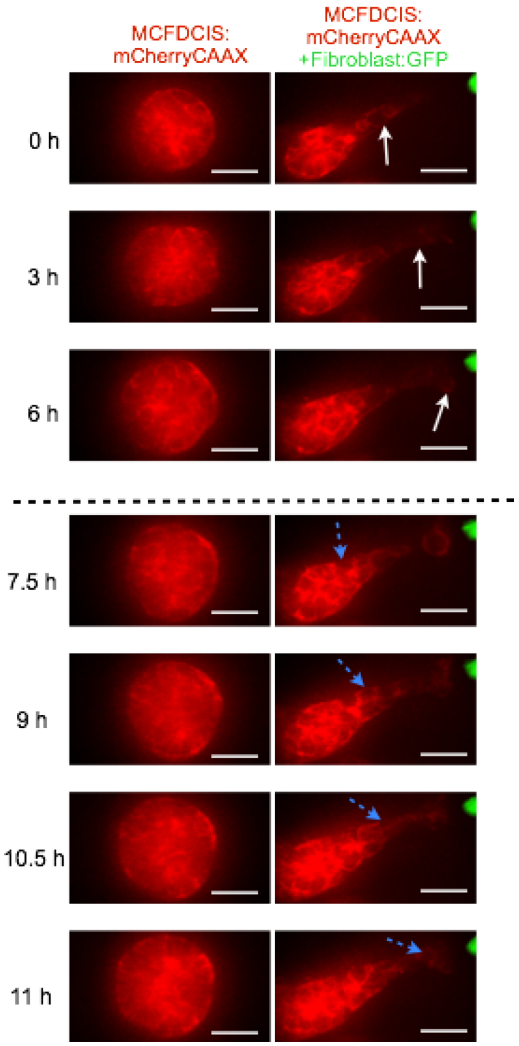

Figure 2-4: Subsequent invasive cells follow the initial invasive path. Time-lapse images of MCFDCIS:mCherry-CAAX spheroids with and without mammary fibroblasts GFP. Top panel traces the location of an invasive cell at the middle of the invasive structure migrating and extending the invasive protrusion towards the mammary fibroblast. Bottom panel traces the location of an invasive cell that starts at the base of the invasive structure and migrates away from the primary mass and towards the mammary fibroblast. Scale bar is 20 um.

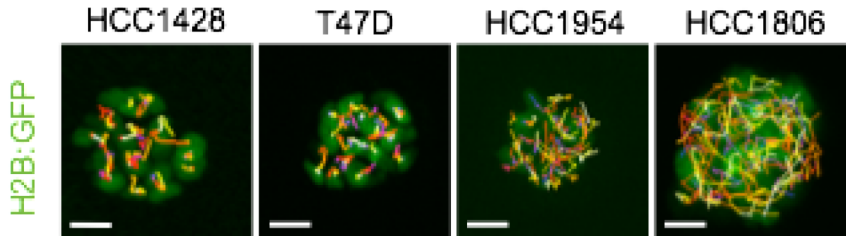

Figure 2-5: The intrinsic motility of breast cancer cells within the spheroid. Real-time imaging of single organotypic cultures of two luminal-subtypes, HCC1428 and T47D and two basal-subtypes HCC1954 and HCC1806. Lines represent the tracks of the cells during the imaging period. H2B-GFP labels the nuclei and shows the position of the cells after 14 hours of imaging. Scale bar is 20 um.

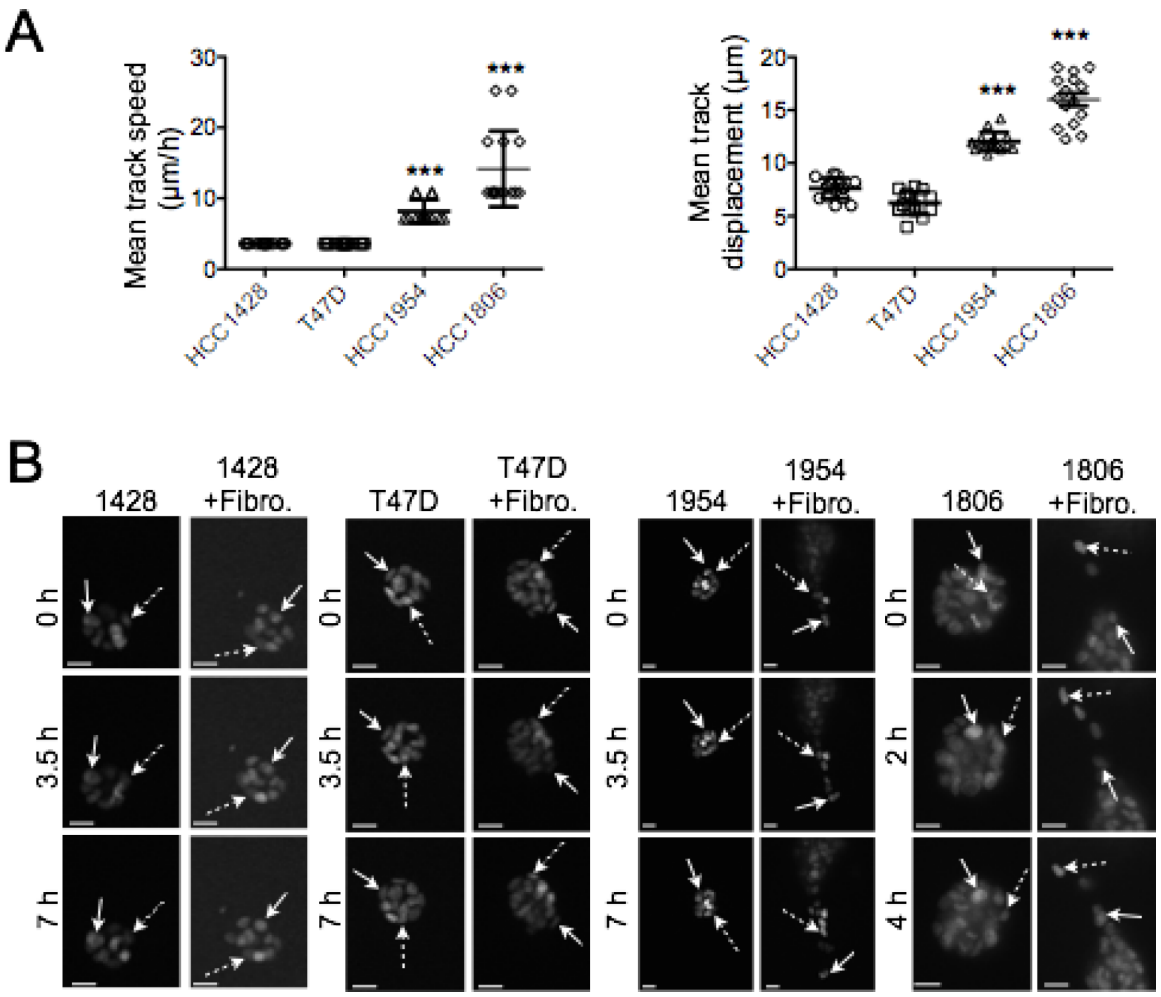

Figure 2-6: Basal-subtype breast cancer cells are intrinsically motile and are able to be induced to invade by mammary fibroblasts. A. Quantification of speed and displacement of single organotypic cultures of listed luminal and basal-subtypes. Graphs show means and standard deviation bars. T-test against HCC1428. ***p-value <= 0.001. **B.** Time lapse images of single and co-cultures of listed luminal- and basal- subtypes with and without mammary fibroblasts. Arrows show the relative position of two cells within the spheroid over time. H2B-GFP (nuclei, gray). Scale bars are 20 um.

Mammary fibroblasts reorganize the microenvironment for invasion:

Cancer associated fibroblasts have been shown to induce invasion of cancer cells through secretion of pro-migratory proteins such as EGF, SDF, etc. (20). To determine if conditioned media from mammary fibroblasts was sufficient to induce invasion, we cultured MCFDCIS alone, with mammary fibroblasts, or alone with mammary fibroblast conditioned media applied on day 2 of organotypic culture. We found that only the co-culture of MCFDCIS cells with mammary fibroblasts was sufficient to induce collective cell invasion compared to the single culture (Fig 2-7 A and B). These data suggest that secreted factors from mammary fibroblasts are not sufficient to induce collective cell invasion.

Since fibroblasts can reorganize the extracellular matrix, specifically collagen-I in the stroma, we conducted immunofluorescence and stained for collagen-I in the co-culture of breast cancer epithelial cells and mammary fibroblasts. In the single culture of MCFDCIS, the collagen-I is organized in a mesh-like network. Around the spheroid, the collagen-I forms a tight ring around the structure almost like a barricade separating the epithelial cells from the rest of the modeled ECM. With the addition of mammary fibroblasts, the collagen-I is no longer in a mesh-like network but rather have linearized around the mammary fibroblasts. Most importantly the collectively invasive cells of a spheroid run parallel to the linearized collagen-I and nearby mammary fibroblast as though the invasive cells are using the reorganized collagen-I fibers as tracks to migrate away from the primary mass (Fig 2-7 C). In real-time imaging, if we label the collagen-I with FITC, we see that the area for which the invasive cells eventually migrate to have been reorganized preceding the invasion (rectangle, Fig 2-7D). Therefore the site of invasion needs to be reorganized by mammary fibroblasts before motile breast cancer cells can migrate away from the primary mass.

To determine if the mammary fibroblasts' ability to reorganize the collagen-I is independent from the signaling of the breast cancer cells, we cultured mammary fibroblasts alone in organotypic culture. In the ECM devoid of mammary fibroblasts, the collagen-I was in a mesh-like network similar to single cultures of MCFDCIS. With the addition of mammary fibroblasts either mock transfected (OptiMEM) or transfected with a non-targeting siRNA, the collagen-I linearizes around the cells. The linearization of the collagen-I by the mammary fibroblasts can be reduced if Cdc42, a GTPase is knocked down in the cells via siRNAs targeting Cdc42. It has been shown that fibroblasts need functional Cdc42 to be able to elongate to functionally remodel the ECM (Fig 2-7 E, (24). As expected, if we knocked down Cdc42 in the mammary fibroblasts and then co-cultured with breast cancer cells, we saw a reduction of collectively invading spheroids as compared to mock (OptiMEM) and non-targeting siRNA controls (Fig 2-7 F and G). Therefore, if we can inhibit the mammary fibroblasts' ability to reorganize the ECM at the DCIS stage of breast cancer development, we can greatly reduce the frequency of invasion.

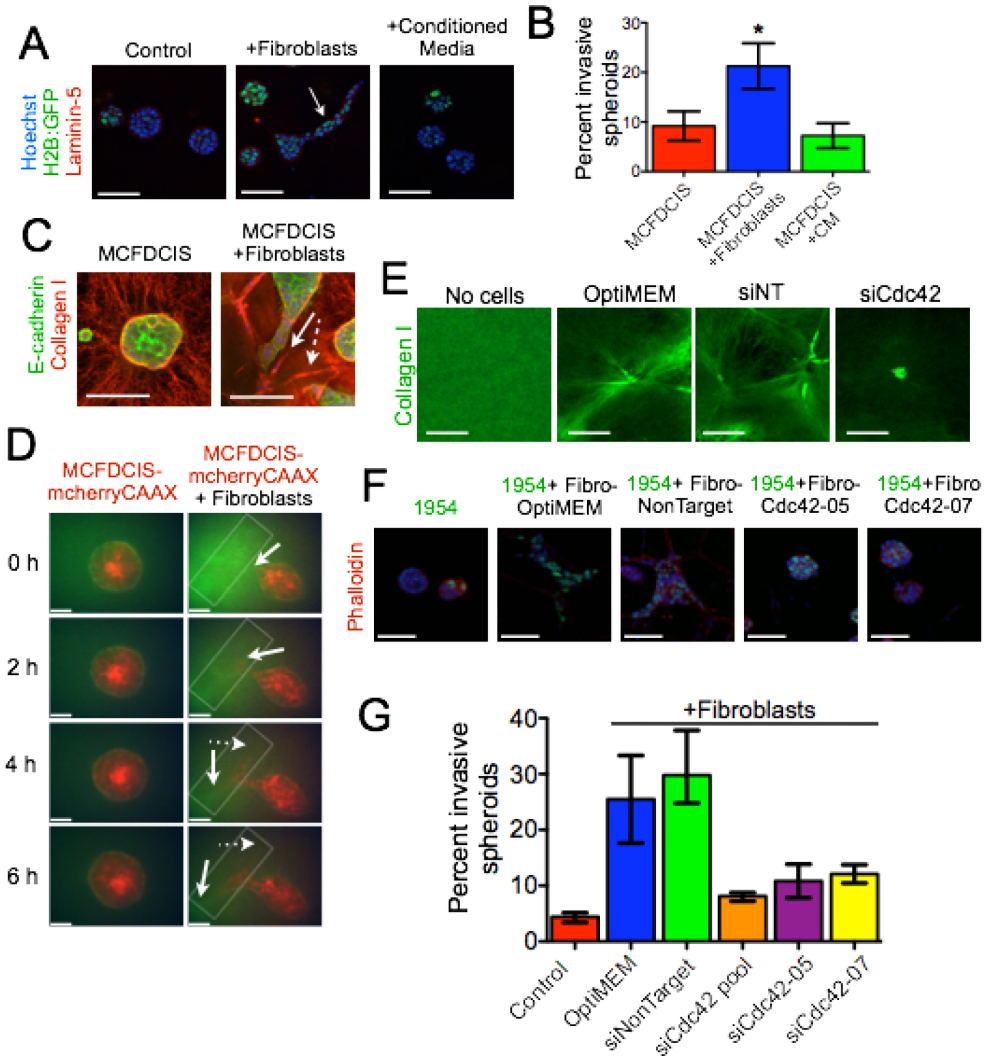

Figure 2-7: Invasive cells utilize mammary fibroblast-reorganized collagen-I tracks to invade. **A.** Immunofluorescence of organotypic cultures of MCFDCIS cells alone, with mammary fibroblasts, or with conditioned mammary fibroblast media. **B.** Quantification of invasive spheroids in the conditions listed in A. **C.** Immunofluorescence of organotypic cultured MCFDCIS with and without mammary fibroblasts. E-cadherin (epithelial marker, green), collagen-I (ECM, red) and counterstained with Hoechst (nuclei, blue). Solid arrow highlights mammary fibroblast parallel to the invasive MCFDCIS structure. Dotted arrow points to another nearby mammary fibroblast. **D.** Time lapse imaging of MCFDCIS:mCherry-CAAX spheroids cultured alone or with mammary fibroblasts (unlabeled) in organotypic cultures where collagen-I is FITC labeled (green). Arrows point to 2 ends of an invasive structure emanating from the MCFDCIS spheroid. The decrease of collagen-I:FITC signal over time is due to photobleaching. **E.** Organotypic cultures of mammary fibroblasts mock (OptiMEM), non-targeting, or Cdc42 siRNAs (siCdc42) transfection. Collagen-I:FITC (green). **F.** Co-cultures of HCC1954 with mammary fibroblasts transfected with mock, non-targeting siRNAs, or Cdc42 siRNAs (shown two oligos from the siCdc42 pool). **G.** Quantification of invasive spheroids in F. Graphs show means and standard deviation bars, and t-test against control conditions. *p-value = 0.01. Immunofluorescence scale bars are 100 um, real-time imaging scale bars are 20 um.

Inhibition of ERK1/2 signaling can decrease mammary fibroblast-induced collective cell invasion:

To induce collective cell invasion by mammary fibroblasts, the mammary fibroblasts need to reorganize the ECM and the breast cancer cells must posses the intrinsic ability of motility. Inhibition of mammary fibroblasts elongation can decrease the frequency of collective invasion. However, if mammary fibroblasts have already reorganized the microenvironment, targeting the breast cancer cells specifically the motile cells could decrease invasion. First, we wanted to determine if the invasive cells had undergone an epithelial to mesenchymal transition during invasion as a means to gain motility. Western blot of luminal and basal-subtypes show that though the luminal-subtype, HCC1428, have a higher E-cadherin expression, basal-subtypes still express more E-cadherin than mammary fibroblasts (Fig 2-8 A). Through E-cadherin and EpCAM stainings, of single and co-cultures, we found that the cells within the spheroid and cells that are collectively invading away from the primary mass still retain epithelial characteristics in both luminal and basal-subtypes (Fig 2-8 C). In xenografts, MCFDCIS cells maintain E-cadherin expression in DCIS-like lesions and in mammary fibroblast induced invasive breast cancer (Fig 2-8 D). Based on these data, the invasive cells have not undergone a complete EMT during the translocation away from the primary mass.

Since EMT does not seem to be the route to gain the intrinsic motility of the breast cancer cells, we investigated if ERK1/2 signaling could be regulating the breast cancer cells' motility. Previously, it has been shown that ERK1/2 signaling can induce the intraspheriod motility of MCF10A (60) and that phospho-ERK1/2 expression was elevated in patient DCIS lesions (57). Therefore to determine if ERK1/2 signaling is required for mammary fibroblast induced invasion, we treated co-cultures of MCFDCIS and mammary fibroblasts with a MEK1/2 inhibitor. As

seen through the track lengths and speed quantification in Fig 2-9 A and B, the addition of the MEK1/2 inhibitor to the organotypic co-cultures of MCFDCIS and mammary fibroblasts decrease the motility of the epithelial cells. If we targeted the activity of epidermal growth factor receptor, EGFR, an upstream stimulator of ERK1/2 signaling, with Erlotinib we saw a decrease in the frequency of invasive spheroids in the co-cultures (Fig 2-9 C and D). Since ERK1/2 signaling is required for mammary fibroblast induced invasion in vitro, we wanted to determine if it is also required in vivo. We treated mice bearing 2 week tumors with the MEK1/2 inhibitor for one week before sacrificing the mice and harvesting the tumors. As shown before, control xenografts of MCFDCIS cells form non-invasive DCIS-like lesions while co-injected with mammary fibroblasts form invasive lesions as shown through the SMA staining (Fig 2-9 E). Upon MEK1/2 inhibitor treatment, the tumor weight of both MCFDCIS and MCFDCIS co-injected with mammary fibroblasts decreased compared to their vehicle treated counterparts (Fig 2-9 F). Immunohistochemistry, shows that most of the MEK1/2 inhibitor treated tumors consisted of necrotic tissue and if there were still MCFDCIS lesions, the lesions were small and DCIS-like (Fig 2-9 E and Fig 2-10). Since MCFDCIS cells are not the only cells exposed to MEK1/2 inhibitor, the inhibitor may also affect mammary fibroblasts. To determine if the decrease in invasion is due to the MEK1/2 inhibitor affecting the mammary fibroblasts' ability to reorganize the ECM, we investigated the inhibitors' effects on the mammary fibroblasts. MEK1/2 inhibitor and Ertlonib did not decrease the mammary fibroblasts' ability to reorganize the ECM (Fig 2-11). Therefore, the decrease in invasion upon MEK1/2 inhibitor treatment in the co-culture is through the inhibition of motility in the breast cancer cells since it does not seem that the inhibitor is affecting the mammary fibroblasts' ability to reorganize the microenvironment. In summation, the intrinsic motility of the breast cancer cells is regulated by

ERK1/2 signaling and inhibition of this pathway leads to decreased mammary fibroblast induced collective invasion in both in vitro and in vivo assays.

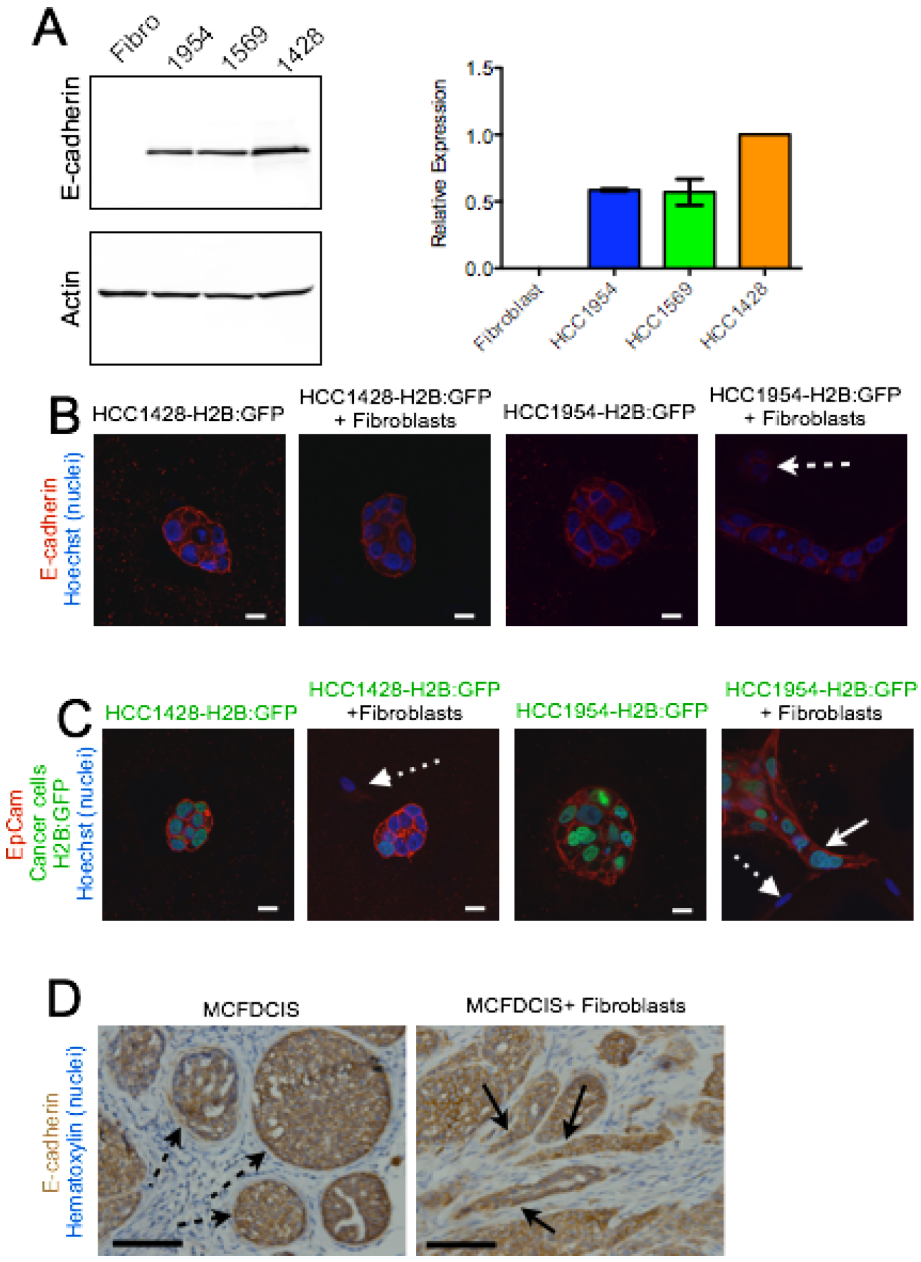

Figure 2-8: Invasive breast cancer cells maintain E-cadherin expression. A. Western blot of E-cadherin and actin of listed cell lines. Quantification is of E-cadherin signal normalized to actin of the corresponding lane. **B.** Immunofluorescence of HCC1428:H2B-GFP and HCC1954:H2B-GFP single and co-cultured with mammary fibroblasts. E-cadherin (epithelial marker, red) and counterstained with Hoechst (nuclei, blue). **C.** Immunofluorescence of HCC1428:H2B-GFP and HCC1954:H2B-GFP single and co-cultured with mammary fibroblasts. EpCAM (epithelial marker, red), H2B-GFP (nuclei, green) and counterstained with Hoechst (nuclei, blue). **D.** Immunohistochemistry of MCFDCIS injected with or without mammary fibroblasts. Dotted arrows point to DCIS-like lesions while solid arrows point to invasive lesions. E-cadherin (epithelial marker, brown) and counterstained with Hematoxylin (nuclei, blue). Immunofluorescence scale bars are 15 um and immunohistochemistry scale bars are 100 um.

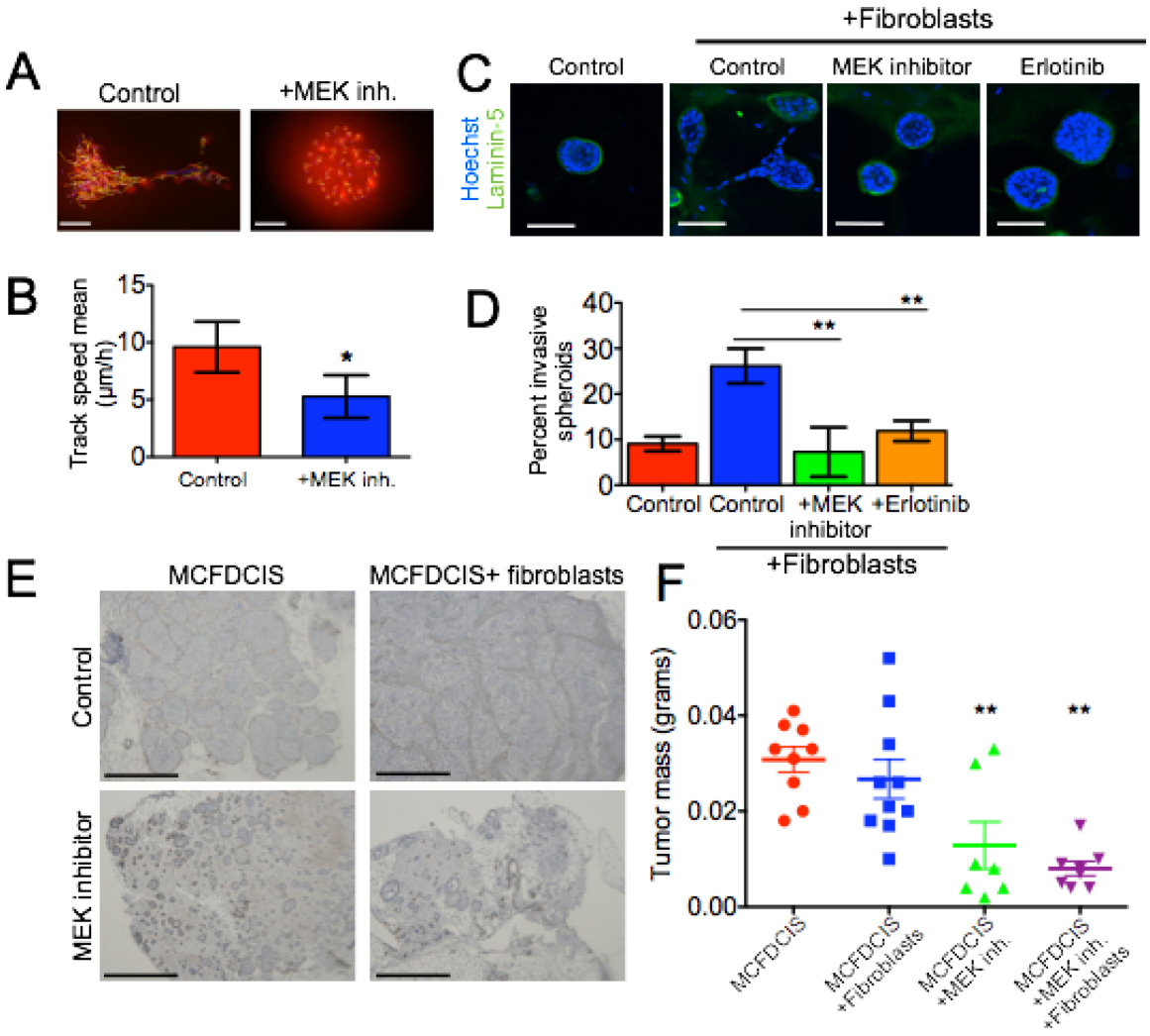

Figure 2-9: ERK1/2 signaling is required for intra-spheroid motility and mammary fibroblast induced invasion. **A**. Real-time imaging tracks of MCFDCIS:H2B-mcherry movement in co-cultures with mammary fibroblasts vehicle or MEK1/2 inhibitor treatment. Scale bars are 40 um. **B.** Tracking quantification of A. **C.** Immunofluorescence of MCFDCIS organotypic cultures treated with vehicle, MEK1/2 inhibitor or Erlotinib, an EGFR inhibitor. Laminin-5 (basement membrane, green) and counterstained with Hoechst (nuclei, blue). Scale bars are 100 um. **D.** Quantification of C. **E.** MCFDCIS xenografts with and without mammary fibroblasts co-injected and treated with vehicle or with MEK1/2 inhibitor. SMA (myoepithelial cells, brown) and counterstained with Hematoxylin (nuclei, blue). Scale bars are 500 um. **F.** Tumor mass quantification of xenografts conditions listed in E. Quantifications were t-tests versus control conditions. *p-value = 0.05, ** p-value = 0.01. Graphs show means with standard deviation bars. Scale bars are 100 um.

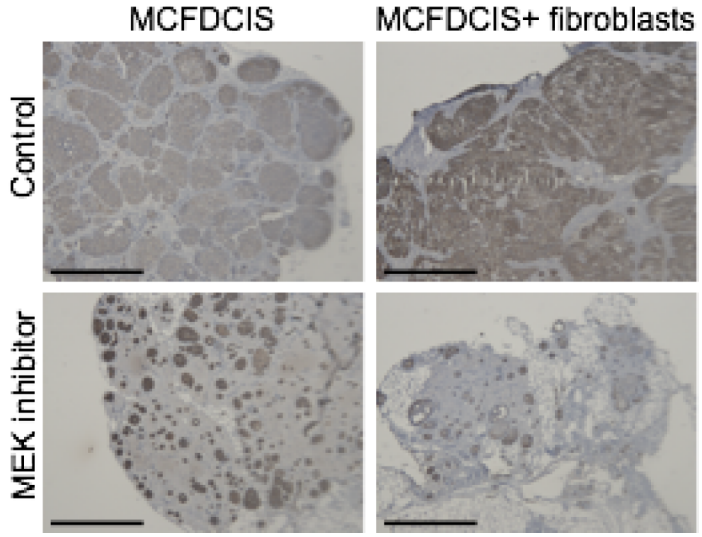

Figure 2-10: Tumors treated with MEK1/2 inhibitor have small DCIS-like lesions. Tumors of MCFDCIS injected alone or with mammary fibroblasts and treated with vehicle or MEK1/2 inhibitor. Pan-cytokeratin (MCFDCIS epithelial cells, brown) and counterstained with Hematoxylin (nuclei, blue). Scale bars are 500 um.

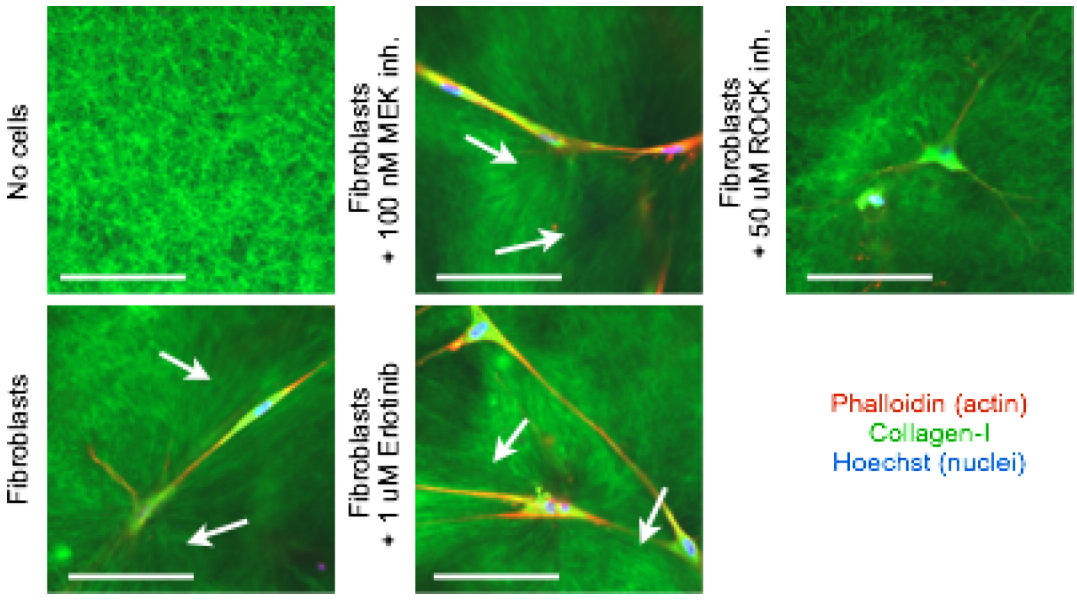

Figure 2-11: Inhibition of ERK1/2 signaling in mammary fibroblasts did not affect the cells ability to reorganize collagen-I. Mammary fibroblasts were embedded in Matrigel:collagen-I for 2 days and then treated with the listed conditions. Arrows point out the linearization of collagen-I from mammary fibroblasts reorganization. Scale bar is 100 um. Collagen-I (ECM, green), Phalloidin (actin, red), and counterstained with Hoechst (nuclei, blue). Scale bars are 100 um.

Discussion

Survival from breast cancer is greatly decreased upon invasion of cancer cells into the surrounding stroma, therefore it is important to understand how breast cancer cells can migrate away from the primary tumor. To study the transition from non-invasive DCIS to invasive breast cancer have been a difficult task due to technical difficulties. In vitro, many breast cancer cells can form DCIS-like lesions or invasive structures, but there have not been a reliable system that can model the transition from DCIS to invasive breast cancer. In vivo, breast cancer models such as PyMT require months for formation of tumors and then for the tumors to progress (62).

In this study, we have shown that the addition of mammary fibroblasts can induce collective cell invasion of breast cancer cells in vitro and in vivo. The co-injection of MCFDCIS with mammary fibroblasts also create an early onset of invasive tumors at week 3 post-injection compared to the spontaneous invasion at week 6 (28, 61). Co-culturing of mammary fibroblasts in organotypic cultures with basal-subtype breast cancer cells can induce E-cadherin positive breast cancer collective migration. Luminal-subtype breast cancer cells were not induced to invade.

To understand how mammary fibroblasts can induce the invasion of one subtype and not the other, we conducted real-time imaging analyses of single and co-cultured organotypic cultures. We found that in single cultures, basal-subtype breast cancer spheroids had motile cells that moved within the structure and did not invade into the ECM; luminal-subtype spheroids did not have motile cells. Upon further investigations, we found that it was the motile cells that can migrate away from the primary mass and into mammary fibroblast-remodeled ECM. This invasion can be stopped by the inhibition of ERK1/2 signaling.

Shown here is the first instance where the intrinsic differences between breast cancer subtypes dictates the responsiveness of mammary fibroblast-induced invasion. Camp et al have shown the co-cultures of fibroblasts with basal- or luminal-subtype breast cancer cells can induce differential gene expression in the breast cancer cells. Luminal-subtype breast cancer cells have an up regulation of pro-growth programs while basal-subtype breast cancer cells have an up regulation in proliferation, migration and EMT factors (63). The change in gene expression by fibroblasts in basal-subtype may contribute to the progression of invasion, but it is the intrinsic motile breast cancer cells that ultimately utilize the collagen-I tracks generated by the mammary fibroblasts to invade away from the primary mass.

The ability of cancer cells to exploit fibroblast-remodeled environment can also be seen in other cancers such as squamous cell carcinoma, SCC (24). SCC cells that are E-cadherin positive are poorly invasive in vitro, however if cultured with fibroblasts they fall in behind the fibroblasts to invade into the modeled stroma. Fibroblast-led invasion of SCC cells can be stopped if the fibroblasts' ability to remodel the microenvironment is inhibited, either through knockdown of Cdc42 expression or inhibition of Rho activity with a ROCK inhibitor (24).

However, if fibroblast induced remodeling have already occurred, targeting the breast cancers' motility program can reduce breast cancer cell invasion. In this study we decreased the intrinsic motility of the breast cancer cells by inhibiting the ERK1/2 signaling pathway. ERK1/2 signaling has been shown to be up regulated in neoplastic breast samples and can induce the motility of mature epithelium (57, 60). Upon treatment with a MEK1/2 inhibitor, we found that the breast cancer cells had reduced motility and more specifically reduced propensity to invade in the presence of mammary fibroblasts. In vivo, the tumors had elevated necrotic tissues, but what tumor lesions did remain were small and DCIS-like.

In summation, the differential response of basal- versus luminal-subtype to mammary fibroblasts may contribute to the poor prognosis of patients who have triple negative compared to ER+/PR+ breast cancer patients. By understanding the functional differences between the two subtypes, we found a targeted method to decrease breast cancer cell invasion.

Chapter Three: Identification of miRNAs that can regulate collective cell migration

Introduction

Overview:

The presence of invasive cells in a breast tumor is highly detrimental to the patient since the risk of metastasis is greater compared to a non-invasive tumor. Understanding how breast cancer cells gain the ability to invade is critical for the treatment of breast cancer. To discover novel mechanisms that control breast cancer cell migration, we conducted a miRNA mimic screen. As readout of cell migration we designed a wounding assay to allow for high throughput screening. The screen identified two novel proteins, RhoT1 and TapT1, for which loss of either protein enhances breast cancer motility.

MiRNAs mechanism of action:

MiRNAs are non-coding RNA sequences that through the actions of Drosha, the RISC complex, and Argonaut reduce gene expression (41). Since the sequence match between the miRNA and its target does not have to be 100% perfect, miRNAs can target multiple genes and therefore multiple signaling pathways (44).

MiRNAs in cancer:

MiRNAs can inhibit or facilitate depending on the target genes that control cancer progression. For example miR21 can drive progression of breast and prostate cancers through the decrease expression of genes associated with tumor inhibition(64, 65). In contrast miR34c increase cell cycle arrest in cancer cells and thus can function as a tumor suppressor (66). Collectively, these few examples strongly suggest that miRNAs have various effects on cancer progression.

RhoT1:

RhoT1 is a mitochondrial GTPase that contain calcium EF-binding domains and consists of 618 amino acids. It is commonly known as Miro-1 and functions in mitochondria morphology and mitochondrial transporting (67-69). RhoT1 is located in the mitochondrial outer membrane on the cytoplasmic side. This protein is involved in the transporting of mitochondria along microtubules. The loss of RhoT1 in lymphocytes inhibits cell migration and polarity (69). However, the contribution of RhoT1 in cancer progression has not been fully vetted.

TapT1:

Little is known about Transmembrane Anterior Posterior Transformation 1, TapT1. TapT1 is expressed ubiquitously in mouse embryos. The loss of TapT1 resulted in malformed vertebrae, ribs and embryonic lethality. TapT1 encodes a protein that contains ~6 transmembrane domains suggesting it may be a receptor. If TapT1 is a receptor, its ligand is yet to be discovered. TapT1 seems to be involved in developmental patterning, though its specific function and its involvement in any signaling pathway is unknown (70).

Methods and Materials

Cell culture and reagents:

See Chapter 2 "Cell culture and reagents" section for the culturing of MCFDCIS and MDA-MB-231.

Transfection:

Cells were reverse transfected with OptiMEM (Life Technologies), Lipofectamine, and RNAiMax at a final concentration of 0.2 ul/200 ul of total volume (Life Technologies) and with siRNAs or miRNAs . See Appendix H for a list of siRNAs and miRNAs and their final concentration used in the project. Transfections were allowed to go for 24 hours for transwell

assays or 72 hours for wounding assays unless noted otherwise. Transfections were done in 96-well plates for transwell and wounding assays.

Wounding Assay and Spontaneous motility:

Cells were reverse transfected and plated for either 24 or 72 hours at a density that generated 100% confluent wells before wounding in a 96-well plate. Wounds were generated with V&P AFIX96FP6 pin tool fixture, FP6-WP pins, and VP 381NW 4.5 library copier (V&P Scientific, see Appendix B for picture of tool). Wells were washed twice with growth media and wounds were allowed to close for 24 hours in growth media before fixation for immunofluorescence. For spontaneous motility, cells were reverse transfected and plated at a density for ~70% confluence at 72 hours post-transfection.

Immunofluorescence:

Media was removed from the 96-well plates and rinsed with 1X PBS. Cells were fixed with 0.2% formaldehyde for 20 minutes and permeablized with 0.05% Triton X-100 for 10 minutes; both solutions were diluted in 1X PBS. Plates were blocked with 10% goat serum diluted in immunofluorescence buffer (0.1% BSA, 0.2% TritionX-100, 0.05% Tween-20 in PBS) for 1 hour and then stained with 1:250 Phalloidin-546 (Life Technologies, cat. no. A22283) and 1:2000 Hoechst (Life Technologies, cat. no. H1399) for 1 hour. Plates were washed 3 times with immunofluorescence buffer at 10 minutes each, then rinsed with 1X PBS and stored in 1X PBS at 4 degrees Celsius until imaged.

Real-time cell imaging:

Cells were imaged on a PerkinElmer microscope using a 10x objective. Z-stacks were either 5-3 slices over a 25 micron span. Imaging conditions were humidified 5% CO2 at 37 degrees Celsius for ~35 time points, each time point was 30 minutes. Wounding assays and

spontaneous motility cultures were imaged within a few hours of wounding or fresh media change.

MiRNA screening:

Dharmacon miRNA mimic master plates were diluted with Dharmacon 1X siRNA buffer to a concentration of 5 uM. Master plates were aliquoted into three replicate plates for a final concentration of 50 nM. 10,000 MCFDCIS cells per well were plated into the replicate plates with 0.2 ul of Lipofectamine RNAiMax per 200 ul total volume. The transfection was allowed to go for 72 hours before wounding. Wounds were made with V&P AFIX96FP6 pin tool fixture, FP6-WP pins, and VP 381NW 4.5 library copier and were allowed to close for 24 hours. Plates were then fixed for imaging on the BD Pathway microscope and PheraStar plate reader. See Appendix A for list of miRNAs screened.

Imaging on high through-put BD Pathway microscope:

Wounded plates were imaged on a BD Pathway 855 microscope with a 10x objective (Olympus, UPlanSApo 10x/0.40, ∞/0.17/FN26.5). Images were either taken as a 4x5 montage (screening condition) or as a 6x4 montage (follow-up conditions) using Phallodin-546 signal. Images were then analyzed with the Pipeline Pilot program for quantification of wound closure.

Imaging on PheraStar plate reader for relative cell number calculation:

Relative Hoechst signal was used to determine relative cell number per well. Wells were imaged in a 6x6 matrix with three flashes per point for Hoechst signal.

MDA-MB-231 Transwell migration:

MDA-MB-231 H2B-GFP cells were reverse transfected with siRNAs or miRNAs in the same matter as previously stated. Cells were harvested and counted to plate 20,000 cells per transwell filter (BD Falcon Cell Culture Inserts, ref. no. 353097) in serum-free RPMI. The

bottom chamber had 10% FBS in RPMI as the chemoattractant. Cells were allowed to migrate for 6 hours. The upper chamber was wiped clean, and cells were counted by hand using an inverted fluorescence microscope. The bottom of the filter was wiped clean and re-counted. The difference between the first count and the second count was the number of cells that had transverse the filter.

Gene expression microarray:

Cells were transfected as described for 72 hours and scaled up to 35 mm dishes. Samples' total RNAs were extracted following manufacturer's protocol for "Qiagen Rneasy Plus, Cat. No. 74134, Appendix D: Purification of Total RNA containing small RNAs". Gene expression microarray was run on an Illumina HT12v4 chip.

Results

Motile cells close the wound:

To discover novel motility pathways that regulate breast cancer cell invasion, we conducted a miRNA mimic screen using a wounding assay as a read out for cell motility. To screen for miRNAs that regulate cell motility, we chose the MCFDCIS cell line. This model was chosen because the cells can collectively invade in organotypic cultures and the cells still maintain epithelial characteristics (Chapter 2 and Fig 3-2). A wounding assay was used to monitor cell migration for transfection and high throughput ease. Cells were plated to 100% confluency in a 96-well plate and wounds were generated using a 96-well pin-wounding tool with a wounding template. To verify that wound closure was driven by cell migration, we conducted real-time imaging of wounds treated with mock or 2 uM Cytochalasin D. Cytochlasin D is an inhibitor of motility, which functions by inhibiting actin polymerization (71) . At 2 uM of Cytochlasin D, cells are non-motile but maintain cell proliferation (data not shown). Time

lapse images of mock treated MCFDCIS:H2B-GFP cells show that motile cells transverse the cleared space as shown through the tracking of the wounded front (arrows) and track lengths on wounds monitored for 19 hours compared to the Cytochlasin D treated condition (Fig 3-1 A and B). The motility of the closing cells can also be seen in a shorter time period of 5 hours (Fig 3-1 C).

However, with the current resources and technology, using real-time imaging to screen hundreds of miRNAs is time consuming and expensive. Therefore, with the help of the High Throughput Screening Core at UT Southwestern Medical Center, we designed a system that can efficiently measure relative migration in a 96-well plate format. With our wounding tool, we can wound 96-well plates, allow the wounds to close for 24 hours, and then fix and stain the plasma membrane of the cells with Phalloidin to determine the spread of cells in the wells. Using the high-content BD Pathway microscope, we automated imaging of each well in a 4 by 5 (for screening conditions) or 6 by 4 (for follow-up studies) montage to capture the extent of migrating cells. The Pipeline Pilot program was used to measure the amount of black pixels or remaining cleared wounding area as a measurement of migration (Fig 3-1 D).

As previously reported in Gilles et al and Aomatsu et al, MCFDCIS cells at the wounding edge do have some mesenchymal characteristics as seen through the increased vimentin and slug expression when compared to non-motile and non-wounded conditions (72, 73). However, these cells have not undergone EMT since they still express epithelial markers such as E-cadherin and EpCAM at similar levels as MCF10A cells (Fig 3-2 A and B). These data suggest that migrating cells do not need to undergo EMT to be motile.

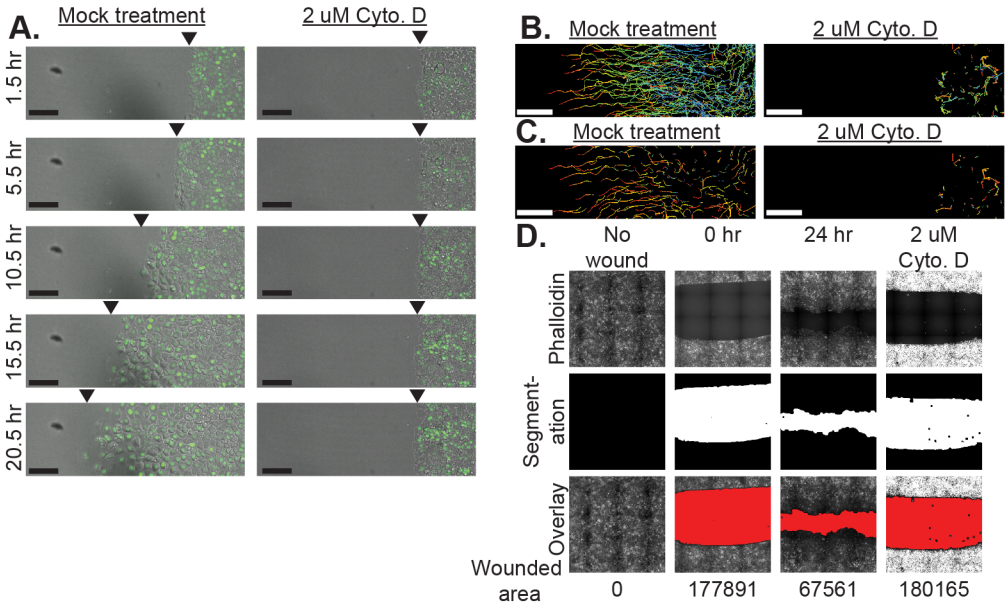

Figure 3-1: Motile cells close the wound. **A.** Time lapse images of MCFDCIS:H2B-GFP mock or Cytochlasin D treatment. Time listed is time after wounding. Arrows mark the wounding front. Phase (gray), MCFDCIS:H2B-GFP (nuclei, green). **B.** Tracks of MCFDCIS wounding cultures over 17 hours of imaging. **C.** Tracks of wounding cultures in B but tracking the last 5 hours of the real-time imaging. **D.** Immunofluorescence, Pipeline Pilot segmentation and overlay of listed conditions. Numbers represent the Pipeline Pilot values of the wounds. Scale bar is 100 um.

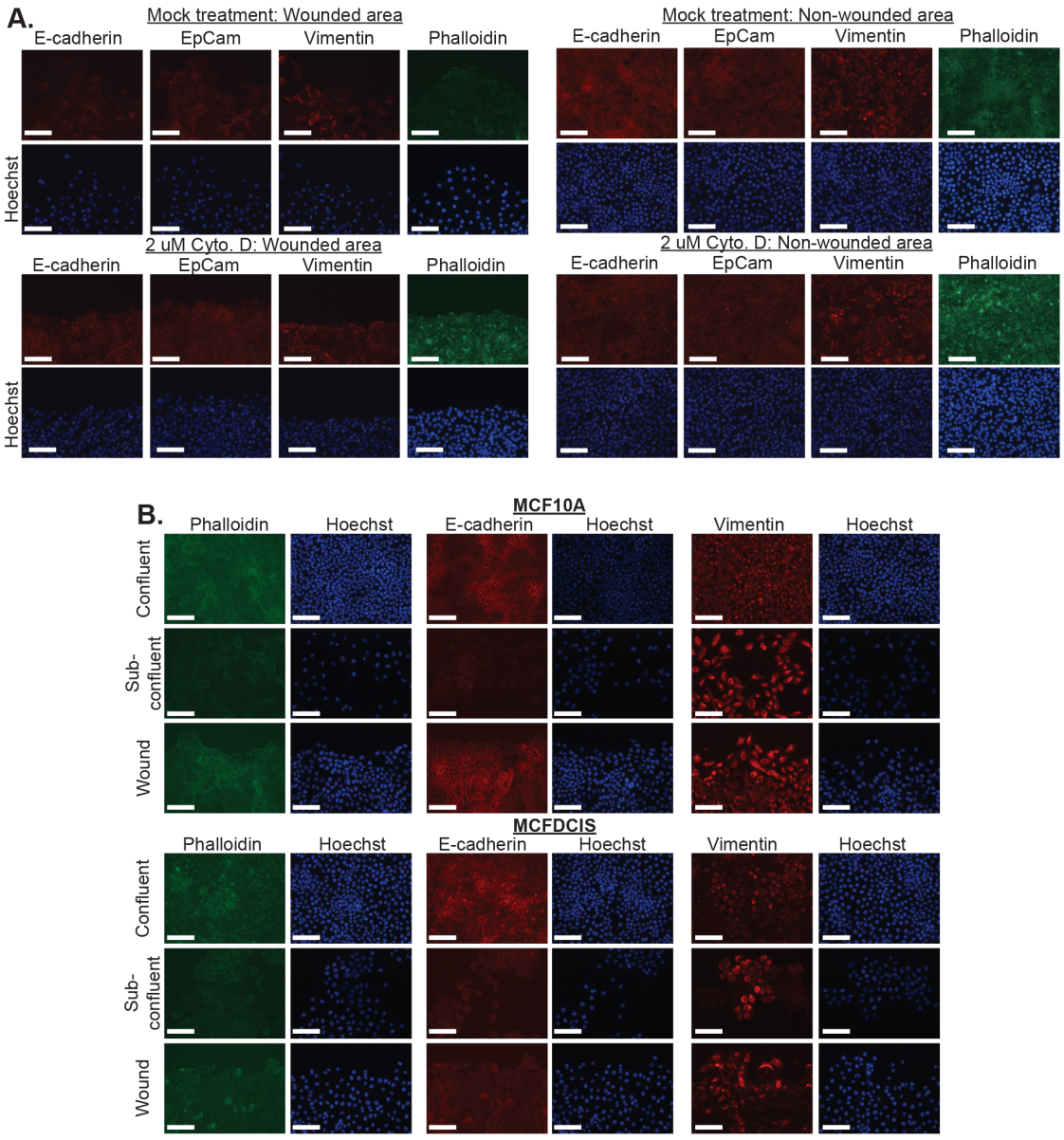

Figure 3-2: Migrating cells express both mesenchymal and epithelial markers. A. Immunofluorescence of MCFDCIS cells mock or Cytochlasin treated. Images are at the wounded or non-wounded area. E-cadherin (epithelial marker, red), EpCAM (epithelial marker, red), Vimentin (mesenchymal marker, red), Phalloidin (actin, green), and counterstained Hoechst (nuclei, blue). B. Immunofluorescence of MCF10A or MCFDCIS at confluent, subconfluent or wounding edge. E-cadherin (epithelial marker, red), Vimentin (mesenchymal marker, red), Phalloidin (actin, green), and counter-stain Hoechst (nuclei, blue). Scale bars are 100 um.

Identification of miRNAs that regulate motility:

We conducted a miRNA mimic screen to identify novel regulators of motility. Using a one-condition per well format, with 3 replicates per condition, we screened 879 Dharmacon miRIDIAN miRNA mimics in a wounding assay (Fig 3-3A). To normalize the wounding activities, we used the following formula:

((Raw value – median value)/ (median value)) *100

The median value of mock treatment conditions was used to normalize the data because the median value of the test conditions was skewed. The median value of the test conditions was skewed because a large number of miRNAs actually reduced cell number in our screen. The normalized value was then corrected for plate-to-plate and well-to-well variation with GeneData's correction factor, a proprietary pattern detection calculation. The miRNA mimics were normalized to their corresponding mock treatment run day. The final value generated after the normalization and correction is now referred as wounding activity.

To focus on miRNAs with a high reproducibility, we looked at miRNA mimics that had a standard deviation of 80 or less between the three replicate wounding activities. A standard deviation of 80 was chosen because the standard deviation of our mock treatment controls in the screen was 80. With the reproducibility filter, there were 750 potential miRNA mimics that may regulate cell motility (Fig 3-3 B). Upon further analysis, of the 750 miRNA mimics there were miRNAs that affected cell number by either inhibiting cell proliferation or were lethal. Since we are only interested in miRNAs that affected cell motility and not cell number, we screened our plates on a PheraStar plate reader and measured the relative Hoechst signal of each well and removed miRNAs that had a greater than -50 relative fluorescence when normalized to the median of the mock treated conditions (Fig 3-3 C). A value of -50 translates to a 50% lower

relative fluorescence to the mock treatment control and thus a possibility of a 50% cell number reduction. After all the calculations, 574 miRNA mimics had high reproducibility and did not lower the relative cell number by greater than 50%.

Of the filtered 574 miRNA mimics, there were some miRNAs that enhanced, inhibited or were innocuous for wound closure. To determine the cutoff for each category, the wounding activity of each miRNA was converted to a z-score using the mean wounding activity of mock treatment conditions and given a cumulative probability (Fig 3-3 A-D). The cumulative probability calculates the chance that a miRNA's wounding activity would be equal to or greater than the mock treatment conditions. The cutoff for a miRNA that enhanced wound closure is a z-score of less than or equal to -2 and for a miRNA that inhibits wound closure the z-score was to be greater than or equal to 8, which produced 53 enhancers and 106 inhibitors (Appendices E and F). Figures 3-4 and 3-5 show the wounding segmentation of some of the enhancers and inhibitors of wound closure. We also chose 160 miRNA mimics from the primary screen to re-screen at 10 nM to determine the reproducibility of the screen. A Pearson correlation of the primary and secondary screen showed a correlation of 0.7918. A Pearson correlation of 1 is a perfect correlation, 0 is no correlation and -1 is a perfect negative correlation (Fig 3-3 E).

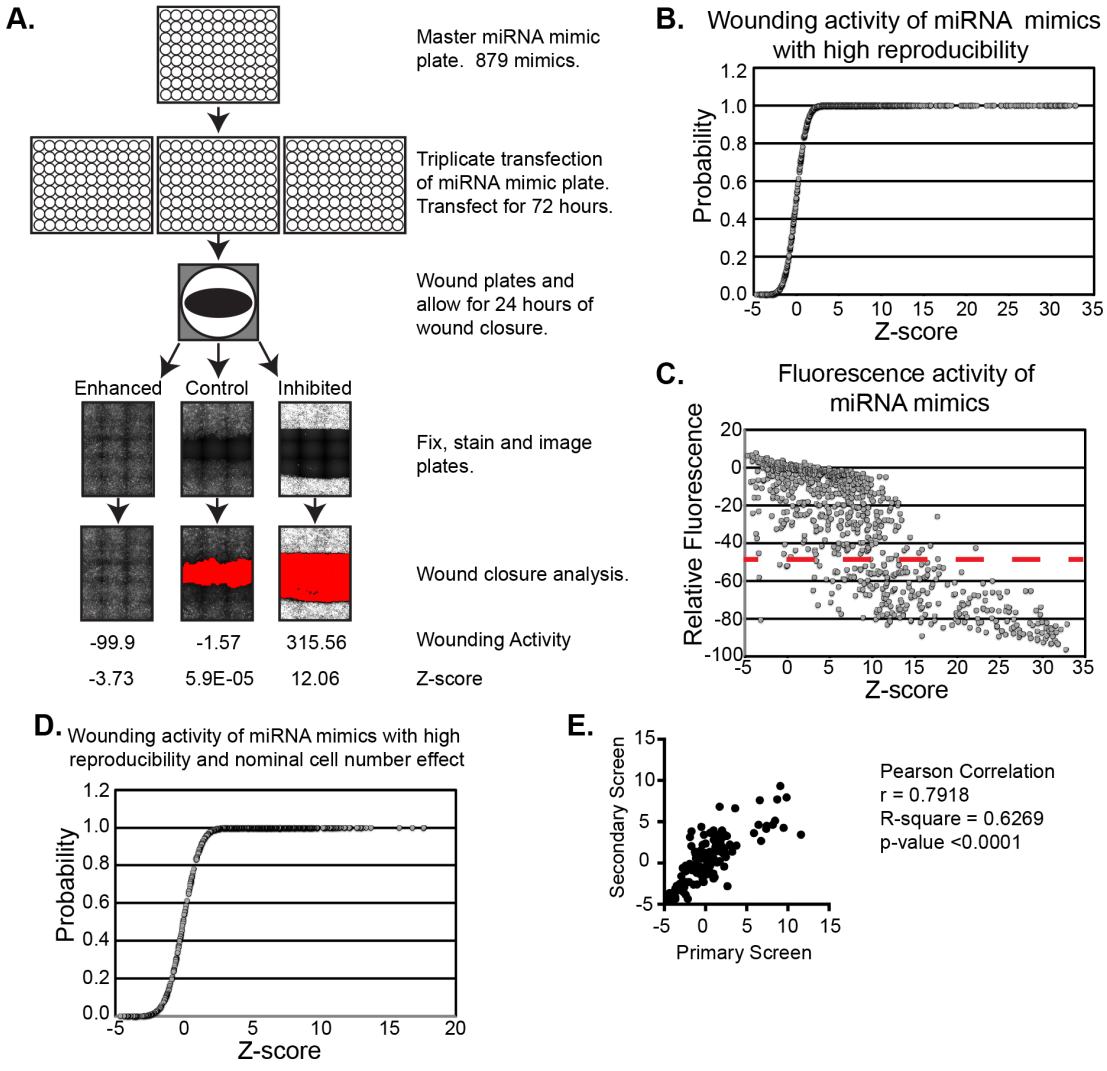

Figure 3-3: Identification of miRNAs that regulate collective cell migration. A. Diagram of miRNA screen. **B.** Graph of miRNAs' z-scores for wounding activity and cumulative probability. These miRNAs have a high reproducibility of a standard deviation less than 80. **C.** Relative fluorescence activity and z-score wounding activity of miRNAs in the screen. The red dotted line signifies the -50 relative fluorescence cutoff. **D.** Graph of miRNAs' z-scores for wounding activity and cumulative probability. These miRNAs have a high reproducibility of a standard deviation less than 80 and a relative fluorescence value of above -50. **E.** Pearson correlation of miRNAs screen in the primary and secondary screens. Raw data from the Primary Screen are in Appendices C and D. Raw data from the Secondary Screen are in Appendices G and H.

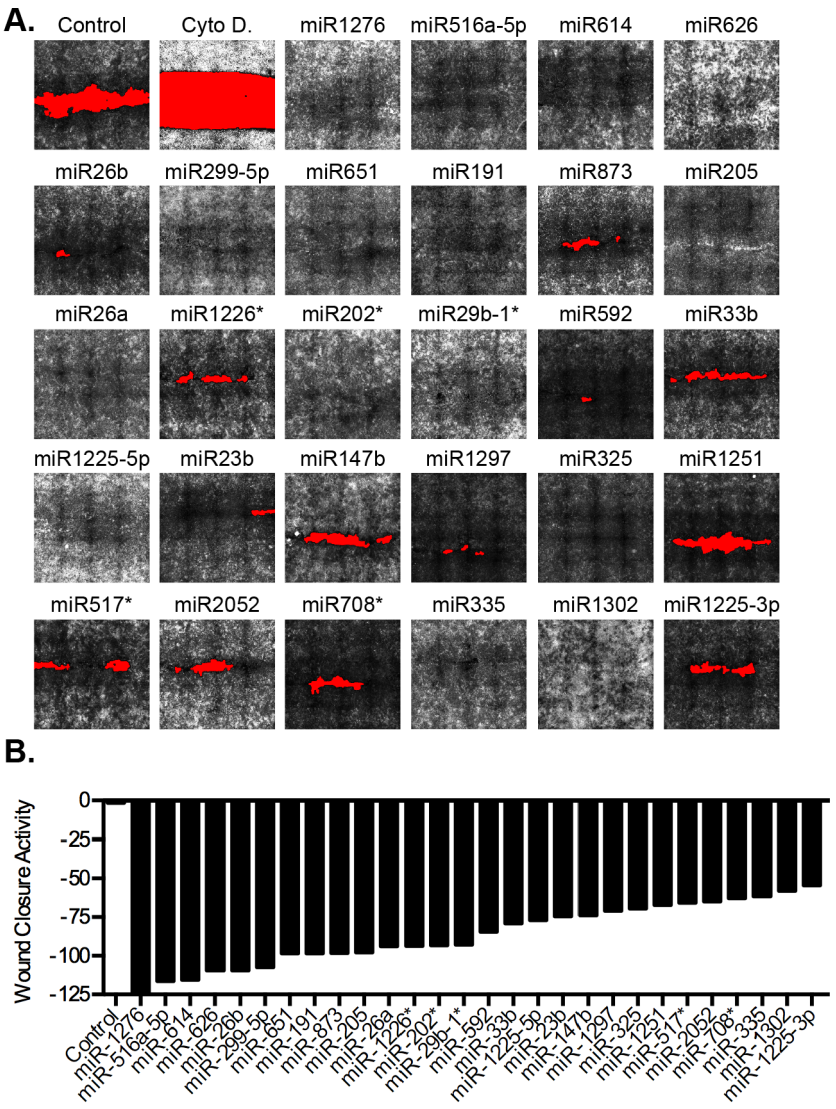

Figure 3-4: Examples of miRNA mimics that enhance wound closure. A. Pipeline Pilot segmentation of miRNA mimics that enhance wound closure. **B.** Wound closure activity of example miRNA mimics that enhance wound closure in A. Values from Primary screen. Full list of enhancer miRNAs are in Appendix C.

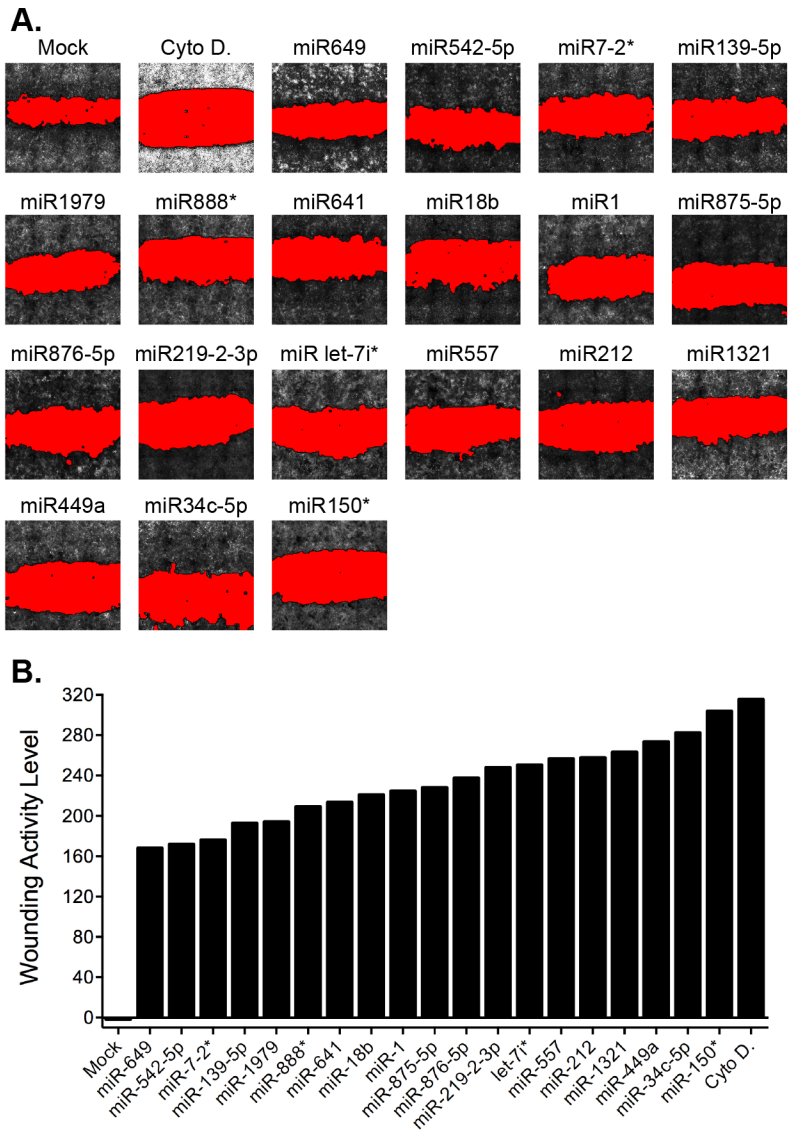

Figure 3-5: Examples of miRNA mimics that inhibited wound closure. A. Pipeline Pilot segmentation of miRNA mimics that inhibited wound closure. **B.** Wound closure activity of example miRNA mimics that inhibit wound closure in A. These values are from the Primary Screen. Full list of inhibitor miRNAs is in Appendix D.

miR614 enhances wound closure and spontaneous cell migration:

To prioritize which enhancer of migration are relevant for further studies, matched normal and breast cancer miRNA expression was investigated. With the help of former student Robert Borkowski in the White lab, the expression of 11 enhancer miRNAs were analyzed from The Cancer Genome Atlas, TCGA database (Fig 3-6). Of these miRNAs, we identified miR614 and miR1276 for further study since they were highly expressed in tumor compared to normal samples (Fig 3-7 A). For both miRNAs, there is little known about their functions in cell migration and cancer progression.

To verify that miR614 and miR1276 enhance wound closure through migration, we perform real-time imaging of the wounding edge in MCFDCIS:H2B-GFP cells transfected with either miR614, miR1276, or control. Both enhancer miRNAs increased the wound closure through motile cells based on the track lengths and speed of the cells (Fig 3-7 B). However, since the act of wounding a confluent culture induces a wounding response, we wanted to determine if the enhancement of migration by miR614 and miR1276 is in response to a wounding stimulus. Therefore, we tracked spontaneous movement of MCFDCIS:H2B-GFP cells transfected with miR614, miR1276 and control (Fig 3-7 B). Surprisingly, we found that miR614 could increase the motility and displacement of spontaneous movement, while miR1276 could not. This differential enhancement of spontaneous movement suggest that miR614 and miR1276 elicit two different motility signaling programs, one that is independent of a wounding response and one that is dependent on a wounding response. For future studies, we focused on miR614.

In summation, our miRNA screen has discovered endogenous miRNAs that have an increased expression upon tumorigenesis and can enhance collective cell migration. These enhancer miRNAs can increase collective cell motility utilizing different signaling pathways.

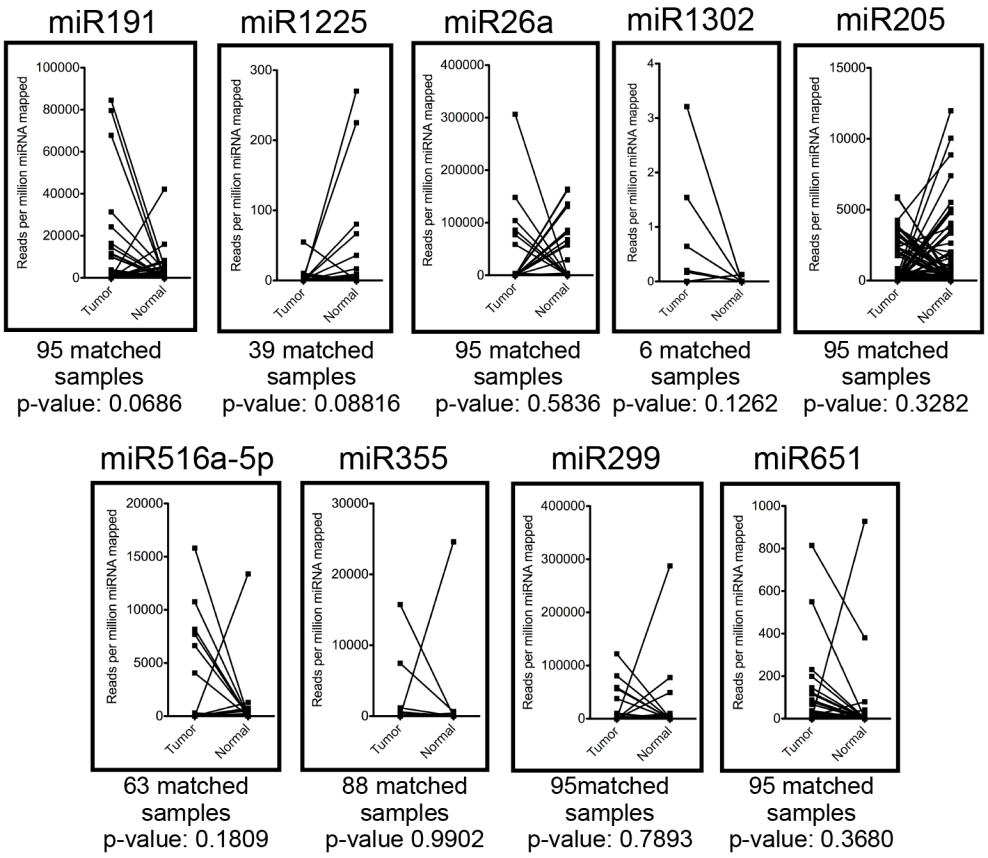

Figure 3-6: TCGA Patient miRNA expression of matched tumor and normal samples. TCGA data mined with the help of Robert Borkowski from the White lab. P-values are t-test comparisons between tumor and normal samples.

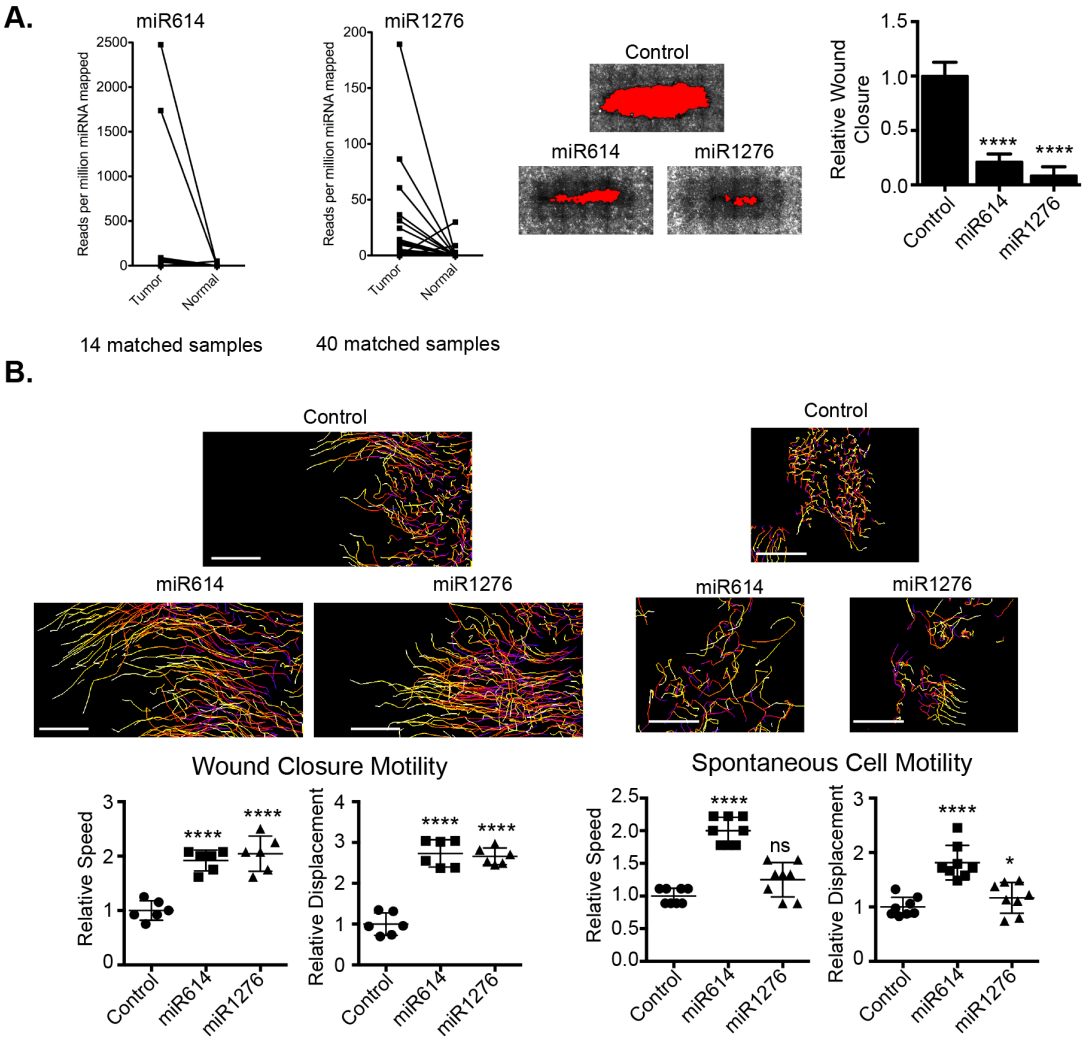

Figure 3-7: miR614 enhances wounding and spontaneous cell motility. A. Matched tumor and normal breast cancer patient sample expression of miR614 and miR1276. Values were from TCGA and were mined with the help of Robert Borkowski, from the White lab. Follow-up wounding images and relative wound closure of MCFDCIS transfected with miR614, miR1276 or Control. **B.** Wounding and spontaneous movement tracks and track quantification of MCFDCIS transfected with miR614, miR1276 or Control. Scale bars are 100 um. Graphs show mean, standard deviation bars and individual data points across two experiments with three replicates. Quantifications were t-test of sample versus control. Ns = not significant, *p-value <= 0.05, **** p-value <=0.0001.

Decreased expression of RhoT1 or TapT1 can enhance cell migration:

Since miR614 can enhance wounding and spontaneous collective cell migration, we wanted to determine if it could also enhance single cell migration. If miR614 can enhance collective and single cell motility, this suggests that miR614 regulates a signaling program that is utilized by both types of migration. MDA-MB-231 cells were transfected with control, miR614 and miR1276 for a transwell assay (Fig 3-8 A). A transwell assay is a single cell migration assay, where single cells are plated in the upper chamber while a chemoattractant is plated in a bottom chamber. A porous membrane separates the two chambers to allow a gradient to form and have pores small enough for single cells to pass through. MDA-MB-231 cells were chosen because the cells can migrate in a transwell in 6 hours, which allows for quick analyses. As expected miR1276 did not enhance single cell migration as compared to control. MiR614 enhanced single cell migration by approximately 2-fold compared to control (Fig 3-8 A). Therefore, miR614 can enhance collective and single cell migration in at least two breast cancer subtypes, basal- (MCFDCIS) and claudin-low (MDA-MB-231).

MiR614 can enhance the collective and single cell motility of breast cancer cells independent of subtype. To identify other players in this unique cell motility program, we conducted a gene expression microarray of MCFDCIS and MDA-MB-231 transfected with control or miR614 mimic. There were 1517 differential probe expression in the MDA-MB-231 and 3261 probes for MCFDCIS when we looked at probes that had a p-value of 0.05 and a 1.5 fold difference between control and miR614 transfected conditions. Since we are interested in direct targets of miR614, we looked at probes that had a down regulation upon miR614 transfection, which gave us 795 probes for MDA-MB-231 cells and 1587 probes for MCFDCIS. There were 120 genes (131 probes) that were common between the two cell lines and of those

120 genes, 83 genes had at least 50 or more expression read values (Appendix E, Fig 3-8 C). We tested 28 genes by transfecting their siRNAs into MCFDCIS cells and conducted a wounding assay (Fig 3-8 D). RhoT1 and TapT1 were our best candidates that enhanced wound closure and upon follow-up wounding assays, were the most reliable targets of miR614 (Fig 3-8 E).

RhoT1 also known as Miro-1 is a mitochondrial Rho GTPase that regulates mitochondria morphology and transportation within the cell. Disruption of RhoT1 function either through constitutively activating or inhibiting activation resulted in mitochondrial aggregation and/or formation of thread-like structures (67). Loss of RhoT1 in lymphocytes results in decreased migration, polarization, and detection of chemotaxis. In neurons, RhoT1 defects leads to improper neuron development, which can result in neurological disease (74). However, RhoT1's role in breast cancer progression is still unknown.

TapT1 is a 567 amino acid transmembrane protein. Ligands for this protein are unknown and the signaling pathway it is involved is also unknown. It has been shown that loss of TapT1 resulted in improper formation of the axial skeleton and embryonic lethality in mice (70). How TapT1 functions in development, cell migration, and cancer is unknown and should be investigated.

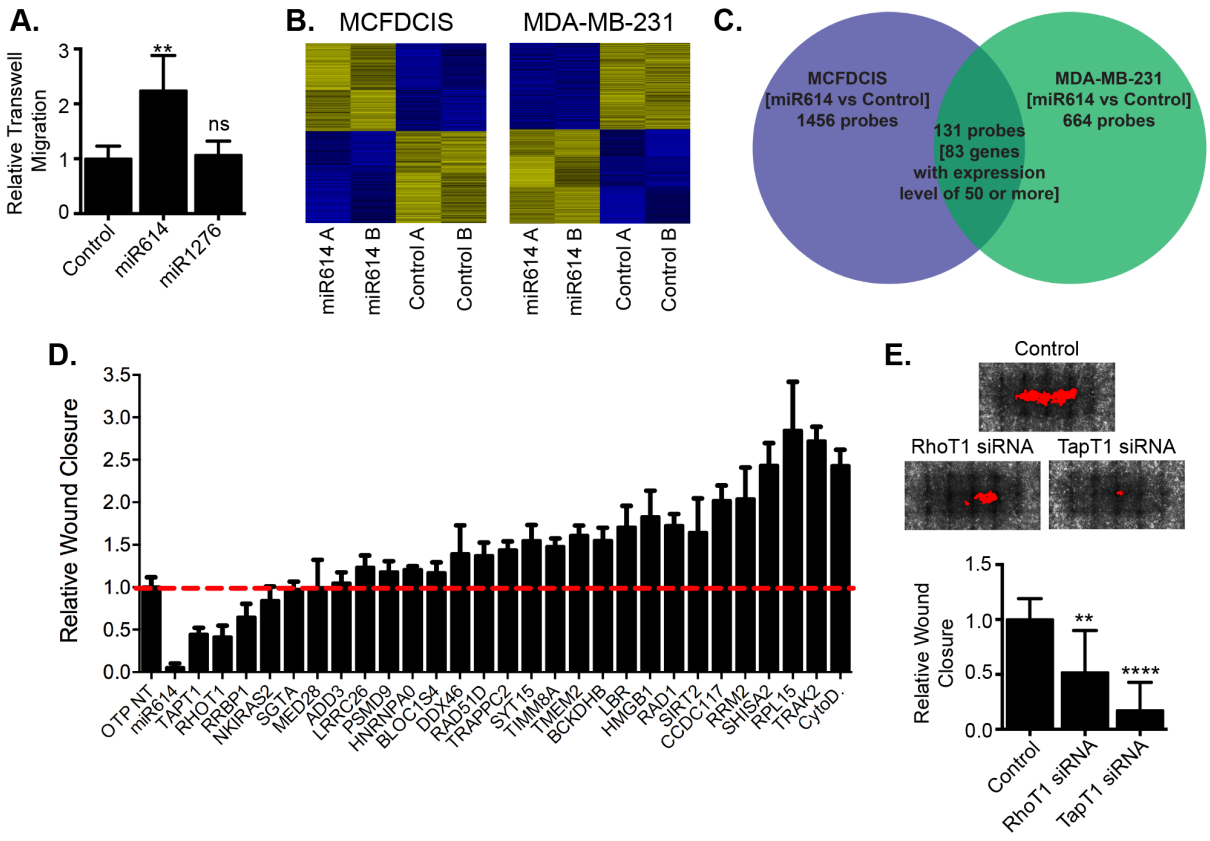

Figure 3-8: miR614 targets, RhoT1 and TapT1 can enhance collective cell migration. A. Relative transwell migration of MDA-MB-231 transfected with miR614, miR1276, and control. **B.** Gene expression microarray heatmaps of MCFDCIS or MDA-MB-231 transfected with miR614 or control. Genes have 1.5-fold or greater difference from control condition and have a p-value of 0.05. Yellow = down regulated, blue = up regulated. **C.** Venn diagram of overlapping probes/genes from B. **D.** Relative wound closure of 28 possible miR614 targets from C. **E.** Relative wound closure of MCFDCIS transfected with RhoT1 siRNA, TapT1 siRNA, or control. All graph quantification are t-tests of sample versus control condition, shown are means with standard deviation bars. Ns = not significant, ** p-value <=0.01, **** p-value <= 0.0001.

Discussion

To discover novel regulators of breast cancer cell motility, we conducted a miRNA screen using a wounding assay as a measurement of cell migration. From the screen, we found 53 miRNAs that enhanced and 106 miRNAs that inhibited cell migration. For subsequent studies, we investigated at miR614 and miR1276. Both miR614 and miR1276 have not been associated with breast cancer progression. In our studies, we found that while both can enhance collective cell migration, only miR614 was able to enhance single-cell motility in MDA-MB-231 cells. Therefore, our miRNA screen was able to detect at least two different signaling pathways that can regulate cell migration.

To uncouple miR614 mechanism of action, we conducted a gene expression comparison of miR614 transfected MCFDCIS and MDA-MB-231 cells. We found two novel miR614 targets, RhoT1 and TapT1. Determination of how miR614 regulates RhoT1 and TapT1 is still in need since according to TargetScan miR614 is predicted to target only 6 genes and none of them are RhoT1 or TapT1. Therefore, it is uncertain if miR614 directly targets RhoT1 and TapT1 through a non-classical 3'UTR or if miR614 regulate an upstream regulator of these genes. Loss of either RhoT1 or TapT1 resulted in an enhancement of cell migration. This connection between miR614 with RhoT1 and TapT1 is the first to be observed. However, exactly how the loss of RhoT1 or TapT1 enhances cell migration is still unknown and needs further investigation.

Chapter Four: p63 regulated cell motility

Introduction

Overview:

Exploiting a miRNA mimic motility screen and the endogenous miRNA expression profile of motile and non-motile cells, we found a novel motility program regulated by p63. P63 was found to be the hub of miR203a and miR205 regulated cell motility, where p63 is required for cell motility and miR205 enhances cell migration. Upon further investigation, we found that Axl and Slug are novel p63 targets.

Background information on p63:

P63, a transcription factor in the p53 family, has 2 transcriptional start sites producing 2 major isoforms TA and deltaN. There are also 3 different C-terminus splice sites, alpha, beta, and gamma, resulting in 6 different p63 isoforms. P63 is a homolog of p53 that can bind to p53 response-elements and can also bind the following sequence:

5'-RRRC(A/G)(A/T)GYYYRRRC(A/T)(C/T)GYYY-3' (75)

R = A/G nucleotide and Y = T/C nucleotide

P63 is involved in development specifically in tissues consisting of epithelial cells. Mice deficient in p63 have severe developmental malformations of limbs and epithelial tissues such as the skin and mammary glands to the point that they do not survive after birth (76). P63 has been found in the myoepithelial layer of breast mammary gland, a cell source of breast progenitor cells (77, 78). Thus, improper functioning of p63 can result in systematic failure in differentiation.

P63 in cancer:

P63 expression is overexpressed in squamous cell carcinoma and was found to be required for cell invasion and migration (79). Patients with head and neck squamous cell carcinoma who have elevated p63 expression have a poor prognosis. Tumors with high p63 expression are poorly differentiated (80).

Axl and cancer:

Axl is part of the TAM receptor tyrosine kinase family, which consists of Tyro3 and Mer. The two ligands of the TAM receptor tyrosine kinase family are Protein S and Gas6. However, the preferred ligand for Axl is Gas6 and upon activation Axl dimerizes and autophosphorylate its kinase domain. Once activated, Axl can stimulate PI3K, ERK1/2, and other signaling pathway (81, 82). Upon Axl phosphorylation, it can associate with Grb2 to stimulate the ERK1/2 signaling pathway (83).

TAM receptors are not necessary for development and mice with triple receptor knockout have been generated (84). Though viable, mice that lack TAM receptors are infertile. The infertility is due to the failure of clearance of apoptotic cells in the seminiferous tubules. These apoptotic cells were generated under normal meiosis and must be removed by phagocytosis for proper spermatogenesis. Proper TAM receptor function is necessary for the signaling of phagocytosis in spermatogenesis (84).

Axl was first discovered in chronic myeloid leukemia (CML) patients and have since to be found elevated in other cancers such as colon, lung, and breast (82). In breast cancer, Axl expression was elevated in basal-subtype compared to luminal subtype breast cancer cell lines (85). Decreased expression of Axl or inhibition of Axl activity has been shown to decrease tumor size in breast cancer models. The reduction in tumor growth may be due to endothelial cells not forming tumor-associated vasculature since these cells are unable to migrate and form

new blood vessels to tumors upon Axl dysfunction (86, 87). R428 is a small molecule inhibitor that can inhibit Axl function by inhibiting Axl phosphorylation (88).

Slug and cancer:

Slug is a transcription factor that can repress E-cadherin expression and induce EMT (89). It is important during development and stem cell maintenance. Slug-deficient mice are viable, though the stem cell compartments of certain cell types such as the hematopoietic cells are aberrant (90). Transgenic overexpression of Slug in mice results in increase incidence of mesenchymal tumors such as sarcomas (91).

In breast cancer, Slug can enhance breast cancer cell migration. FOXM1 can promote single cell breast cancer cell migration through the up regulation of Slug expression (92). Slug can induce migration through the repression of E-cadherin (92, 93). During pregnancy, the mammary gland undergoes an expansion. For expansion to occur there is an increase in mammary stem cells. The expression of Slug seems to be necessary for the maintenance and increase in number of mammary stem cells (94). In this particular situation, Slug expression was dependent on functional alpha5beta3 integrin (94). So, far it is unclear how Slug is regulated and contributes to collective cell migration. It is also uncertain if migrating cells utilizes early developmental or stem cell program(s) as a means for migration.

Methods and Materials

Cell culture and Reagents:

Cell culture of MCFDCIS, HCC1806, HCC1954, and HCC1428 were performed as described in Chapter 2: Methods/Materials.

Western blot, xenografts, transfection, wounding assay, and immunofluorescence:

Western blot, xenografts were performed as described in Chapter 2: Methods and Materials, transfection, wounding assay and immunofluorescence were performed as described in Chapter 3: Methods and Materials. SiRNA and miRNA sequences used are listed in Appendix H.

Gene expression and miRNA expression microarray:

Gene expression microarrays were conducted as described in Chapter 3: Methods/Materials. MiRNA expression microarrays were performed as described in Chapter 3: Methods/Materials, except Exiqon miRNA 7th Generation chip was used instead of a gene expression chip.

Real-time PCR:

For all RT-PCR used to quantify expression level of genes or miRNAs, total RNA was extracted from cells following "Qiagen Rneasy Plus, Cat. No. 74134, Appendix D: Purification of Total RNA containing small RNAs protocol" and each cDNA reaction had 300 ng of total RNA. BioRad iScript cDNA Synthesis kit was used to generate cDNA from mRNA and Life Technologies's TaqMan microRNA Reverse Transcriptase kit was used to generate cDNA for miRNAs.

RT-PCR was conducted following TaqMan Universal PCR Master Mix's protocol for ABI 7500 RT-PCR machine. Appendix I list all TaqMan primers used.

Immunofluorescence on paraffin-embedded tissue:

Paraffin sections were incubated in xylene for 10 minutes 3 times, 100% ethanol for 3 minutes twice, 95% ethanol for 3 minutes, twice, and 1X PBS for 3 minutes. A boiling sodium citrate bath for 20 minutes was used as an antigen retrieval method. Slides were allowed to cool in the sodium citrate solution for 20 minutes, incubated in 1X PBS for 3 minutes and then blocked in 20% AquaBlock in 1X TBS for 30 minutes. Primary antibodies were diluted in 5%

BSA in 1X TBS and incubated on the sections overnight at 4 degrees Celsius in a humidified chamber. Sections were washed 3 times at 5 minutes each with 0.05% Tween-20 in 1X PBS, incubated for 1 hour at room temperature with secondary antibodies that were diluted in 5% BSA in 1X TBS, washed 3 times at 5 minutes each of 0.05% Tween-20 in 1X PBS and rinsed in 1X PBS. Slides were mounted with Prolong Gold (Life Technologies).

Chromatin immunoprecipitation, ChIP:

ChIP protocol was modified from Ramsey et al (95). Cells were grown in 10 dishes of 15 cm diameter under normal cell culturing methods. Cells were cross-linked with a final concentration of 1% (v/v) formaldehyde in the existing cell culture media at room temperature for 15 minutes with gentle shaking. Cross-linking was stopped with an addition of glycine at a final concentration of 0.125M. Adherent cells were scraped from the dishes and spun down for 5 minutes at 4 degrees Celsius at 3,000 rpm. Pellet was resuspended in cold PIPES hypotonic buffer (5 mM PIPES pH8.0, 85 mM KCl, 0.5% NP-40, in sterile water), incubated at 4 degrees for 30 minutes with gentle shaking and pelleted at 4 degrees Celsius for 5 minutes at 3,000 rpm. Pellet was resuspended in cold RIPA buffer (10 mM Tris-HCl pH 7.5, 150 mM NaCl, 1 mM EDTA pH 8.0, 1% (w/v) DOC, 0.1% w/v SDS, 1% (v/v) NP-40, 0.2mM $NaVO_4$, in sterile water) with 1X protease cocktail (Calbiochem) and incubated at 4 degrees Celsius overnight with rotation. Samples were sonicated in volumes of 300 ul in a ice bath using a Diagenode Bioruptor for 3 times at 7.5 minutes on High with 30 seconds ON and 30 seconds OFF, and 1 time at 5 minutes on High with 30 seconds ON and 30 seconds OFF. Samples were pre-cleared with 50 ul of pre-blocked beads (Sepherose-A beads (Life Technologies) blocked in 1mg/ml BSA, 0.25 mg/ml sonicated sperm DNA in RIPA buffer at a final 50:50 concentration overnight at 4 degrees) for 2 hours. Chromatin concentration was measured and separated into samples of 1000

ug IP samples but save 100 ug for the 10% Input. Add 2 ug of antibody per 1000 ug IP and incubate at 4 degrees Celsius with rotation overnight. Add 50 ul of pre-blocked beads to each IP and incubate at 4 degrees Celsius for 2 hours with rotation. Spin down IPs for 1 minute at 14,000 rpm at 4 degrees Celsius, remove supernant, resuspend in 500 ml cold Wash Buffer 1 (150 mM NaCl, 20 mM Tris pH 8.1, 2 mM EDTA pH 8.0, 0.1% (w/v) SDS, 1% (v/v) Triton X-100, in sterile water), and incubate at 4 degrees with rotation for 10 minutes. Repeat spin down, resuspension, and incubation for Wash Buffer 2 (500 mM NaCl, 20 mM Tris pH 8.1, 2 mM EDTA pH 8.0, 0.02% (w/v) SDS, 1% (v/v) Triton X-100, in sterile water), Wash Buffer 3 (250 mM LiCl, 10 mM Tris pH 8.1, 1 mM EDTA pH 8.0, 1% (w/v) DOC, 1% (v/v) NP40, in sterile water), and Wash Buffer 4 (10 mM Tris pH 7.9, 1 mM EDTA pH 8.0, in sterile water). Pellet sample and resuspend in 500 ml of room temperature Resuspension Buffer (10 mM Tris pH 7.9, 1 mM EDTA pH 8.0, 0.5% (w/v) SDS, in sterile water) that has 10 ug of RNAse A and 10 ug of Proteinase K per sample. Incubate at 55 degrees Celsius for 3 hours and then at 65 degrees Celsius for ~16 hours. Clean up chromatin with Qiaquick PCR purification kit as per manufacturer's instructions and eluting in a total volume of 60 ul.

ChIP RT-PCR:

For ChIP RT-PCR, BioRAD iTaq Universal SYBR Green Master Mix was used. In a 20 ul reaction, 2 ul of chromatin, 10 ul of SYBR Green, 1 uM of primers and up to 20 ul of water. % Input was calculated using the following formula: (2^(Average Ct for Input/ Ct of sample)) x (% Input used in qPCR) x 100. The following primers were used for p63 binding of Axl: 5'ATTTGGTGTCCCATTTAGGC-3' and 5'-TCGATTCCTGGAGAAACCTC-3'. The following primers were used for non-binding (12^{th} exon of Axl): 5'-

CCTGGCCTGGATCTAAAGG-3' and 5'-GGGTCTGTGGTTCTGACATTC-3'. Temperatures and times for RT-PCR followed manufacturer's protocol for ABI 7500 instrument.

BP and LR cloning to generate p63 overexpression plasmid:

Transient deltaNp63alpha-FLAG and pLX302 plasmids were obtained from Addgene (26979, 25896 respectively) and pDONR221 plasmid from Life Technologies (12536-017). DeltaNp63alpha was sequenced out using the following primers: 5'-ATGTGGTACCTGGAAAACAATGCCCAGACTCAATTT-3' and 5'-ACACTCCCCCTCCTCTTTGATGCGCTGTTGCTTATTGCG -3'. PCR fragment was then recombined into pDONR221 and then pLX302 as prescribed by manufacturer's protocol for BP and LR recombination except scaled down to a 6 ul total reaction volume.

Colony formation assay:

Cells were transfected with siRNAs in a 96-well plate for 72 hours before re-plating and seeding 300 cells per well in a 6-well plate. Colonies were grown out for 7 days before being fixed with 2% formaldehyde for 20 minutes, rinsed twice with 1X PBS and stained for at least 5 hours to overnight with 1:6 diluted Giemsa stain (Sigma Aldrich). Plates were then rinsed with water, dried, scanned, and then colonies were counted by hand.

Results

P63 is a hub between miR203a and miR205 regulated cell motility:

From the miRNA motility screen conducted in Chapter 3 "Identification of miRNAs that regulate motility", there were over 50 potential miRNA signaling pathways to follow up. To prioritize, we looked at the endogenous miRNA expression of motile basal- versus non-motile luminal subtypes MCFDCIS and HCC1428. We found 45 differential expressed miRNAs with a 2-fold or more differential expression, a p-value of 0.05 that appeared in the miRNA mimic

screen, and had a relative fluorescence of -40 or greater (Fig 4-1 A, Appendix F). By graphing the relative log expression difference of basal- over luminal subtype and each miRNAs wounding z-scores, we found two interesting miRNAs, miR203a and miR205 (Fig 4-1 B). MiR203a expression is high in non-motile luminal cell and inhibited wound closure in the screen. MiR203a is known to be a negative regulator of stem cell maintenance in keratinocytes and mammary epithelium (96, 97). MiR205 expression is high in the motile basal-subtype cell line and enhanced wound closure. To identify targets of miR203a that may regulate cell motility, we conducted a gene expression microarray on MCFDCIS transfected with miR203a mimic and found that among the targets, p63 and miR205 expression were decreased (Fig 4-1C and E). It has been previously shown that p63, specifically deltaNp63alpha is a direct target of miR203a (96).

P63 is a transcription factor in the p53 family and has six isoforms (98). This transcription factor is of interest because it can induce the expression of miR205 in bladder cells (99), which coincide with our RT-PCR results. Knockdown of p63 via siRNAs decreased the expression of miR205 (Fig 4-1 C). We also tested if miR205 can regulate p63 expression through a feed-forward mechanism for enhanced migration and found that miR205 did not affect p63 expression (Fig 4-1 D). Therefore, miR203a can inhibit motility through the direct repression of p63, a positive regulator of miR205.

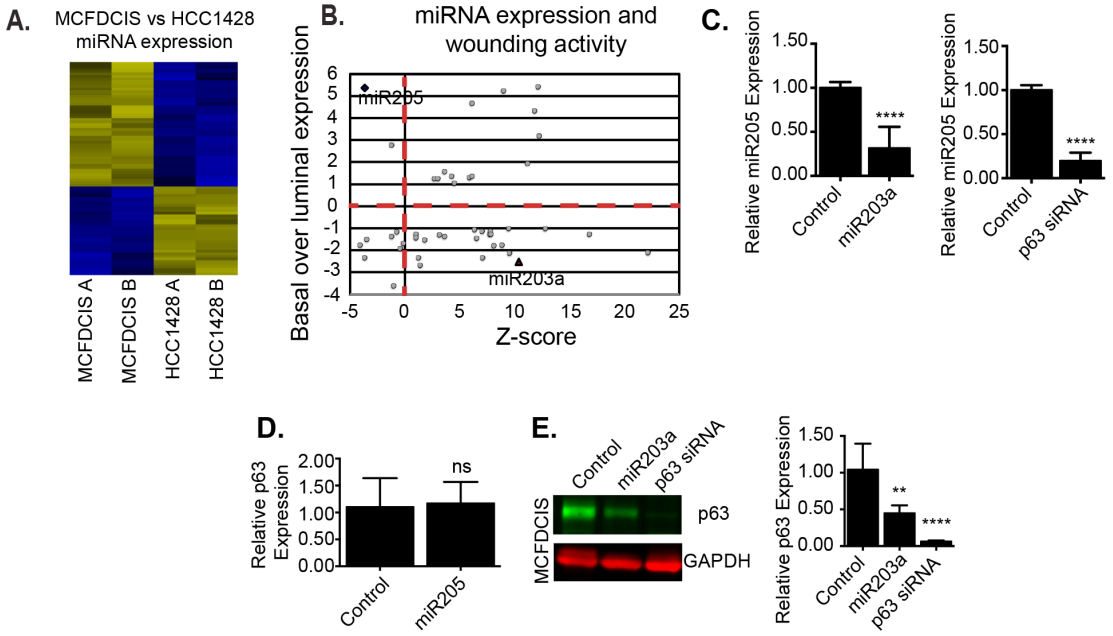

Figure 4-1: P63 is a hub between miR203a and miR205 regulated cell motility. **A.** Heatmap of MCFDCIS (basal-subtype) and HCC1428 (luminal-subtype) miRNA expression profile. Shown are probes that have at least 2-fold difference in expression and a p-value of 0.05. Yellow = down regulated, blue = up regulated. **B.** Graph of miRNAs differential expressed from A. and their wounding z-score activity. Of note, miR205 is highly expressed in the basal-subtype with a low z-score (enhancer of migration) and miR203a is highly expressed in the luminal-subtype and have a high z-score (inhibitor of migration). **C.** RT-PCR expression of relative miR205 in MCFDCIS cells when transfected with miR203a, p63 siRNA, or control. **D.** RT-PCR expression of relative p63 expression in MCFDCIS cells transfected with miR205 or control. **E.** Western immuno-blot of MCFDCIS lysates from transfection of miR203, p63 siRNA, or control. P63 (green), GAPDH (loading control, red). Graph from RT-PCR of relative p63 expression in MCFDCIS cells transfected with miR203a, p63 siRNA, or control. All graph quantification are t-tests of sample versus control condition, shown are means with standard deviation bars. Ns = not significant, ** p-value <=0.01, **** p-value <= 0.0001.

P63 is required for motility:

We hypothesized that p63 is required for cell motility since p63 is a target of an inhibitor of cell motility and a required transcription factor of an enhancer of cell motility. To test this observation, we transfected p63 siRNAs in MCFDCIS and HCC1806. MCFDCIS and HCC1806 were chosen because they express p63 and can collectively invade. We found that p63 is required for not only wound closure but also spontaneous movement (Fig 4-2A, B and D). As expected, MCFDCIS cells transfected with miR203a or p63 siRNA had shorter tracks and slower motilities compared to control, while miR205 had a greater displacement and cell speed compared to control (Fig 4-2 A and B).

To pinpoint which isoform of p63 is required for motility, we deconvoluted Dharmacon's siGENOME p63 siRNA pool. When the deltaNp63alpha isoform is targeted, we get the most inhibition of wound closure (Fig 4-2 C). As of yet, we have not tested with siRNAs that specifically targets deltaNp63alpha and not the TA versions. For convenience, we used Sigma's p63 siRNA pool for the rest of the project (Fig 4-2 E), unless noted otherwise, to knockdown p63 expression. In addition, when we refer to p63, we specifically mean the deltaNp63alpha isoform.

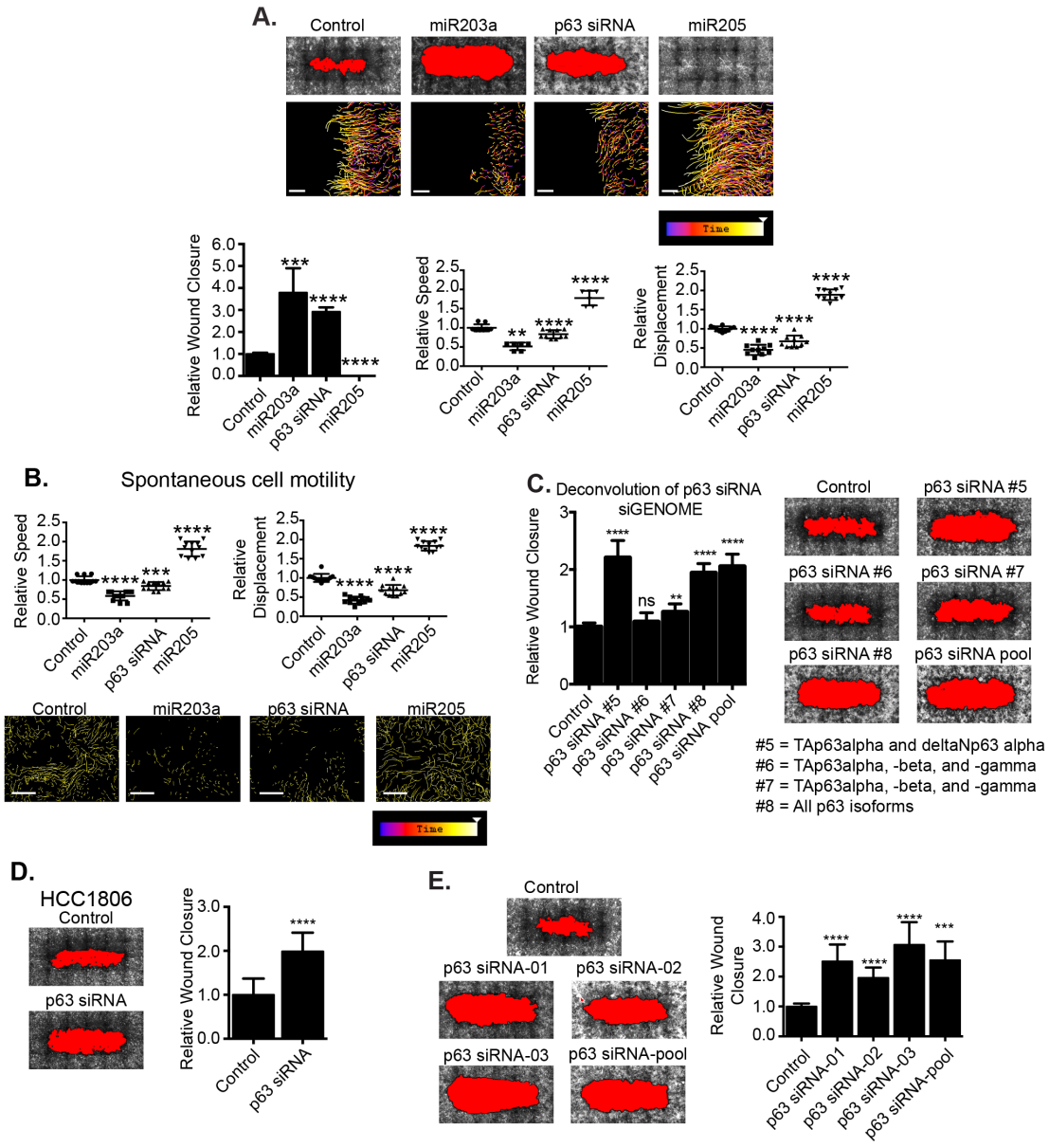

Figure 4-2: DeltaNp63alpha is required for cell motility. A. Immunofluorescence and real-time imaging tracks of MCFDCIS wound closures. Cells were transfected with miR203a, p63 siRNA, miR205, or control. Graphs are of relative wound closure, relative speed of cells, and relative displacement of cells compared to control. **B.** Quantification of spontaneous MCFDCIS cell speed and displacement relative to control. Images are of tracks over 5 time points. **C.** Deconvolution of p63 siRNA from Dharamcon siGENOME. Quantification and images of MCFDCIS transfected with individual p63 siRNA oligos. Listed are the specific isoforms each siRNA oligo targets. **D.** Wounding of HCC1806 transfected with p63 siRNA or control. Graph shows relative wound closure. **E.** Deconvolution of the p63 siRNA pool used in this project. All graph quantification are t-tests of sample versus control condition, shown are means with standard deviation bars. Ns = not significant, ** p-value <=0.01, ***p-value <= 0.001, **** p-value <= 0.0001. Scale bars are 100 um.

P63 expression increases upon breast cancer invasion:

Since p63 is required for cell motility in vitro, we wanted to determine its expression in breast cancer progression. First we looked at the epithelial status of invasive breast cancer cells. As shown in Chapter 2 and in Hu et al, MCFDCIS lesions can be induced to invade at three weeks when co-injected with mammary fibroblasts (Fig 4-3) (61). Since the cells that were collectively invading in organotypic culture still retain their epithelial characteristics (Chapter 2, Fig 2-8,(61)), we immunostained tumor paraffin sections with E-cadherin and collagen-IV. In non-invasive DCIS lesions, the breast cancer cells retain their E-cadherin expression and the collagen-IV is organized around the circular lesion and in the stroma. However, upon induction of invasion, the collagen-IV staining is dispersed within the tumor and along invasive tracks while the invasive cells still express E-cadherin (Fig 4-3 A). Thus, invasive cells in vivo do not need to undergo complete EMT to become invasive.

In non-invasive DCIS lesions, p63 is co-expressed with SMA in the myoepithelial layer, which coincide with previous reports (Fig 4-3 B, (61)). Myoepithelial cells are the stem cells of the mammary gland (78). Upon collective invasion, invasive cells are positive for p63, but most importantly not all p63 positive cells co-express SMA, thus these invasive cells are not an expansion of the myoepithelial cell layer (Fig 4-3 B). In addition, p63 positive cells in both invasive and non-invasive lesions express E-cadherin and are therefore still epithelial (Fig 4-3 C). The increased expression of p63 is not only seen in the MCFDCIS mammary fibroblast induced model but also in the genetic PyMT breast cancer model where p63 expression increased by week 10 (Fig 4-4 A, (100)).

Based on the increase of p63 expression in the invasive cells in vivo, we tried to knockdown p63 using the short-hairpin RNA, shRNA system to target the gene. Even though

we were able to knockdown p63 expression by western blot (not shown), the knockdown was not sustained in vivo (Fig 4-4 B). During infection of MCFDCIS cells with p63 shRNAs, there was some cell death, suggesting that p63 is required for cell survival. We conducted a colony formation assay on MCFDCIS cells transfected with control and p63 siRNAs to determine if p63 is required for growth (Fig 4-4 C). Indeed p63 is required for growth in MCFDCIS cells and therefore MCFDCIS cells that may have p63 knockdown by shRNAs may have died off leaving p63 expressing cells to grow out in vivo. A possible solution to achieve p63 knockdown in vivo is to generate a cell line with a p63 shRNA inducible construct, inject the cell line into mice and treat the mice before invasion in vivo to determine if p63 is required for breast cancer invasion.

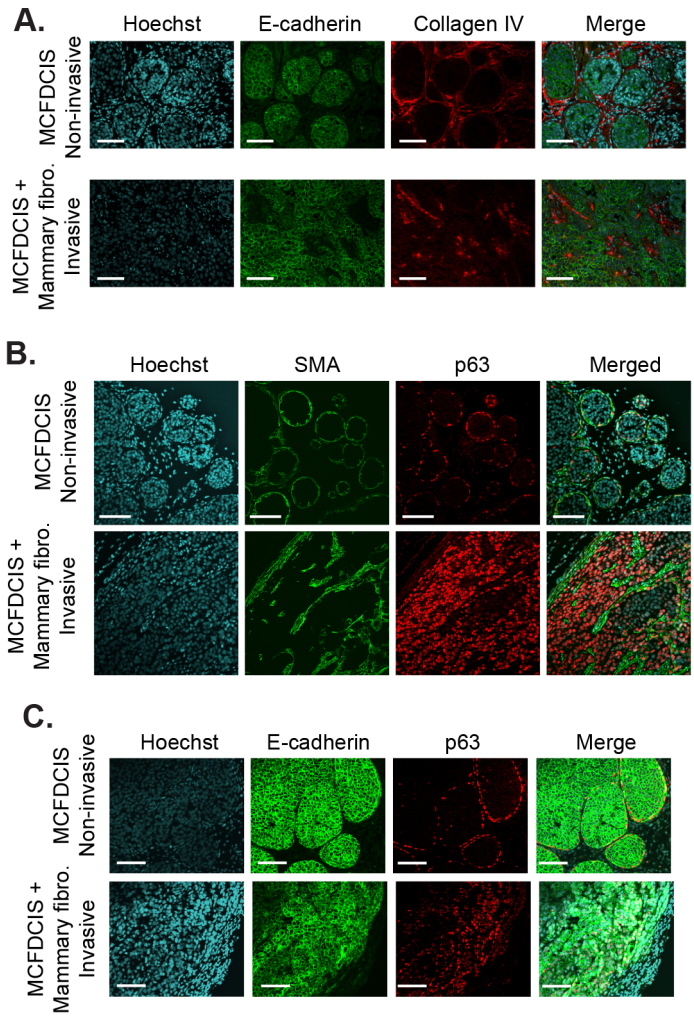

Figure 4-3: P63 expression increases upon breast cancer invasion in vivo and maintain E-cadherin expression. Immunofluorescence on MCFDCIS (non-invasive tumor) or MCFDCIS co-injected with mammary fibroblasts (invasive tumor). **A.** Collectively invading cells maintain E-cadherin expression. E-cadherin (epithelial marker, green), collagen IV (ECM marker, red), counterstained with Hoechst (nuclei, cyan). **B.** P63 expression is restricted in the myoepithelial layer of non-invasive lesions and is up regulated in invading cells. Smooth muscle actin (myoepithelial marker, green), p63 (red), counterstained with Hoechst (nuclei, cyan). **C.** Invasive p63 positive cells express E-cadherin. E-cadherin (epithelial marker, green), p63 (red), Hoechst (nuclei, cyan). Scale bars are 100 um.

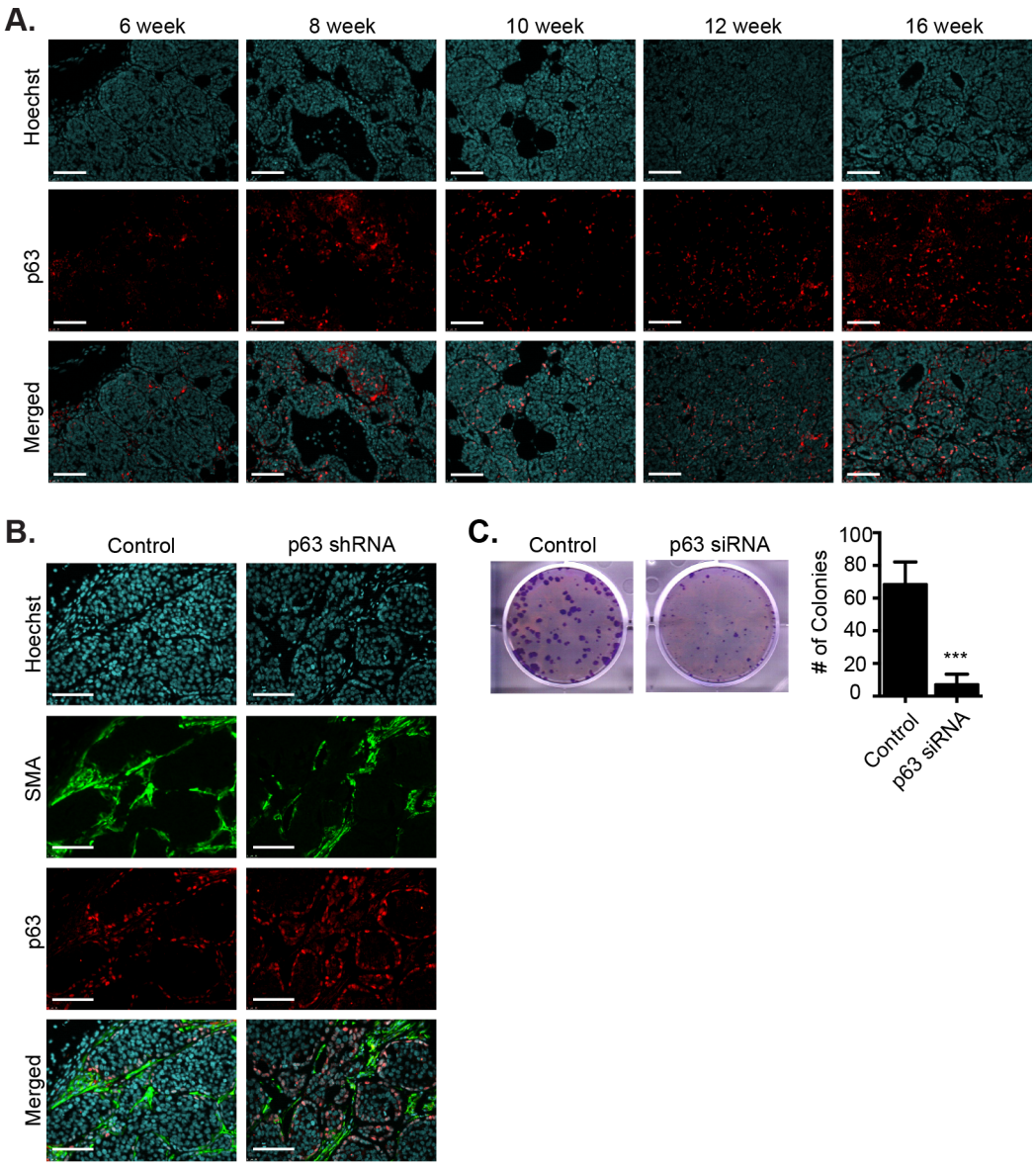

Figure 4-4: P63 expression is required for growth. A. PyMT breast cancer model immuno-stained for p63 (red) expression and counterstained with Hoechst (nuclei, cyan). Tumor samples were a gift from Noah Sorelle (Brekken lab). **B.** P63 shRNA was not able to sustain p63 knockdown in vivo. Xenografts of MCFDCIS control and p63 shRNA immuno-stained for SMA (myoepithelial marker, green), p63 (red) and counterstained with Hoechst (nuclei, cyan). **C.** Colony formation assay of MCFDCIS transfected with either control or p63 siRNA. Graph shows the mean of the number of colonies over three experiments with two replicates per experiment. Erin A. Pineda conducted colony formation. Scale bars are 100 um. Graph quantification is a t-test of sample versus control condition, shown are means with standard deviation bars. ***p-value <= 0.001.

P63 overexpression is insufficient to induce cell motility:

Since p63 is required for cell motility in vitro, the next question is whether or not p63 is sufficient to induce motility in a non-motile condition. We generated a constitutive deltaNp63alpha overexpression construct and infected MCFDCIS and HCC1428 (Fig 4-5 A and B). The exogenous deltaNp63alpha is functionally active since it was able to induce the expression of its target, miR205 in HCC1428 (Fig 4-5 C). The Exogenous deltaNp63alpha, increased the expression of miR205, but did not induce motility in the HCC1428 as seen through a wounding assay (Fig 4-5 D). Further co-transfection of MiR205 with p63 siRNA in MCFDCIS, did not sustain cell motility in p63 knocked down cells (Fig 4-5 E). Therefore, there must be other p63-regulated targets that act in conjunction with miR205 to regulate cell motility. Another possibility of why miR205 was not able to sustain motility in p63 knocked down cells is that the p63 siRNAs may have an off-target effect. However, this seems to be not as likely since we utilized 11 siRNA oligos and at least three shRNAs targeting p63 and found that p63 is required for cell motility.

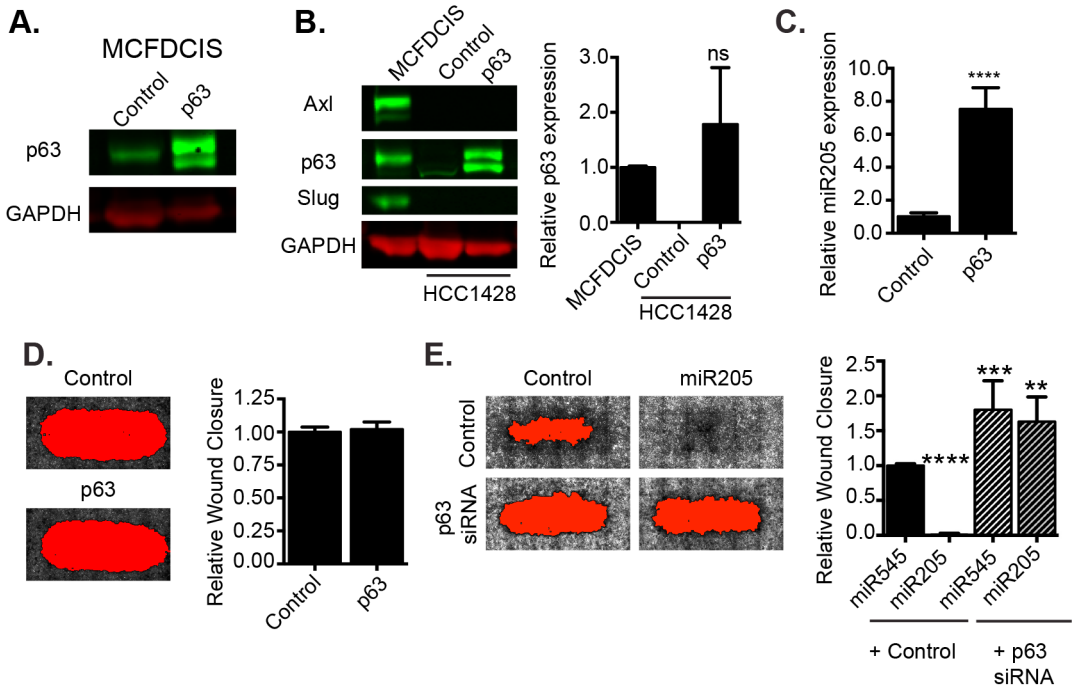

Figure 4-5: P63 is not sufficient to induce cell migration in a non-motile cell line. A. Western blot of MCFDCIS control and overexpression of p63. P63 (green), GAPDH (loading control, red). **B.** Western immuno-blot and quantification of MCFDCIS, HCC1428 and HCC1428 with p63 overexpression. Immuno-blot for p63, Axl, and Slug (green) and GAPDH (loading control, red). **C.** RT-PCR of relative miR205 expression in control and p63 overexpression HCC1428. **D.** Wounding images and quantification of HCC1428 control and p63 overexpressing cells. **E.** Wounding assay of MCFDCIS co-transfected with the listed conditions. For the Control along the miRNA axis, it is miR545 an innocuous wounding miRNA found in the miRNA screen. All graph quantification are t-tests of sample versus control condition, shown are means with standard deviation bars. ** p-value <=0.01, ***p-value <= 0.001, **** p-value <= 0.0001.

Identification of p63 regulated cell motility targets:

To identify other p63 regulated cell motility targets, we conducted gene expression microarrays on MCFDCIS and HCC1806 cells transfected with p63 siRNAs and motile and non-motile cells. For probes that changed due to p63 loss, we found 1430 probes in MCFDCIS transfected with p63 siRNA versus control and 1521 probes for the HCC1806 transfection. In the comparison of motile cells, MCFDCIS and HCC1806 versus non-motile cells HCC1428 and MCF-7, there were 3753 differential probe expressions. Once we compared the overlap and removed duplicate probes for the same gene, we found 99 genes that changed upon p63 loss and had the same expression trend when comparing motile versus non-motile cells (Fig 4-6 A). Of these 99 p63-regulated targets, 61 of these genes required p63 expression and are expressed highly in the motile cells versus non-motile cells (Fig 4-6 B, Appendix G). Of these 61 p63 motile regulated genes, we were able to find TP63, which is the gene name of p63, miR205 which we have already established as a p63 regulated target that can enhance cell motility (Fig 4-2) and two interesting targets, Axl and SNAI2 otherwise known as Slug (highlighted features in Fig 4-6 B).

A.

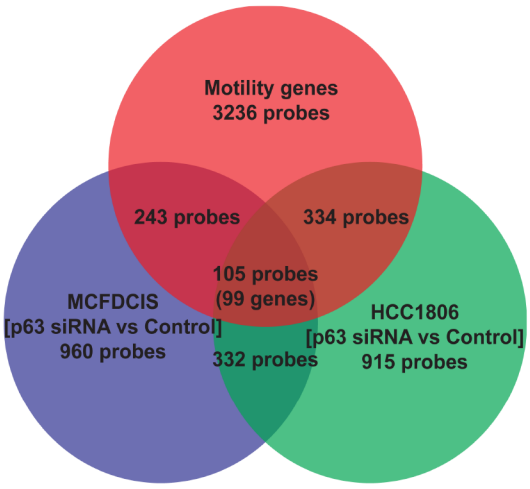

B.

p63 motile regulated genes/miRNAs						
ABCC4	BDKRB1	CTGF	HS.12876	MIR205	PM20D2	SNAI2
ALDH3A1	BCL11A	DLK2	HS.551128	MTMR15	POLR3G	SNCA
ANTXR1	C17ORF81	DST	HS.554203	NEK1	PPFIBP1	TP63
ANXA8L1	C3ORF54	DYRK3	IKBIP	NFASC	PROCR	TP73L
ANXA8L2	CASP1	EXTL2	IRF6	NFIX	PSTPIP2	TWIST2
APOBEC3G	CD44	FAM189B	KCTD12	NKX3-1	PTPRZ1	UGT1A6
ARHGAP22	CDH13	FAT2	LOC653110	NOTCH1	RFC3	VSNL1
AXL	CKAP4	GNG11	MAMDC2	PALMD	SIM2	
BBS7	CPNE8	GPX8	MFNG	PLXNA2	SLC47A1	

Figure 4-6: Identification of p63 regulated motility genes. A. Venn diagram of genes that have differential expression upon p63 knockdown (MCFDCIS and HCC1806 transfected with control or p63 siRNA) or genes differentially expressed in motile versus non-motile cells (HCC1806 and MCFDCIS versus HCC1428 and MCF-7). Probes/genes must exhibit 2-fold or more change compared to control and have a p-value of 0.05. **B.** List of genes from A that require p63 expression and are highly expressed in motile cells versus non-motile cells. Of note are Axl, miR205, Slug (SNAI2), and p63 (TP63). An extensive list of overlapping genes is located in Appendix G.

Axl is required for cell motility:

Axl is a tyrosine receptor kinase. It has been shown that in a p63 ChIP-Seq, the transcription factor was able to pull down the Axl gene in keratinocytes (101). Looking at publicly available ChIP-Seq data of keratinocytes (102, 103) we found that p63 binds in the promoter region of Axl in progenitor and differentiated keratinocytes and in two different patient samples using two different antibodies that recognize p63alpha (Fig 4-7 A). Aligning the common binding sequences of the five ChIP-Seq samples, we found a p53 response element in the Axl promoter for which p63 may use to regulate Axl expression (Fig 4-7 B). P63 can bind in p53 response elements to regulate genes (75). Since most of the published data showing p63 binding to the Axl gene were in keratinocytes, we wanted to determine if p63 can directly regulate Axl expression in breast cancer cells. By performing a direct ChIP priming for the sequence around the Axl's p53 response element, we found that in our p63 expressing motile cells, MCFDCIS, p63 can pull down Axl's promoter region compared to our IgG negative control and in a MDA-MB-231 cells which have undetectable p63 protein expression (Fig 4-7 C). P63 regulation of Axl expression can be seen through the knockdown of Axl protein expression upon p63 siRNA treatment in two motile breast cancer cell lines, HCC1954 and HCC1806 (Fig 4-7 D).

To determine if Axl is required for cell motility, we conducted a wounding assay of MCFDCIS cells transfected with siRNAs targeting Axl or treated with an Axl inhibitor, R428 (Fig 4-8 A and B) (88). Inhibition of Axl function via siRNA or with R428 decreased cell migration (Fig 4-8 B). However, overexpression of Axl was not sufficient to overcome the loss of migration due to the knockdown of p63 (Fig 4-8 C). The reason why Axl overexpression was not sufficient to sustain cell migration in the loss of p63 is probably because Axl, like miR205

works in conjunction with other p63 regulated targets to control cell migration. If another p63-regulated target is knocked down in Axl overexpressed cells such as Slug, cell migration can be reduced (Fig 4-8 C). Therefore, Axl a direct p63 target, functions in parallel with other p63 regulated targets to control cell migration.

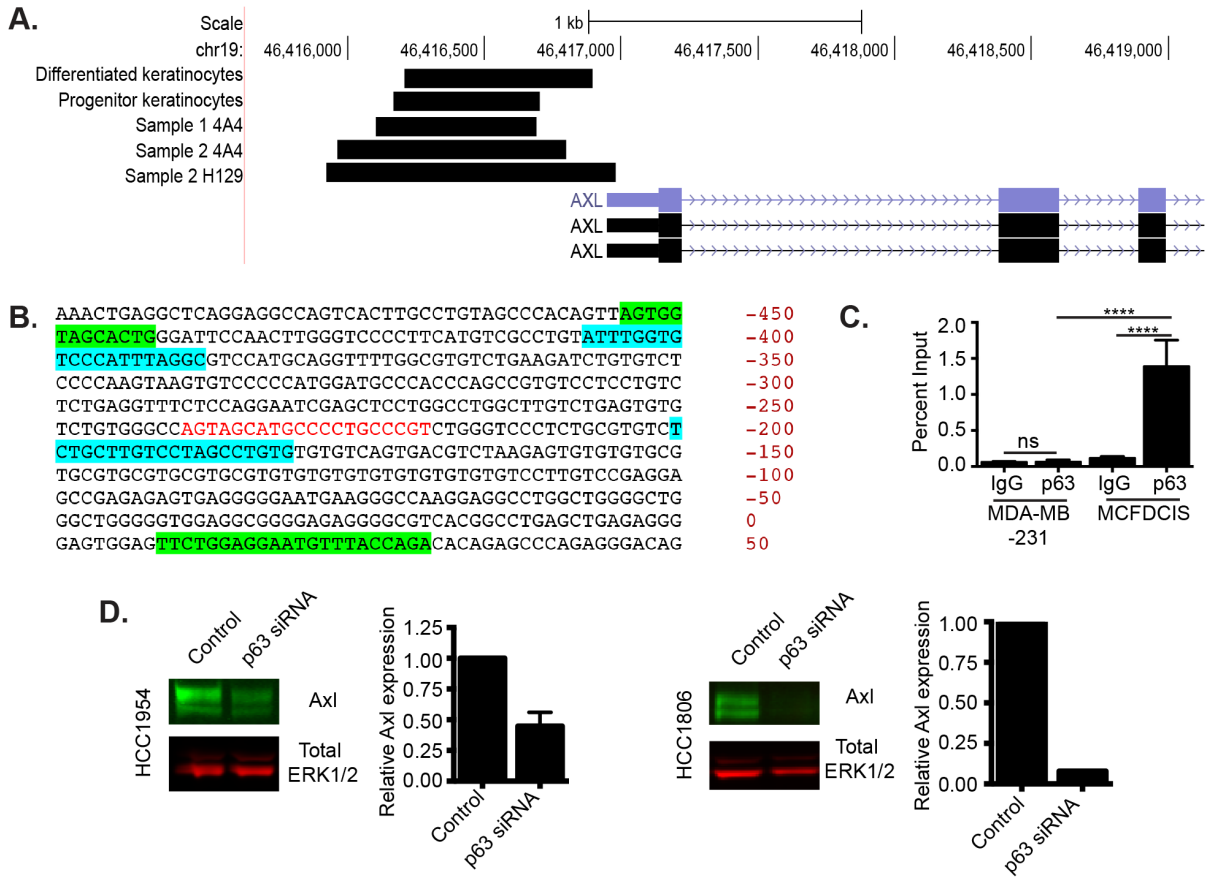

Figure 4-7: p63 directly binds to Axl's promoter region to regulate Axl expression. A. Diagram of p63 ChIP-Sequence binding sites in the promoter region of Axl. **B.** Sequence of overlapping ChIP-Sequence binding site from A. Green sequences bracket the overlapping region of p63 binding, Blue sequences are primer sequences for directed p63 ChIP, red sequence is the p53 response element and red numbers are the base pair location in respect to the transcription start site of Axl. **C.** RT-PCR of directed p63 ChIP for the Axl promoter. Priming sequence is the blue sequences in B. **D.** Western immuno-blots of Axl expression in control and p63 siRNA transfected HCC1954 and HCC1806, both are motile breast cancer cell lines. Axl (green) and ERK1/2 (loading control, red).

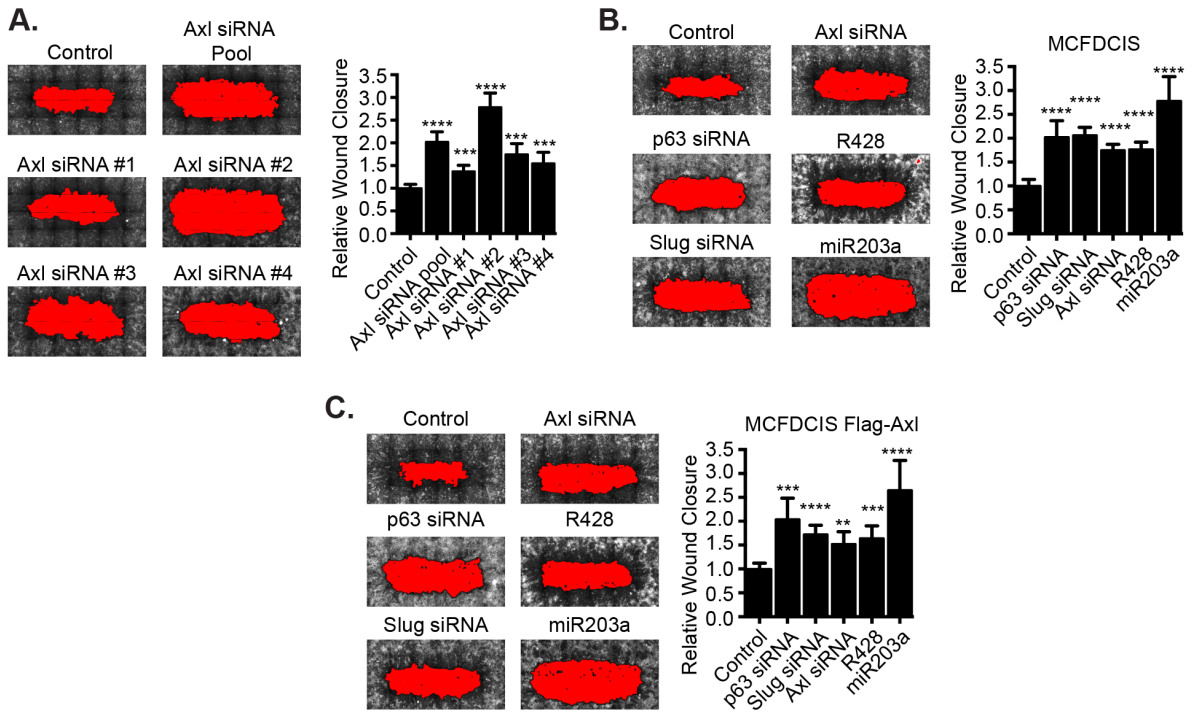

Figure 4-8: Axl is required for cell motility. A. Wounding assay of MCFDCIS deconvolution of Axl siRNA pool. **B.** Wounding assay of MCFDCIS cells transfected with p63, Axl, and Slug siRNAs, miR203a, or pre-treated for 24 hours with R428, an Axl specific inhibitor. **C.** Wounding assay of MCFDCIS infected with a Flag-Axl (Addgene, #20428) overexpression construct transfected or treated with the listed conditions. All graph quantification are t-tests of sample versus control condition, shown are means with standard deviation bars. ** p-value <=0.01, ***p-value <= 0.001, **** p-value <= 0.0001. Matthew Esparza generated wounding data.

Slug is required for cell motility:

As shown in Fig 4-6 B, Slug is a possible target of p63 regulated motility program. Slug is a transcription factor that has been associated with the transformation of epithelial cells to mesenchymal cells (104). It is thought to be a transcriptional repressor of E-cadherin (89) and is elevated upon a wounding stimulus (72).

To determine if p63 can regulate Slug protein expression, we blotted for Slug expression in three of our motile cell lines, MCFDCIS, HCC1806, and HCC1954 upon transfection with p63 siRNA (Fig 4-9 A). As shown with a Slug siRNA control, loss of p63 decreased Slug protein expression when compared to control, though not as efficiently as the Slug siRNA. Analyses of cell migration upon loss of Slug reveal decreases in cell migration in wounding and spontaneous movement in both MCFDCIS and HCC1806 (Fig 4-9 B to D). Thus, Slug expression is required for cell migration.

As shown in Fig 4-8 C, knockdown of Slug expression reduced cell migration even though there was endogenous expression of Axl. It has been suggested that Axl expression could be regulated by Slug activity (105). To determine if the reduction of cell migration when Slug is knocked down is due to the decrease in Axl expression, we blotted for Axl expression in Slug siRNA transfected cells (Fig 4-10 A). Knock down of Slug in MCFDCIS cells did not decrease the expression of Axl, while p63 siRNA and Axl siRNA did. Also, exogenous expression of Slug in MCFDCIS cells did not sustain Axl expression upon p63 siRNA transfection. Together these data suggest that in the context of this current study, Slug does not regulate motility through Axl expression.

Exogenous expression of Slug had a slight enhancement of cell motility in MCFDCIS cells (Fig 4-10 B). However, like miR205 and Axl, the overexpression of Slug was not able to sustain cell motility during the loss of p63, Axl, or inhibition of Axl function (Fig 4-10 B). Therefore, p63 regulates cell motility through the parallel actions of Slug, Axl and miR205.

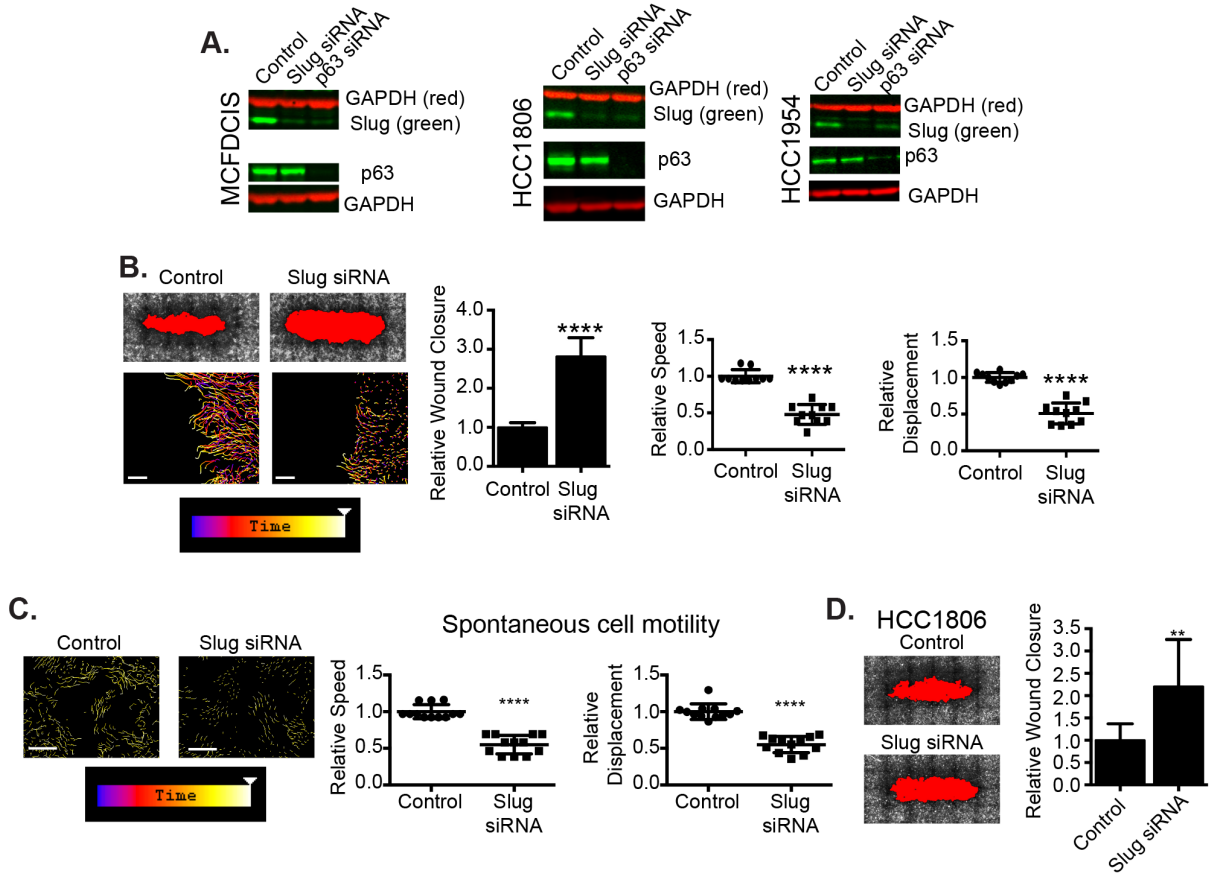

Figure 4-9: Slug is required for cell motility. **A**. Loss of p63 decreases Slug expression in motile breast cancer cell lines, MCFDCIS, HCC1806 and HCC1954. P63 (green), Slug (green), and GAPDH (loading control, red). **B.** Immunofluorescence and real-time imaging tracks of MCFDCIS wounding assay transfected with control or Slug siRNA. Graphs quantify relative wound closure, relative cell speed, and relative cell displacement. **C.** Real-time imaging tracks of MCFDCIS spontaneous cell motility. Shown are track of the last 5 time points. Graphs are quantifications of relative speed and cell displacement. **D.** Wounding assay of HCC1806 transfected with control or Slug siRNA. All graph quantification are t-tests of sample versus control condition, shown are means with standard deviation bars. ** p-value <=0.01, **** p-value <= 0.0001.

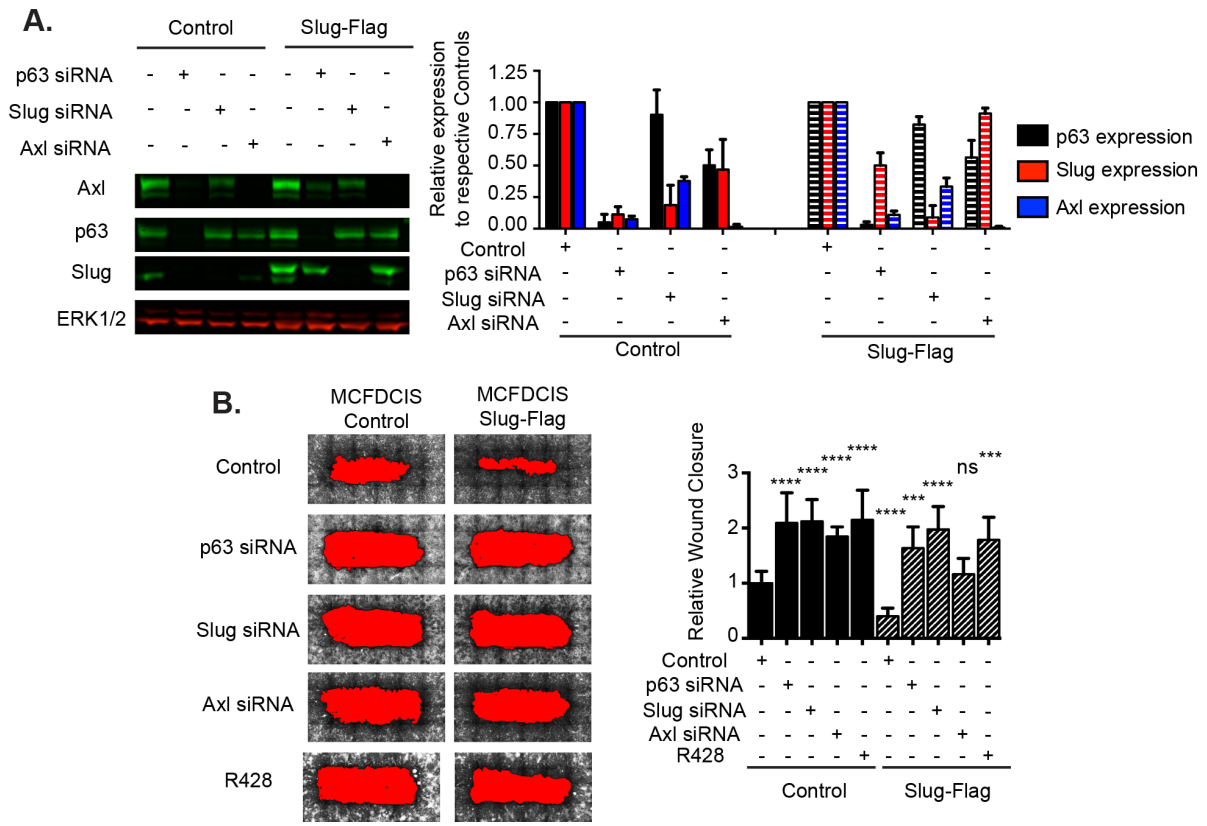

Figure 4-10: Slug does not regulate motility through Axl expression. A. Western immuno-blots and graph of relative protein expression of control and Slug-Flag overexpressing MCFDCIS transfected and blotted for with the listed conditions. **B.** Wounding assay of control and Slug-Flag overexpressing MCFDCIS cells transfected with the listed conditions. All graph quantification are t-tests of sample versus Control condition, shown are means with standard deviation bars. Ns = not significant, ***p-value <= 0.001, **** p-value <= 0.0001. Western blot and wounding assay conducted by Matthew Esparza.

Slug is sufficient to induce invasion in vivo:

As shown in Figure 4-3, p63 expression increases in MCFDCIS cells upon mammary fibroblast induced invasion in vivo. To understand how Slug is regulated during breast cancer progression, we stained for Slug in non-invasive and invasive breast cancer tumors. We found that Slug expression was restricted to the myoepithelial layer in non-invasive lesions. Like p63, Slug expression increased upon mammary fibroblast induced invasion. These invasive Slug positive cells also express E-cadherin, suggesting that though there is an elevated expression of Slug, these invasive cells are still E-cadherin positive epithelial cells (Fig 4-11 A).

Since the exogenous expression of Slug in MCFDCIS had a slight enhancement of cell migration (Fig 4-10 B), we wanted to determine if the overexpression of Slug could induce breast cancer invasion (Fig 4-11 A). Tumors with Slug overexpression had an elevated Slug expression and invasion compared to control tumors (Fig 4-11 B). The sufficiency of Slug to induce breast cancer invasion is a surprise since we were not able to maintain exogenous p63 (data not shown) to induce breast cancer invasion. Nonetheless, Slug overexpression was sufficient to induce breast cancer cell invasion in vivo. The sufficiency of Slug to induce breast cancer invasion in vivo shows that the overexpression of a p63 target is sufficient to induce breast cancer invasion.

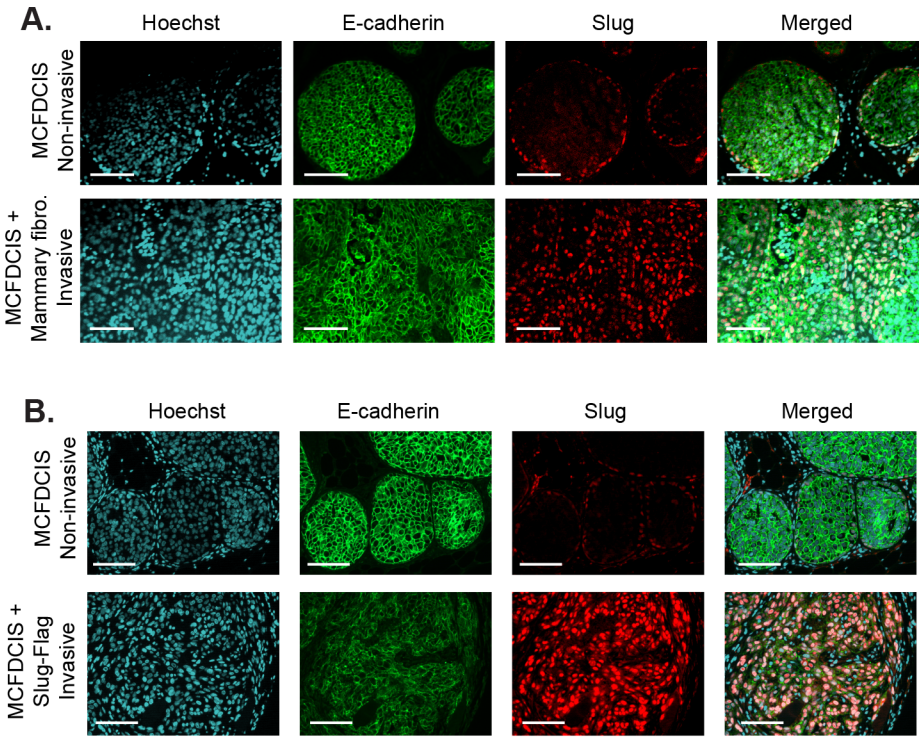

Figure 4-11: Slug is sufficient to induce invasion in vivo. A. Immunofluorescence of MCFDCIS or MCFDCIS co-injected with mammary fibroblasts xenografts for E-cadherin (epithelial marker, green) and Slug (red) and counterstained with Hoechst (nuclei, cyan). **B.** Immunofluorescence of control or Slug-Flag overexpressing MCFDCIS tumors for E-cadherin (epithelial marker, green) and Slug (red) and counterstained with Hoechst (nuclei, cyan). Scale bars are 100 um.

MiR203a is a safety switch against p63 regulated cell motility:

Previously, we have shown that overexpression of Slug enhanced MCFDCIS migration and was sufficient to induce breast cancer cell invasion. However, the overexpression of p63 alone failed to induce the motility of non-motile HCC1428. This failure of p63 to convert HCC1428 into a motile cell line is perplexing since the exogenous p63 was able to induce miR205 expression in HCC1428 (Fig 4-5 C and D). However, upon further analyses, p63 was not able to induce the expression of its two other targets, Axl and Slug (Fig 4-5 B). To understand why p63 was not sufficient to induce motility and perhaps induce invasion in vivo, we looked at a basic characteristic of HCC1428. HCC1428 expresses miR203a at a greater level than our motile cell line, MCFDCIS (Fig 4-1 A and B). Since miR203a is a negative regulator of p63, we wanted to determine if somehow miR203a was targeting the exogenous p63 expression through a non-3'UTR mechanism. Transfection of miR203a in p63 overexpressing cells did not significantly reduce the expression of p63. The slight reduction in protein and mRNA level is most likely the reduction of endogenous p63 expression. We believe that the slight reduction of p63 by miR203a in the overexpressing p63 cell line was not significant because the miR205 expression was sustained in the presence of miR203a (Fig 4-12 C). Surprisingly, we found that miR203a was able to knockdown the expression of Slug and Axl in both protein and mRNA levels (Fig 4-12 A and B). We also noted that the overexpression of Axl or Slug was not able to overcome miR203a inhibition of cell migration (Fig 4-8 C and 4-10 B). This suggests that miR203a may act as a safety switch against p63 induced migration by targeting p63's downstream players Slug and Axl. However, the mechanism of how miR203a targets Slug and Axl expression is currently unknown.

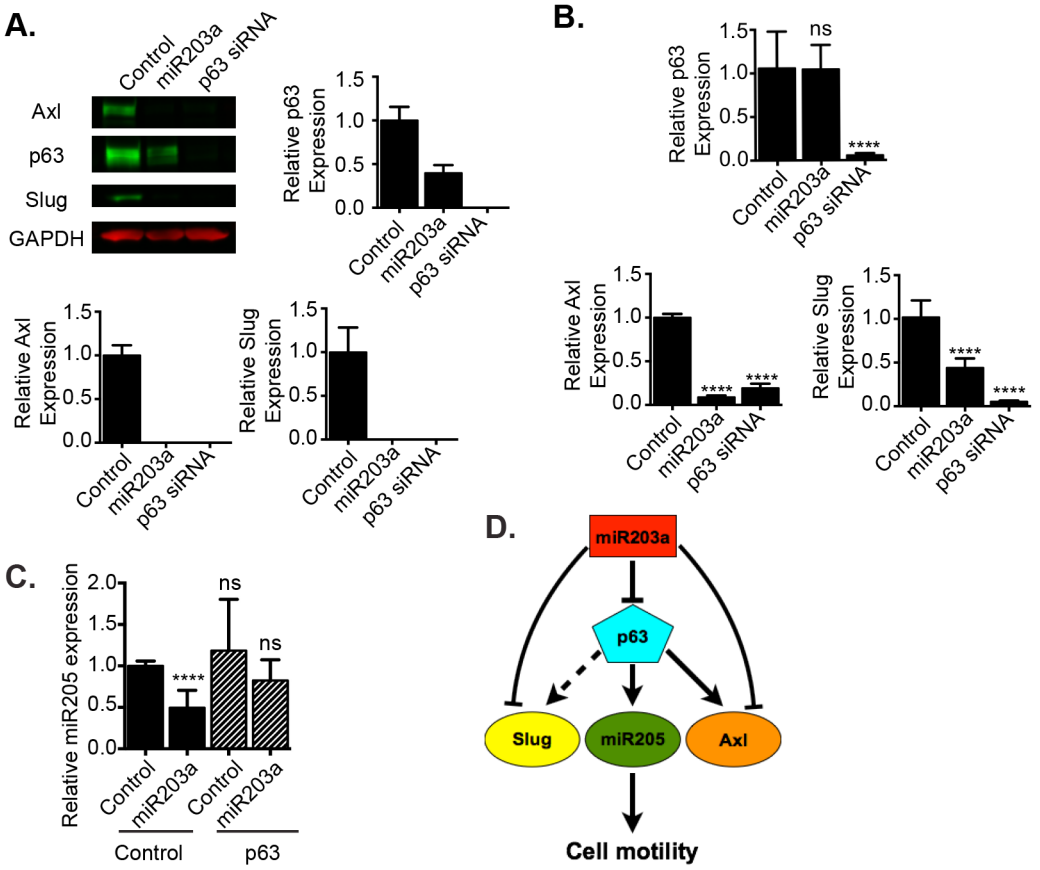

Figure 4-12: miR203a is a safety switch against p63 regulated motility. **A.** Western immuno-blot of Axl, p63, Slug (green), and GAPDH (loading control, red) of MCFDCIS overexpressing p63 and transfected with control, miR203a, or p63 siRNA. **B.** RT-PCR of relative expression of p63, Axl, and Slug in MCFDCIS overexpressing p63 transfected with control, miR203a, or p63 siRNA. **C.** RT-PCR of relative miR205 expression in control or p63 overexpressing MCFDCIS transfected with control or miR203a. **D.** Putative p63 regulated motility signaling program. All graph quantification are t-tests of sample versus control, shown are means with standard deviation bars. Ns = not significant, **** p-value <= 0.0001.

Discussion

Using a combinatorial effort of functional and expression profiling of miRNAs, we found a unique signaling pathway that regulated E-cadherin positive collective-cell migration. We found that miR203a, which decreases cell migration and is highly expressed in non-motile cells, can regulate the expression of miR205, an enhancer of cell motility and is highly expressed in motile cells. The hub that connects these two very different miRNAs is p63, a transcription factor (96, 97, 99). P63 was found to be required for cell motility not only in our system but also in SCC (79).

To identify targets of p63, we conducted a gene expression comparison of motile cells with p63 knocked down and motile versus non-motile cells. From the analyses, we found 61 genes that are regulated by p63 and may play a role in cell migration, which include Axl, Slug, and miR205. We found that Axl and Slug are required for cell motility but neither of them alone can overcome the inhibition of cell migration in p63 knocked down cells. Also, if one or the other is knocked down, the overexpression of Axl or Slug could not overcome decrease in cell motility. In contrast to Vuoriluoto et al, Slug was not found to regulate Axl expression (105). Surprisingly, Slug was sufficient to slightly enhance cell migration and induce breast cancer invasion. Therefore, the downstream targets of p63, Axl, miR205, and Slug work in concert to regulate cell migration.

Overexpression of p63 is not sufficient to induce the expression of Axl or Slug enhanced cell migration. By taking a step back, we looked at the function of miR203a, which is highly expressed in the non-motile cells, and discovered that even though our exogenous p63 was resistant to miR203a targeting, miR203a can decrease the expression of Axl and Slug. Therefore, miR203a can act as a safety measure against p63 induced cell migration. Based on the presented

data, we have shown a novel p63 motility regulated mechanism that may regulate the transition between non-invasive DCIS to invasive breast cancer.

Chapter Five: Conclusions and Future Directions

Overview:

The primary cause of death in breast cancer patients is the metastatic growths. Therefore, it is important to elucidate the mechanism of metastasis. An early and necessary step in metastasis is the invasion of breast cancer cells into the tumor stroma. In this study we have shown that induction of invasive breast cancer can be assisted through the reorganization of collagen-I fibers by mammary fibroblasts. The breast cancer cells that utilize the newfound collagen tracks are motile cells. Motility can be gained through the increased signaling of p63 and its targets miR205, Axl and Slug.

Intrinsic motility dictates the propensity of mammary fibroblast-induced invasion:

During breast cancer progression, the stroma undergoes drastic changes to confer tumor growth and invasion. These changes in the microenvironment elicit pro-growth and pro-invasion responses in the cancer cells. One important component in the tumor microenvironment is the mammary fibroblast.

Transformed fibroblasts are called cancer-associated fibroblasts, CAFs or myofibroblasts. The origin of CAFs is resident fibroblasts that are transformed by signaling from the cancer cells, specifically the secretion of TGFbeta1 (21, 22). In turn, CAFs can secrete pro-growth factors such as HGF and induce angiogenesis with VEGF and SDF-1 (21, 23). In our system, conditioned media from the mammary fibroblasts was not sufficient to induce invasion. This is not surprisingly since Camp et al have shown that fibroblasts induce different gene expression patterns on breast cancer cells if cultured in direct or indirect contact with the epithelial cells (63).

CAFs are present and align with the invasive front in breast cancer patient tumors(55, 56). Squamous cell carcinomas (SCC), which are not particularly invasive, can be induced to invade

into the modeled stroma by fibroblasts. Fibroblasts can induce invasion by reorganizing the modeled ECM, forming tracks, which the SCC cells can follow (24). In our studies we find that the mammary fibroblasts must be able to reorganize the collagen-I in the modeled stroma to precede the basal-subtype breast cancer cells for invasion.

What is innovative about our study is that, even if the collagen-I has been reorganized by the mammary fibroblasts, breast cancer invasion may not occur. This lack of invasion is seen through the co-culturing of mammary fibroblasts with luminal-subtype breast cancer cells. The absence of invasion in a reorganized ECM was due to the fact that the luminal-subtype breast cancer cells were non-motile. Whereas, the basal-subtype breast cancer cells were very motile within the spheroid and it is the motile cells that eventually take advantage of the collagen-I tracks formed by the mammary fibroblasts to invade into the modeled ECM.

Prevention of invasion in the presence of mammary fibroblasts at the tumor site can occur if we target the migration ability of the breast cancer cells. In our studies we have achieved this by inhibiting ERK1/2 signaling. ERK1/2 signaling is elevated during breast cancer progression and it has been shown to induce motility in a non-motile setting (59, 60). Though inhibition of ERK1/2 signaling was able to reduce breast cancer cell invasion in vivo and in vitro, it was not able to inhibit the reorganization of the microenvironment by the mammary fibroblasts. Inhibition of mammary fibroblasts' ability to reorganize the ECM occurs through the application of a Rho inhibitor or through the knockdown of Cdc42 (24).

Based on our data and previous studies, we have come with a model of mammary fibroblast induced invasion (Fig 5-1). This model can explain in part how patients with triple negative breast cancer (basal-subtype) have a poor prognosis than those with amplification of the ER and PR receptors (luminal subtype). This project then opens up to avenues for further

investigations: 1) mammary fibroblast function during breast cancer progression and 2) breast cancer motility.

Shown here and in other studies is that the microenvironment needs to be primed preceding breast cancer cell invasion. Cancer cells can convert fibroblasts to CAFs through the secretion of TGFbeta1 (21, 22). The first step in the transformation of fibroblasts to CAFs is the recruitment of the fibroblasts to the cancerous site. Therefore, identifying how breast cancer cells signal for mammary fibroblasts to migrate to the tumor may reveal a vulnerability in cancer progression. To determine if a secreted factor(s) from the breast cancer is sufficient to induce migration in the mammary fibroblasts, we can do a transwell migration assay where the conditioned media from breast cancer cells would be used as the chemoattractant. The mammary fibroblasts would need to migrate from the upper chamber and through a collagen-I plug to the lower chamber. Plating a collagen-I plug for which fibroblasts must migrate through would mimic in vivo conditions. If conditioned media from the breast cancer cells was sufficient to induce migration of the mammary fibroblasts, we can conduct mass spectrometry to determine the composition of the secretions. After identifying the secreted factors, we can screen and identify which secreted factor(s) is sufficient for migration. It would be interesting to see if different breast cancer subtypes would induce different rates of migration in mammary fibroblasts. If the conditioned media from the breast cancer cells is insufficient to induce migration, perhaps the breast cancer signal for fibroblast recruitment goes through an intermediary such as macrophages. Another explanation is that the fibroblasts must elicit the breast cancer cells to secrete pro-migratory factors.

Once at the cancer site mammary fibroblasts need to reorganize the ECM to induce invasion. Determining how mammary fibroblasts reorganize the collagen around the lesion is

important. Levental, et al suggested that the enzyme lysyl oxidase can reorganize collagen. It is suggested that the stroma produces this enzyme, yet the exact cell source is unknown (37). We can first determine if fibroblasts express lysyl oxidase. If fibroblasts do express lysyl oxidase, we can determine if its expression in the fibroblasts is required for breast cancer cell invasion. Again we can conduct mass spectrometry on fibroblast-conditioned media to identify which novel enzymes that may reorganize the ECM.

However, if the microenvironment has been reorganized at the point of tumor detection, the next line of defense is to target the breast cancer cells. Determining how breast cancer cells gain migratory ability can prevent invasion into the stroma. Since we have shown that motility is a pre-existing state before the reorganization of the modeled stroma, our next endeavor is to discover novel regulators of cell motility.

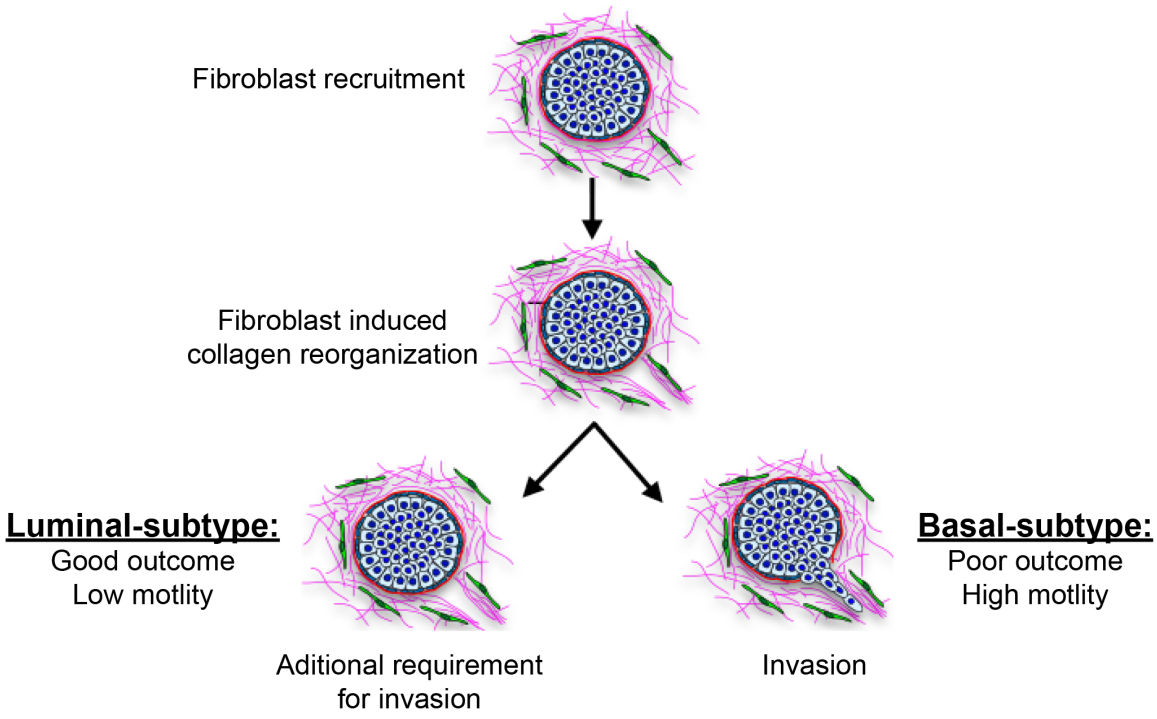

Figure 5-1: Model of mammary fibroblast induced-invasion. Collagen-I (extracellular matrix, pink), fibroblasts (green), basement membrane (red), neoplastic epithelium (blue), and myoepithelial cells (cyan).

Identification of novel regulators of breast cancer cell motility:

To identify novel regulators of breast cancer cell motility, we conducted a miRNA screen with a wounding assay as a readout of migration. From this screen we found 53 miRNAs that enhanced wound closure. To prioritize the follow-up we looked at the endogenous expression of enhancer miRNAs in matched tumor and normal breast cancer patient samples. MiR614 and miR1276 were up regulated upon tumorigenesis and were found to increase migration in our wounding assay. Neither of these genes has been connected to cancer progression.

However, in spontaneous cell motility and transwell assays we found that only miR614 can increase cell motility. This differential cell motility shows that our screen was able to detect two different motility programs. To identify the targets of miR614 regulated motility, we compared the gene expression of MCFDCIS and MDA-MB-231 cells transfected with miR614. MCFDCIS cells are capable of collective cell migration while MDA-MB-231 cells are capable of single cell migration. After conducting a small screen of common miR614 targets, we found that the loss of RhoT1 or TapT1 was sufficient to induce collective cell migration.

Desai, et al has found that during cell migration mitochondria localizes in the anterior front of the migrating cells in microfluidic channels. It has been suggested that mitochondria congregate toward areas where energy is needed most such as the motile front (106). Loss of RhoT1 leads to mitochondria unable to move to the anterior in gradient induced migration. The mis-compartmentalization of the mitochondria correlated to a slower and more random motility (69, 106).

On the surface, our data contradict that loss of RhoT1 leads to decrease in migration. However, investigations showing that RhoT1 loss led to decrease migration were done with single-cell assays such as microfluidic channels and in cells that migrate/invade using a single

cell motility program (leukocytes and MDA-MB-231). Here we show that in MCFDCIS, collective cell migration enhances upon RhoT1 knockdown. Therefore, it would be interesting to determine if in collective cell migration, mitochondrial placement does not have an effect on motility. To test this we could treat our wounding assays with MitoTracker to label the mitochondria and conduct a real-time imaging of wound closure. We can also test if loss other proteins that are involved in mitochondrial displacement can increase cell motility such as Milton, a binding partner of RhoT1 (68).

There is little known about the function of TapT1 in cancer. TapT1 have been implicated in the proper formation of the axial skeletal system and seem to be a cell surface receptor (70). However, its ligand is unknown. To understand how TapT1 contributes to cancer progression, we can stain for TapT1 expression in normal, DCIS, and invasive breast cancer. If TapT1 is a negative regulator of motility, it would be interesting to see if overexpression of TapT1 can inhibit collective cell migration. Since there is nothing known about TapT1 signaling, we can overexpress the protein and conduct an immunoprecipitation, IP and mass spectrometry for binding partners of TapT1.

As shown previously, miR1276 can only increase the motility of breast cancer cells in response to a wounding stimulus. We can conduct a small spontaneous motility screen of the remaining enhancer miRNAs to determine if there are other miRNAs that enhance wound closure but not spontaneous motility. By doing a gene expression microarray we can find overlapping targets of miR1276 and phenocopying miRNAs. The resulting gene list would identify a novel motility program.

P63 regulated motility program:

To prioritize the miRNAs in our screen, we looked at the endogenous miRNA expression levels in non-motile and motile cells. MiR203a was found to be highly expressed in the non-motile cells and was inhibitory in collective cell migration. Gene expression microarray of motile cells transfected with miR203a showed that p63 and miR205 to be down regulated. It has been shown that miR203a can target p63 and suppress its expression (96, 97). It has also been shown that p63 can induce the expression of miR205 (99). However, this is the first time where it has been shown that miR203a can down regulate miR205 through p63 expression.

P63 was required for collective-cell migration. MiR205 was one of the enhancer of wound migration in the screen and was highly expressed in the motile cell line. However, miR205 was not sufficient to sustain cell migration in a p63 knockdown condition. Gene expression analyses of non-motile and motile conditions, led us to investigate Axl and Slug as possible targets of p63 regulation. Both were required for cell migration but neither was sufficient to sustain cell migration under p63 loss. Therefore, miR205, Axl, and Slug work in concert to regulate cell migration in a p63 regulated motility program. Based on our data we have generated a model of p63 regulated motility program (Fig 5-2).

We have shown that p63 expression is required for collective cell migration. However, the mechanism by which p63 expression is induced is unclear. To determine how p63's expression can be induced we can conduct a DNA pull down in the promoter region of p63 and mass spectrometry to determine the proteins that bind in the p63 promoter region.

P63 is not required for all breast cancer cell motility. MDA-MB-231 cells are motile and can metastasis in vivo. However, overexpression of miR205 inhibits cell migration and metastasis (107). It would be interesting if overexpression of p63 or its motility regulated targets

such as Axl or Slug can act as a negative regulator of cell migration in this claudin-low background. In addition SUM149, a basal-subtype breast cancer cell line is motile and yet it does not seem to express p63 (data not shown). Therefore, not all motile basal-subtype breast cancer cells require p63 for motility. However, the overexpression of miR205 was able to increase the motility of SUM149 (data not shown). It would be interesting to see if overexpression of p63 in the SUM149 would cause an increase or a decrease in cell motility.

This is the first time where it has been shown that p63 is required for Slug and Axl expression. We have shown that p63 can regulate Axl expression through direct binding in the Axl promoter. Osada et al have also seen that p63 can pull down Axl chromatin (101). However, we have been able to pinpoint the binding area down to ~150 base pairs. To determine if p63 is sufficient to induce the expression of Axl, we can fuse the Axl promoter region to a luciferase gene and see if p63 can drive the expression of luciferase. By mutating the Axl promoter, we can also pinpoint the exact sequence that p63 utilize to regulate Axl expression.

Slug was sufficient to induce breast cancer cell invasion in vivo. The next endeavor is to identify which Slug target(s) is responsible for the increase in motility. To determine direct targets of Slug we can conduct a ChIP-Seq to identify genes that Slug binds to. Using gene expression microarrays of motile cells treated with Slug siRNAs, we can determine which genes require Slug expression. Combining the ChIP-Seq and gene expression microarrays we can prioritize Slug targets.

Based on published keratinocyte ChIP-Seq data, there was no obvious p63 binding of Slug's promoter region (102, 103). Currently we are conducting a ChIP-Seq with p63 in our MCFDCIS cells to determine if in our system does p63 bind to the Slug promoter to regulate its expression. If p63 could not pull down Slug chromatin, we can conduct a DNA pull down of

Slug's promoter region. From the DNA pull down we can compare those transcription factors to genes that require p63 expression from our gene expression microarray.

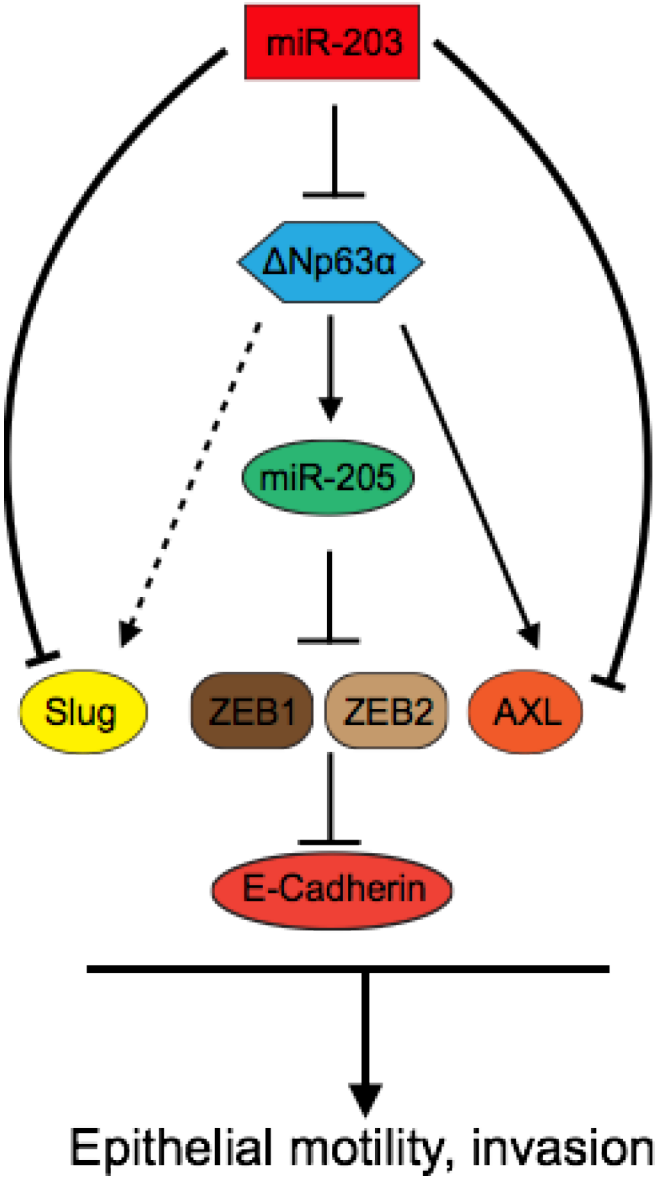

Figure 5-2: Schematic of p63 regulated motility program.

Appendix A: Dharmacon miRNA mimics screen sequences

Dharmacon miRIDIAN® microRNA Library - Human Mimic		
CS-001010 Lot 09167		
Catalog Number	**Mature Sanger ID**	**Mature Sequence**
C-300879-01	hsa-miR-561	CAAAGUUUAAGAUCCUUGAAGU
C-301123-01	hsa-miR-615-5p	GGGGGUCCCCGGUGCUCGGAUC
C-301117-01	hsa-miR-589	UGAGAACCACGUCUGCUCUGAG
C-300597-07	hsa-miR-128	UCACAGUGAACCGGUCUCUUU
C-300875-01	hsa-miR-557	GUUUGCACGGGUGGGCCUUGUCU
C-301168-01	hsa-miR-500	UAAUCCUUGCUACCUGGGUGAGA
C-301282-01	hsa-miR-1225-3p	UGAGCCCCUGUGCCGCCCCCAG
C-301364-00	hsa-miR-1305	UUUUCAACUCUAAUGGGAGAGA
C-300919-01	hsa-miR-595	GAAGUGUGCCGUGGUGUGUCU
C-300877-01	hsa-miR-559	UAAAGUAAAUAUGCACCAAAA
C-301213-01	hsa-miR-891a	UGCAACGAACCUGAGCCACUGA
C-301093-01	hsa-miR-193b*	CGGGGUUUUGAGGGCGAGAUGA
C-301160-01	hsa-miR-374a*	CUUAUCAGAUUGUAUUGUAAUU
C-301030-01	hsa-miR-92a-1*	AGGUUGGGAUCGGUUGCAAUGCU
C-301066-01	hsa-miR-146a*	CCUCUGAAAUUCAGUUCUUCAG
C-300551-07	hsa-miR-34a	UGGCAGUGUCUUAGCUGGUUGU
C-301020-01	hsa-miR-19a*	AGUUUUGCAUAGUUGCACUACA
C-300746-03	hsa-miR-486-5p	UCCUGUACUGAGCUGCCCCGAG
C-301045-01	hsa-miR-30b*	CUGGGAGGUGGAUGUUUACUUC
C-300618-05	hsa-miR-9	UCUUUGGUUAUCUAGCUGUAUGA
C-300931-01	hsa-miR-606	AAACUACUGAAAAUCAAAGAU
C-301116-01	hsa-miR-548b-5p	AAAAGUAAUUGUGGUUUUGGCC
C-301245-01	hsa-miR-887	GUGAACGGGCGCCAUCCCGAGG
C-300680-03	hsa-miR-373	GAAGUGCUUCGAUUUUGGGGUGU
C-300864-03	hsa-miR-363*	CGGGUGGAUCACGAUGCAAUUU
C-301467-00	hsa-miR-2113	AUUUGUGCUUGGCUCUGUCAC
C-301351-00	hsa-miR-1299	UUCUGGAAUUCUGUGUGAGGGA
C-300724-07	hsa-miR-450a	UUUUGCGAUGUGUUCCUAAUAU
C-301256-01	hsa-miR-921	CUAGUGAGGGACAGAACCAGGAUUC
C-300509-07	hsa-miR-33a	GUGCAUUGUAGUUGCAUUGCA
C-301218-01	hsa-miR-220b	CCACCACCGUGUCUGACACUU
C-301100-01	hsa-miR-518d-5p	CUCUAGAGGGAAGCACUUUCUG
C-301259-01	hsa-miR-924	AGAGUCUUGUGAUGUCUUGC
C-301235-01	hsa-miR-876-5p	UGGAUUUCUUUGUGAAUCACCA

C-300796-05	hsa-miR-518f	GAAAGCGCUUCUCUUUAGAGG
C-300633-03	hsa-miR-154	UAGGUUAUCCGUGUUGCCUUCG
C-300754-03	hsa-miR-146b-5p	UGAGAACUGAAUUCCAUAGGCU
C-301292-01	hsa-miR-1236	CCUCUUCCCCUUGUCUCUCCAG
C-300862-01	hsa-miR-487b	AAUCGUACAGGGUCAUCCACUU
C-300707-07	hsa-miR-339-5p	UCCCUGUCCUCCAGGAGCUCACG
C-301164-01	hsa-miR-302d*	ACUUUAACAUGGAGGCACUUGC
C-300947-01	hsa-miR-621	GGCUAGCAACAGCGCUUACCU
C-301181-01	hsa-miR-32*	CAAUUUAGUGUGUGUGAUAUUU
C-301070-01	hsa-miR-200c*	CGUCUUACCCAGCAGUGUUUGG
C-300764-05	hsa-miR-193b	AACUGGCCCUCAAAGUCCCGCU
C-300639-03	hsa-miR-190	UGAUAUGUUUGAUAUAUUAGGU
C-301470-00	hsa-miR-1973	ACCGUGCAAAGGUAGCAUA
C-300795-05	hsa-miR-518f*	CUCUAGAGGGAAGCACUUUCUC
C-300602-03	hsa-miR-135a	UAUGGCUUUUUAUUCCUAUGUGA
C-301427-00	hsa-miR-1255b	CGGAUGAGCAAAGAAAGUGGUU
C-300656-03	hsa-miR-299-3p	UAUGUGGGAUGGUAAACCGCUU
C-300482-03	hsa-miR-15a	UAGCAGCACAUAAUGGUUUGUG
C-300748-05	hsa-miR-488*	CCCAGAUAAUGGCACUCUCAA
C-301175-01	hsa-miR-106b*	CCGCACUGUGGGUACUUGCUGC
C-301180-01	hsa-miR-16-2*	CCAAUAUUACUGUGCUGCUUUA
C-301209-01	hsa-miR-671-3p	UCCGGUUCUCAGGGCUCCACC
C-301111-01	hsa-miR-556-3p	AUAUUACCAUUAGCUCAUCUUU
C-301031-01	hsa-miR-99a*	CAAGCUCGCUUCUAUGGGUCUG
C-300972-01	hsa-miR-645	UCUAGGCUGGUACUGCUGA
C-301009-01	hsa-miR-802	CAGUAACAAAGAUUCAUCCUUGU
C-301179-01	hsa-miR-29c*	UGACCGAUUUCUCCUGGUGUUC
C-300942-01	hsa-miR-548c-3p	CAAAAAUCUCAAUUACUUUUGC
C-301018-01	hsa-miR-15a*	CAGGCCAUAUUGUGCUGCCUCA
C-300640-05	hsa-miR-193a-3p	AACUGGCCUACAAAGUCCCAGU
C-300861-05	hsa-miR-545	UCAGCAAACAUUUAUUGUGUGC
C-301202-01	hsa-miR-181a-2*	ACCACUGACCGUUGACUGUACC
C-300675-03	hsa-miR-369-3p	AAUAAUACAUGGUUGAUCUUU
C-301264-01	hsa-miR-935	CCAGUUACCGCUUCCGCUACCGC
C-301433-00	hsa-miR-1306	ACGUUGGCUCUGGUGGUG
C-300671-05	hsa-miR-302c	UAAGUGCUUCCAUGUUUCAGUGG
C-301212-01	hsa-miR-298	AGCAGAAGCAGGGAGGUUCUCCCA
C-301192-01	hsa-miR-185*	AGGGGCUGGCUUUCCUCUGGUC
C-301439-00	hsa-miR-1324	CCAGACAGAAUUCUAUGCACUUUC
C-300638-07	hsa-miR-188-5p	CAUCCCUUGCAUGGUGGAGGG
C-301397-00	hsa-miR-1268	CGGGCGUGGUGGUGGGGG

C-300989-01	hsa-miR-655	AUAAUACAUGGUUAACCUCUUU
C-300631-07	hsa-miR-149	UCUGGCUCCGUGUCUUCACUCCC
C-301001-01	hsa-miR-668	UGUCACUCGGCUCGGCCCACUAC
C-301254-01	hsa-miR-208b	AUAAGACGAACAAAAGGUUUGU
C-301230-01	hsa-miR-541	UGGUGGGCACAGAAUCUGGACU
C-300505-03	hsa-miR-30a	UGUAAACAUCCUCGACUGGAAG
C-301446-00	hsa-miR-1468	CUCCGUUUGCCUGUUUCGCUG
C-301017-01	hsa-let-7e*	CUAUACGGCCUCCUAGCUUUCC
C-301233-01	hsa-miR-875-5p	UAUACCUCAGUUUUAUCAGGUG
C-301412-00	hsa-miR-548p	UAGCAAAAACUGCAGUUACUUU
C-300652-07	hsa-miR-302a*	ACUUAAACGUGGAUGUACUUGCU
C-301443-00	hsa-miR-1825	UCCAGUGCCCUCCUCUCC
C-300823-03	hsa-miR-516-3p	UGCUUCCUUUCAGAGGGU
C-300676-05	hsa-miR-370	GCCUGCUGGGGUGGAACCUGGU
C-300592-05	hsa-miR-124	UAAGGCACGCGGUGAAUGCC
C-300691-03	hsa-miR-382	GAAGUUGUUCGUGGUGGAUUCG
C-300550-07	hsa-miR-10b	UACCCUGUAGAACCGAAUUUGUG
C-301377-00	hsa-miR-1250	ACGGUGCUGGAUGUGGCCUUU
C-300777-03	hsa-miR-519e*	UUCUCCAAAAGGGAGCACUUUC
C-300697-05	hsa-miR-337-3p	CUCCUAUAUGAUGCCUUUCUUC
C-301462-00	hsa-miR-1913	UCUGCCCCCUCCGCUGCUGCCA
C-301108-01	hsa-miR-194*	CCAGUGGGGCUGCUGUUAUCUG
C-300515-05	hsa-miR-98	UGAGGUAGUAAGUUGUAUUGUU
C-300870-01	hsa-miR-553	AAAACGGUGAGAUUUUGUUUU
C-300902-01	hsa-miR-583	CAAAGAGGAAGGUCCCAUUAC
C-300967-01	hsa-miR-640	AUGAUCCAGGAACCUGCCUCU
C-301130-01	hsa-miR-33b*	CAGUGCCUCGGCAGUGCAGCCC
C-301215-01	hsa-miR-886-3p	CGCGGGUGCUUACUGACCCUU
C-301125-01	hsa-miR-548c-5p	AAAAGUAAUUGCGGUUUUUGCC
C-301080-01	hsa-miR-379*	UAUGUAACAUGGUCCACUAACU
C-300683-03	hsa-miR-376a	AUCAUAGAGGAAAAUCCACGU
C-300828-05	hsa-miR-518a-3p	GAAAGCGCUUCCCUUUGCUGGA
C-301065-01	hsa-miR-138-1*	GCUACUUCACAACACCAGGGCC
C-300982-01	hsa-miR-662	UCCCACGUUGUGGCCCAGCAG
C-300487-05	hsa-miR-18a	UAAGGUGCAUCUAGUGCAGAUAG
C-301330-00	hsa-miR-663b	GGUGGCCCGGCCGUGCCUGAGG
C-300923-01	hsa-miR-599	GUUGUGUCAGUUUAUCAAAC
C-300948-01	hsa-miR-622	ACAGUCUGCUGAGGUUGGAGC
C-300956-01	hsa-miR-630	AGUAUUCUGUACCAGGGAAGGU
C-300672-05	hsa-miR-302d	UAAGUGCUUCCAUGUUUGAGUGU
C-300662-05	hsa-miR-30e*	CUUUCAGUCGGAUGUUUACAGC

C-300660-05	hsa-miR-130b	CAGUGCAAUGAUGAAAGGGCAU
C-300871-01	hsa-miR-554	GCUAGUCCUGACUCAGCCAGU
C-300941-01	hsa-miR-616*	ACUCAAAACCCUUCAGUGACUU
C-300599-06	hsa-miR-132	UAACAGUCUACAGCCAUGGUCG
C-300655-03	hsa-miR-34c-5p	AGGCAGUGUAGUUAGCUGAUUGC
C-300698-05	hsa-miR-323-3p	CACAUUACACGGUCGACCUCU
C-301196-01	hsa-miR-130b*	ACUCUUUCCCUGUUGCACUAC
C-301407-00	hsa-miR-1275	GUGGGGGAGAGGCUGUC
C-301429-00	hsa-miR-1280	UCCCACCGCUGCCACCC
C-301084-01	hsa-miR-337-5p	GAACGGCUUCAUACAGGAGUU
C-300556-03	hsa-miR-181c	AACAUUCAACCUGUCGGUGAGU
C-301043-01	hsa-let-7g*	CUGUACAGGCCACUGCCUUGC
C-300863-05	hsa-miR-542-5p	UCGGGGAUCAUCAUGUCACGAGA
C-301153-01	hsa-miR-214*	UGCCUGUCUACACUUGCUGUGC
C-300649-05	hsa-miR-106b	UAAAGUGCUGACAGUGCAGAU
C-300615-07	hsa-miR-153	UUGCAUAGUCACAAAAGUGAUC
C-300491-03	hsa-miR-20a	UAAAGUGCUUAUAGUGCAGGUAG
C-300975-01	hsa-miR-648	AAGUGUGCAGGGCACUGGU
C-300577-05	hsa-miR-220a	CCACACCGUAUCUGACACUUU
C-300905-01	hsa-miR-548a-3p	CAAAACUGGCAAUUACUUUUGC
C-301086-01	hsa-miR-151-5p	UCGAGGAGCUCACAGUCUAGU
C-301151-01	hsa-miR-149*	AGGGAGGGACGGGGGCUGUGC
C-301076-01	hsa-miR-296-3p	GAGGGUUGGGUGGAGGCUCUCC
C-300856-05	hsa-miR-455-5p	UAUGUGCCUUUGGACUACAUCG
C-301112-01	hsa-miR-551b*	GAAAUCAAGCGUGGGUGAGACC
C-300659-03	hsa-miR-296-5p	AGGGCCCCCCCUCAAUCCUGU
C-301311-00	hsa-miR-1323	UCAAAACUGAGGGGCAUUUUCU
C-300929-01	hsa-miR-604	AGGCUGCGGAAUUCAGGAC
C-300868-01	hsa-miR-551a	GCGACCCACUCUUGGUUUCCA
C-300881-01	hsa-miR-563	AGGUUGACAUACGUUUCCC
C-301465-00	hsa-miR-1915	CCCCAGGGCGACGCGGCGGG
C-300766-05	hsa-miR-181d	AACAUUCAUUGUUGUCGGUGGGU
C-300987-01	hsa-miR-411	UAGUAGACCGUAUAGCGUACG
C-301237-01	hsa-miR-708*	CAACUAGACUGUGAGCUUCUAG
C-301309-00	hsa-miR-320c	AAAAGCUGGGUUGAGAGGGU
C-301110-01	hsa-miR-92b*	AGGGACGGGACGCGGUGCAGUG
C-300738-05	hsa-miR-409-3p	GAAUGUUGCUCGGUGAACCCCU
C-301389-00	hsa-miR-1262	AUGGGUGAAUUUGUAGAAGGAU
C-301473-00	hsa-miR-1976	CCUCCUGCCCUCCUUGCUGU
C-300855-05	hsa-miR-18a*	ACUGCCCUAAGUGCUCCUUCUGG
C-300625-05	hsa-miR-126*	CAUUAUUACUUUUGGUACGCG

C-301344-00	hsa-miR-1290	UGGAUUUUUGGAUCAGGGA
C-300661-07	hsa-miR-30e	UGUAAACAUCCUUGACUGGAAG
C-300847-05	hsa-miR-507	UUUUGCACCUUUUGGAGUGAA
C-300573-05	hsa-miR-218	UUGUGCUUGAUCUAACCAUGU
C-301475-00	hsa-miR-1978	GGUUUGGUCCUAGCCUUUCUA
C-301075-01	hsa-miR-99b*	CAAGCUCGUGUCUGUGGGUCCG
C-300586-05	hsa-miR-1	UGGAAUGUAAAGAAGUAUGUAU
C-300713-05	hsa-miR-384	AUUCCUAGAAAUUGUUCAUA
C-301174-01	hsa-miR-20b*	ACUGUAGUAUGGGCACUUCCAG
C-300688-03	hsa-miR-380*	UGGUUGACCAUAGAACAUGCGC
C-300993-01	hsa-miR-658	GGCGGAGGGAAGUAGGUCCGUUGGU
C-300629-03	hsa-miR-136	ACUCCAUUUGUUUUGAUGAUGGA
C-301278-01	hsa-miR-1224-3p	CCCCACCUCCUCUCUCCUCAG
C-301289-01	hsa-miR-1231	GUGUCUGGGCGGACAGCUGC
C-300859-01	hsa-miR-539	GGAGAAAUUAUCCUUGGUGUGU
C-300793-05	hsa-miR-525-3p	GAAGGCGCUUCCCUUUAGAGCG
C-300565-03	hsa-miR-210	CUGUGCGUGUGACAGCGGCUGA
C-300832-03	hsa-miR-517c	AUCGUGCAUCCUUUUAGAGUGU
C-300701-07	hsa-miR-135b	UAUGGCUUUUCAUUCCUAUGUGA
C-300991-01	hsa-miR-549	UGACAACUAUGGAUGAGCUCU
C-300965-01	hsa-miR-638	AGGGAUCGCGGGCGGGUGGCGGCCU
C-300692-03	hsa-miR-383	AGAUCAGAAGGUGAUUGUGGCU
C-301071-01	hsa-miR-155*	CUCCUACAUAUUAGCAUUAACA
C-301340-00	hsa-miR-1286	UGCAGGACCAAGAUGAGCCCU
C-300579-07	hsa-miR-222	AGCUACAUCUGGCUACUGGGU
C-301366-00	hsa-miR-548f	AAAAACUGUAAUUACUUUU
C-300960-01	hsa-miR-633	CUAAUAGUAUCUACCACAAUAAA
C-301318-00	hsa-miR-1298	UUCAUUCGGCUGUCCAGAUGUA
C-300894-01	hsa-miR-575	GAGCCAGUUGGACAGGAGC
C-301451-00	hsa-miR-1538	CGGCCCGGGCUGCUGCUGUUCCU
C-300763-05	hsa-miR-496	UGAGUAUUACAUGGCCAAUCUC
C-301099-01	hsa-miR-518a-5p	CUGCAAAGGGAAGCCCUUUC
C-301166-01	hsa-miR-509-5p	UACUGCAGACAGUGGCAAUCA
C-300811-05	hsa-miR-517a	AUCGUGCAUCCCUUUAGAGUGU
C-301479-00	hsa-miR-2054	CUGUAAUAUAAAUUUAAUUUAUU
C-300501-07	hsa-miR-26b	UUCAAGUAAUUCAGGAUAGGU
C-300690-03	hsa-miR-381	UAUACAAGGGCAAGCUCUCUGU
C-300867-01	hsa-miR-532-5p	CAUGCCUUGAGUGUAGGACCGU
C-301073-01	hsa-miR-34b	CAAUCACUAACUCCACUGCCAU
C-301205-01	hsa-miR-148a*	AAAGUUCUGAGACACUCCGACU
C-301432-00	hsa-miR-664	UAUUCAUUUAUCCCCAGCCUACA

C-300804-03	hsa-miR-518c*	UCUCUGGAGGGAAGCACUUUCUG
C-300834-05	hsa-miR-522	AAAAUGGUUCCCUUUAGAGUGU
C-301139-01	hsa-miR-19b-2*	AGUUUUGCAGGUUUGCAUUUCA
C-301380-00	hsa-miR-1254	AGCCUGGAAGCUGGAGCCUGCAGU
C-301452-00	hsa-miR-1539	UCCUGCGCGUCCCAGAUGCCC
C-300485-05	hsa-miR-17	CAAAGUGCUUACAGUGCAGGUAG
C-301127-01	hsa-miR-625*	GACUAUAGAACUUUCCCCCUCA
C-301083-01	hsa-miR-342-5p	AGGGGUGCUAUCUGUGAUUGA
C-300516-03	hsa-miR-99a	AACCCGUAGAUCCGAUCUUGUG
C-301146-01	hsa-miR-15b*	CGAAUCAUUAUUUGCUGCUCUA
C-300488-03	hsa-miR-19a	UGUGCAAAUCUAUGCAAAACUGA
C-301194-01	hsa-miR-362-3p	AACACACCUAUUCAAGGAUUCA
C-301253-01	hsa-miR-216b	AAAUCUCUGCAGGCAAAUGUGA
C-300645-05	hsa-miR-320a	AAAAGCUGGGUUGAGAGGGCGA
C-301250-01	hsa-miR-374b	AUAUAAUACAACCUGCUAAGUG
C-300478-07	hsa-let-7d	AGAGGUAGUAGGUUGCAUAGUU
C-301468-00	hsa-miR-1204	UCGUGGCCUGGUCUCCAUUAU
C-300981-01	hsa-miR-661	UGCCUGGGUCUCUGGCCUGCGCGU
C-301287-01	hsa-miR-1228*	GUGGGCGGGGGCAGGUGUGUG
C-300665-05	hsa-miR-363	AAUUGCACGGUAUCCAUCUGUA
C-301162-01	hsa-miR-331-5p	CUAGGUAUGGUCCCAGGGAUCC
C-300908-01	hsa-miR-548b-3p	CAAGAACCUCAGUUGCUUUUGU
C-301238-01	hsa-miR-708	AAGGAGCUUACAAUCUAGCUGGG
C-300739-03	hsa-miR-412	ACUUCACCUGGUCCACUAGCCGU
C-301222-01	hsa-miR-450b-3p	UUGGGAUCAUUUUGCAUCCAUA
C-301286-01	hsa-miR-1228	UCACACCUGCCUCGCCCCCC
C-300669-05	hsa-miR-302b	UAAGUGCUUCCAUGUUUUAGUAG
C-300886-01	hsa-miR-568	AUGUAUAAAUGUAUACACAC
C-301270-01	hsa-miR-941	CACCCGGCUGUGUGCACAUGUGC
C-301231-01	hsa-miR-541*	AAAGGAUUCUGCUGUCGGUCCCACU
C-300865-03	hsa-miR-376a*	GUAGAUUCUCCUUCUAUGAGUA
C-300737-05	hsa-miR-409-5p	AGGUUACCCGAGCAACUUUGCAU
C-300874-03	hsa-miR-556-5p	GAUGAGCUCAUUGUAAUAUGAG
C-300730-03	hsa-miR-433	AUCAUGAUGGGCUCCUCGGUGU
C-300786-03	hsa-miR-519c-3p	AAAGUGCAUCUUUUUAGAGGAU
C-301469-00	hsa-miR-1972	UCAGGCCAGGCACAGUGGCUCA
C-300634-03	hsa-miR-154*	AAUCAUACACGGUUGACCUAUU
C-301121-01	hsa-miR-593	UGUCUCUGCUGGGGUUUCU
C-301126-01	hsa-miR-624	CACAAGGUAUUGGUAUUACCU
C-300792-03	hsa-miR-525-5p	CUCCAGAGGGAUGCACUUUCU
C-300722-05	hsa-miR-429	UAAUACUGUCUGGUAAAACCGU

C-300980-01	hsa-miR-548d-3p	CAAAAACCACAGUUUCUUUUGC
C-300492-03	hsa-miR-21	UAGCUUAUCAGACUGAUGUUGA
C-300839-05	hsa-miR-501-5p	AAUCCUUUGUCCCUGGGUGAGA
C-301055-01	hsa-miR-140-3p	UACCACAGGGUAGAACCACGG
C-301394-00	hsa-miR-548o	CCAAAACUGCAGUUACUUUUGC
C-301015-03	hsa-miR-675	UGGUGCGGAGAGGGCCCACAGUG
C-301386-00	hsa-miR-1260	AUCCCACCUCUGCCACCA
C-300613-05	hsa-miR-145	GUCCAGUUUUCCCAGGAAUCCCU
C-301382-00	hsa-miR-1256	AGGCAUUGACUUCUCACUAGCU
C-300840-05	hsa-miR-502-5p	AUCCUUGCUAUCUGGGUGCUA
C-301430-00	hsa-miR-1308	GCAUGGGUGGUUCAGUGG
C-301293-01	hsa-miR-1237	UCCUUCUGCUCCGUCCCCCAG
C-301379-00	hsa-miR-1253	AGAGAAGAAGAUCAGCCUGCA
C-300699-03	hsa-miR-326	CCUCUGGGCCCUUCCUCCAG
C-300962-01	hsa-miR-635	ACUUGGGCACUGAAACAAUGUCC
C-301350-00	hsa-miR-1297	UUCAAGUAAUUCAGGUG
C-300916-01	hsa-miR-592	UUGUGUCAAUAUGCGAUGAUGU
C-300951-03	hsa-miR-625	AGGGGGAAAGUUCUAUAGUCC
C-301098-01	hsa-miR-518e*	CUCUAGAGGGAAGCGCUUUCUG
C-301078-01	hsa-miR-371-5p	ACUCAAACUGUGGGGGCACU
C-300720-05	hsa-miR-20b	CAAAGUGCUCAUAGUGCAGGUAG
C-300682-05	hsa-miR-375	UUUGUUCGUUCGGCUCGCGUGA
C-300946-01	hsa-miR-620	AUGGAGAUAGAUAUAGAAAU
C-301408-00	hsa-miR-1276	UAAAGAGCCCUGUGGAGACA
C-301294-01	hsa-miR-1238	CUUCCUCGUCUGUCUGCCCC
C-300846-05	hsa-miR-506	UAAGGCACCCUUCUGAGUAGA
C-301279-01	hsa-miR-877	GUAGAGGAGAUGGCGCAGGG
C-300646-05	hsa-miR-200c	UAAUACUGCCGGGUAAUGAUGGA
C-301079-01	hsa-miR-377*	AGAGGUUGCCCUUGGUGAAUUC
C-300818-03	hsa-miR-520g	ACAAAGUGCUUCCCUUUAGAGUGU
C-300986-03	hsa-miR-653	GUGUUGAAACAAUCUCUACUG
C-300587-05	hsa-miR-15b	UAGCAGCACAUCAUGGUUUACA
C-301206-01	hsa-miR-96*	AAUCAUGUGCAGUGCCAAUAUG
C-300955-01	hsa-miR-629*	GUUCUCCCAACGUAAGCCCAGC
C-301161-01	hsa-miR-335*	UUUUUCAUUAUUGCUCCUGACC
C-300963-03	hsa-miR-636	UGUGCUUGCUCGUCCCGCCCGCA
C-300496-05	hsa-miR-24	UGGCUCAGUUCAGCAGGAACAG
C-300997-01	hsa-miR-425	AAUGACACGAUCACUCCCGUUGA
C-301333-00	hsa-miR-1207-5p	UGGCAGGGAGGCUGGGAGGGG
C-300528-03	hsa-miR-192	CUGACCUAUGAAUUGACAGCC
C-300740-03	hsa-miR-410	AAUAUAACACAGAUGGCCUGU

C-301387-00	hsa-miR-548g	AAAACUGUAAUUACUUUUGUAC
C-300858-03	hsa-miR-493	UGAAGGUCUACUGUGUGCCAGG
C-301402-00	hsa-miR-1274a	GUCCCUGUUCAGGCGCCA
C-300964-01	hsa-miR-637	ACUGGGGGCUUUCGGGCUCUGCGU
C-300873-01	hsa-miR-555	AGGGUAAGCUGAACCUCUGAU
C-300841-05	hsa-miR-503	UAGCAGCGGGAACAGUUCUGCAG
C-301050-01	hsa-miR-125b-1*	ACGGGUUAGGCUCUUGGGAGCU
C-301391-00	hsa-miR-548n	CAAAAGUAAUUGUGGAUUUUGU
C-300529-05	hsa-miR-196a	UAGGUAGUUUCAUGUUGUUGGG
C-301258-01	hsa-miR-923	GUCAGCGGAGGAAAAGAAACU
C-300750-05	hsa-miR-490-3p	CAACCUGGAGGACUCCAUGCUG
C-300517-03	hsa-miR-100	AACCCGUAGAUCCGAACUUGUG
C-301375-00	hsa-miR-1248	ACCUUCUUGUAUAAGCACUGUGCUAAA
C-300477-03	hsa-let-7c	UGAGGUAGUAGGUUGUAUGGUU
C-300693-05	hsa-miR-340*	UCCGUCUCAGUUACUUUAUAGC
C-300549-03	hsa-miR-10a	UACCCUGUAGAUCCGAAUUUGUG
C-301327-00	hsa-miR-1201	AGCCUGAUUAAACACAUGCUCUGA
C-301268-01	hsa-miR-939	UGGGGAGCUGAGGCUCUGGGGGUG
C-300788-03	hsa-miR-520a-3p	AAAGUGCUUCCCUUUGGACUGU
C-300494-03	hsa-miR-23a	AUCACAUUGCCAGGGAUUUCC
C-300495-07	hsa-miR-24-1*	UGCCUACUGAGCUGAUAUCAGU
C-301169-01	hsa-miR-505*	GGGAGCCAGGAAGUAUUGAUGU
C-300560-05	hsa-miR-187	UCGUGUCUUGUGUUGCAGCCGG
C-300666-03	hsa-miR-365	UAAUGCCCCUAAAAAUCCUUAU
C-300940-03	hsa-miR-615-3p	UCCGAGCCUGGGUCUCCCUCUU
C-300762-05	hsa-miR-495	AAACAAACAUGGUGCACUUCUU
C-300744-03	hsa-miR-485-5p	AGAGGCUGGCCGUGAUGAAUUC
C-300508-07	hsa-miR-32	UAUUGCACAUUACUAAGUUGCA
C-301152-01	hsa-miR-7-1*	CAACAAAUCACAGUCUGCCAUA
C-301448-00	hsa-miR-1470	GCCCUCCGCCCGUGCACCCCG
C-301236-01	hsa-miR-876-3p	UGGUGGUUUACAAAGUAAUUCA
C-300952-01	hsa-miR-626	AGCUGUCUGAAAAUGUCUU
C-300673-05	hsa-miR-367	AAUUGCACUUUAGCAAUGGUGA
C-301474-00	hsa-miR-1977	GAUUAGGGUGCUUAGCUGUUAA
C-300733-05	hsa-miR-453	AGGUUGUCCGUGGUGAGUUCGCA
C-301026-01	hsa-miR-24-2*	UGCCUACUGAGCUGAAACACAG
C-301142-01	hsa-let-7a*	CUAUACAAUCUACUGUCUUUC
C-300702-03	hsa-miR-148b	UCAGUGCAUCACAGAACUUUGU
C-301246-01	hsa-miR-665	ACCAGGAGGCUGAGGCCCCU
C-301064-01	hsa-miR-136*	CAUCAUCGUCUCAAAUGAGUCU
C-300769-03	hsa-miR-512-3p	AAGUGCUGUCAUAGCUGAGGUC

C-301092-01	hsa-miR-146b-3p	UGCCCUGUGGACUCAGUUCUGG
C-301308-00	hsa-miR-320b	AAAAGCUGGGUUGAGAGGGCAA
C-301074-01	hsa-miR-34c-3p	AAUCACUAACCACACGGCCAGG
C-300990-01	hsa-miR-656	AAUAUUAUACAGUCAACCUCU
C-300729-03	hsa-miR-431	UGUCUUGCAGGCCGUCAUGCA
C-300936-01	hsa-miR-611	GCGAGGACCCCUCGGGGUCUGAC
C-301059-01	hsa-miR-145*	GGAUUCCUGGAAAUACUGUUCU
C-300790-05	hsa-miR-526b*	GAAAGUGCUUCCUUUUAGAGGC
C-300949-01	hsa-miR-623	AUCCCUUGCAGGGGCUGUUGGGU
C-300977-01	hsa-miR-650	AGGAGGCAGCGCUCUCAGGAC
C-300641-05	hsa-miR-194	UGUAACAGCAACUCCAUGUGGA
C-300721-05	hsa-miR-448	UUGCAUAUGUAGGAUGUCCCAU
C-301090-01	hsa-miR-431*	CAGGUCGUCUUGCAGGGCUUCU
C-300650-07	hsa-miR-29c	UAGCACCAUUUGAAAUCGGUUA
C-300899-01	hsa-miR-580	UUGAGAAUGAUGAAUCAUUAGG
C-301081-01	hsa-miR-340	UUAUAAAGCAAUGAGACUGAUU
C-300710-05	hsa-miR-325	CCUAGUAGGUGUCCAGUAAGUGU
C-301269-01	hsa-miR-940	AAGGCAGGGCCCCCGCUCCCC
C-301349-00	hsa-miR-1295	UUAGGCCGCAGAUCUGGGUGA
C-300612-05	hsa-miR-144	UACAGUAUAGAUGAUGUACU
C-300765-03	hsa-miR-497	CAGCAGCACACUGUGGUUUGU
C-301216-01	hsa-miR-886-5p	CGGGUCGGAGUUAGCUCAAGCGG
C-301431-00	hsa-miR-664*	ACUGGCUAGGGAAAAUGAUUGGAU
C-301094-01	hsa-miR-497*	CAAACCACACUGUGGUGUUAGA
C-300531-05	hsa-miR-197	UUCACCACCUUCUCCACCCAGC
C-300581-07	hsa-miR-224	CAAGUCACUAGUGGUUCCGUU
C-300745-03	hsa-miR-485-3p	GUCAUACACGGCUCUCCUCUCU
C-300703-05	hsa-miR-331-3p	GCCCCUGGGCCUAUCCUAGAA
C-301277-01	hsa-miR-1224-5p	GUGAGGACUCGGGAGGUGG
C-301390-00	hsa-miR-1263	AUGGUACCCUGGCAUACUGAGU
C-300533-03	hsa-miR-199a-5p	CCCAGUGUUCAGACUACCUGUUC
C-300524-07	hsa-miR-105	UCAAAUGCUCAGACUCCUGUGGU
C-300978-01	hsa-miR-651	UUUAGGAUAAGCUUGACUUUUG
C-301028-01	hsa-miR-27a*	AGGGCUUAGCUGCUUGUGAGCA
C-301362-00	hsa-miR-1303	UUUAGAGACGGGGUCUUGCUCU
C-301158-01	hsa-miR-367*	ACUGUUGCUAAUAUGCAACUCU
C-301171-01	hsa-miR-508-5p	UACUCCAGAGGGCGUCACUCAUG
C-301012-01	hsa-miR-768-5p	GUUGGAGGAUGAAAGUACGGAGUGAU
C-300595-03	hsa-miR-125b	UCCCUGAGACCCUAACUUGUGA
C-300572-07	hsa-miR-217	UACUGCAUCAGGAACUGAUUGGA
C-301260-01	hsa-miR-509-3-	UACUGCAGACGUGGCAAUCAUG

	5p	
C-301239-01	hsa-miR-147b	GUGUGCGGAAAUGCUUCUGCUA
C-300944-01	hsa-miR-618	AAACUCUACUUGUCCUUCUGAGU
C-300716-05	hsa-miR-423-3p	AGCUCGGUCUGAGGCCCCUCAGU
C-301165-01	hsa-miR-502-3p	AAUGCACCUGGGCAAGGAUUCA
C-300994-01	hsa-miR-659	CUUGGUUCAGGGAGGGUCCCCA
C-300643-03	hsa-miR-195	UAGCAGCACAGAAAUAUUGGC
C-301228-01	hsa-miR-888	UACUCAAAAAGCUGUCAGUCA
C-300687-05	hsa-miR-379	UGGUAGACUAUGGAACGUAGG
C-301296-01	hsa-miR-513c	UUCUCAAGGAGGUGUCGUUUAU
C-301285-01	hsa-miR-1227	CGUGCCACCCUUUUCCCCAG
C-300791-05	hsa-miR-519b-3p	AAAGUGCAUCCUUUUAGAGGUU
C-301413-00	hsa-miR-548i	AAAAGUAAUUGCGGAUUUUGCC
C-300935-01	hsa-miR-610	UGAGCUAAAUGUGUGCUGGGA
C-300971-01	hsa-miR-644	AGUGUGGCUUUCUUAGAGC
C-300837-05	hsa-miR-499-5p	UUAAGACUUGCAGUGAUGUUU
C-301136-01	hsa-miR-33a*	CAAUGUUUCCACAGUGCAUCAC
C-300911-01	hsa-miR-589*	UCAGAACAAAUGCCGGUUCCCAGA
C-300741-03	hsa-miR-376b	AUCAUAGAGGAAAAUCCAUGUU
C-301315-00	hsa-miR-1283	UCUACAAAGGAAAGCGCUUUCU
C-301312-00	hsa-miR-1271	CUUGGCACCUAGCAAGCACUCA
C-300742-05	hsa-miR-483-3p	UCACUCCUCUCCUCCCGUCUU
C-300805-05	hsa-miR-518c	CAAAGCGCUUCUCUUUAGAGUGU
C-301342-00	hsa-miR-1289	UGGAGUCCAGGAAUCUGCAUUUU
C-301445-00	hsa-miR-1827	UGAGGCAGUAGAUUGAAU
C-301024-01	hsa-miR-22*	AGUUCUUCAGUGGCAAGCUUUA
C-301276-01	hsa-miR-944	AAAUUAUUGUACAUCGGAUGAG
C-300999-01	hsa-miR-758	UUUGUGACCUGGUCCACUAACC
C-300927-01	hsa-miR-602	GACACGGGCGACAGCUGCGGCCC
C-300812-05	hsa-miR-519d	CAAAGUGCCUCCCUUUAGAGUG
C-300906-01	hsa-miR-586	UAUGCAUUGUAUUUUUAGGUCC
C-300717-05	hsa-miR-424	CAGCAGCAAUUCAUGUUUUGAA
C-301325-00	hsa-miR-1184	CCUGCAGCGACUUGAUGGCUUCC
C-301378-00	hsa-miR-1251	ACUCUAGCUGCCAAAGGCGCU
C-301338-00	hsa-miR-1285	UCUGGGCAACAAAGUGAGACCU
C-301041-01	hsa-miR-196a*	CGGCAACAAGAAACUGCCUGAG
C-301013-01	hsa-miR-770-5p	UCCAGUACCACGUGUCAGGGCCA
C-300580-07	hsa-miR-223	UGUCAGUUUGUCAAAUACCCCA
C-300907-01	hsa-miR-587	UUUCCAUAGGUGAUGAGUCAC
C-300815-05	hsa-miR-520d-5p	CUACAAAGGGAAGCCCUUUC
C-301396-00	hsa-miR-1267	CCUGUUGAAGUGUAAUCCCCA

C-301399-00	hsa-miR-1270	CUGGAGAUAUGGAAGAGCUGUGU
C-301295-01	hsa-miR-513b	UUCACAAGGAGGUGUCAUUUAU
C-300686-05	hsa-miR-378	ACUGGACUUGGAGUCAGAAGG
C-300736-07	hsa-miR-452*	CUCAUCUGCAAAGAAGUAAGUG
C-300705-05	hsa-miR-324-3p	ACUGCCCCAGGUGCUGCUGG
C-300557-07	hsa-miR-182	UUUGGCAAUGGUAGAACUCACACU
C-301466-00	hsa-miR-1915*	ACCUUGCCUUGCUGCCCGGGCC
C-300518-07	hsa-miR-101	UACAGUACUGUGAUAACUGAA
C-300514-07	hsa-miR-96	UUUGGCACUAGCACAUUUUUGCU
C-300636-07	hsa-miR-185	UGGAGAGAAAGGCAGUUCCUGA
C-301409-00	hsa-miR-302e	UAAGUGCUUCCAUGCUU
C-301463-00	hsa-miR-1914	CCCUGUGCCCGGCCCACUUCUG
C-301319-00	hsa-miR-1178	UUGCUCACUGUUCUUCCCUAG
C-301242-01	hsa-miR-744	UGCGGGGCUAGGGCUAACAGCA
C-301419-00	hsa-miR-1274b	UCCCUGUUCGGGCGCCA
C-300974-01	hsa-miR-647	GUGGCUGCACUCACUUCCUUC
C-300880-01	hsa-miR-562	AAAGUAGCUGUACCAUUUGC
C-300887-01	hsa-miR-551b	GCGACCCAUACUUGGUUUCAG
C-300755-07	hsa-miR-202*	UUCCUAUGCAUAUACUUCUUUG
C-300901-01	hsa-miR-582-5p	UUACAGUUGUUCAACCAGUUACU
C-300833-03	hsa-miR-520h	ACAAAGUGCUUCCCUUUAGAGU
C-300489-03	hsa-miR-19b	UGUGCAAAUCCAUGCAAAACUGA
C-300476-05	hsa-let-7b	UGAGGUAGUAGGUUGUGUGGUU
C-301457-00	hsa-miR-1909*	UGAGUGCCGGUGCCUGCCCUG
C-300848-05	hsa-miR-508-3p	UGAUUGUAGCCUUUUGGAGUAGA
C-300897-01	hsa-miR-578	CUUCUUGUGCUCUAGGAUUGU
C-300957-01	hsa-miR-631	AGACCUGGCCCAGACCUCAGC
C-301326-00	hsa-miR-1200	CUCCUGAGCCAUUCUGAGCCUC
C-301056-01	hsa-miR-141*	CAUCUUCCAGUACAGUGUUGGA
C-301007-01	hsa-miR-769-5p	UGAGACCUCUGGGUUCUGAGCU
C-300700-05	hsa-miR-151-3p	CUAGACUGAAGCUCCUUGAGG
C-300507-05	hsa-miR-31	AGGCAAGAUGCUGGCAUAGCU
C-300988-01	hsa-miR-654-5p	UGGUGGGCCGCAGAACAUGUGC
C-301063-01	hsa-miR-129-3p	AAGCCCUUACCCCAAAAAGCAU
C-301042-01	hsa-miR-218-2*	CAUGGUUCUGUCAAGCACCGCG
C-300608-03	hsa-miR-141	UAACACUGUCUGGUAAAGAUGG
C-301210-01	hsa-miR-297	AUGUAUGUGUGCAUGUGCAUG
C-301198-01	hsa-let-7b*	CUAUACAACCUACUGCCUUCCC
C-301423-00	hsa-miR-1284	UCUAUACAGACCCUGGCUUUUC
C-301022-01	hsa-miR-20a*	ACUGCAUUAUGAGCACUUAAAG
C-301186-01	hsa-miR-490-5p	CCAUGGAUCUCCAGGUGGGU

C-300743-03	hsa-miR-484	UCAGGCUCAGUCCCCUCCCGAU
C-300943-01	hsa-miR-617	AGACUUCCCAUUUGAAGGUGGC
C-300761-05	hsa-miR-494	UGAAACAUACACGGGAAACCUC
C-301147-01	hsa-miR-513a-3p	UAAAUUUCACCUUUCUGAGAAGG
C-301211-01	hsa-miR-486-3p	CGGGGCAGCUCAGUACAGGAU
C-300814-03	hsa-miR-521	AACGCACUUCCCUUUAGAGUGU
C-301411-00	hsa-miR-1277	UACGUAGAUAUAUAUGUAUUUU
C-300527-03	hsa-miR-107	AGCAGCAUUGUACAGGGCUAUCA
C-300570-05	hsa-miR-215	AUGACCUAUGAAUUGACAGAC
C-300504-07	hsa-miR-29a	UAGCACCAUCUGAAAUCGGUUA
C-300872-03	hsa-miR-92b	UAUUGCACUCGUCCCGGCCUCC
C-300976-01	hsa-miR-649	AAACCUGUGUUGUUCAAGAGUC
C-300668-07	hsa-miR-302b*	ACUUUAACAUGGAAGUGCUUUC
C-301284-01	hsa-miR-1226	UCACCAGCCCUGUGUUCCCUAG
C-301137-01	hsa-miR-92a-2*	GGGUGGGGAUUUGUUGCAUUAC
C-301067-01	hsa-miR-150*	CUGGUACAGGCCUGGGGGACAG
C-301331-00	hsa-miR-1205	UCUGCAGGGUUUGCUUUGAG
C-300526-07	hsa-miR-106a	AAAAGUGCUUACAGUGCAGGUAG
C-301046-01	hsa-miR-122*	AACGCCAUUAUCACACUAAAUA
C-301244-01	hsa-miR-885-3p	AGGCAGCGGGGUGUAGUGGAUA
C-300611-05	hsa-miR-143	UGAGAUGAAGCACUGUAGCUC
C-301109-01	hsa-miR-532-3p	CCUCCCACACCCAAGGCUUGCA
C-301156-01	hsa-miR-26b*	CCUGUUCUCCAUUACUUGGCUC
C-300543-03	hsa-miR-30d	UGUAAACAUCCCCGACUGGAAG
C-300798-03	hsa-miR-518b	CAAAGCGCUCCCCUUUAGAGGU
C-300758-03	hsa-miR-493*	UUGUACAUGGUAGGCUUUCAUU
C-301438-00	hsa-miR-1197	UAGGACACAUGGUCUACUUCU
C-300677-05	hsa-miR-371-3p	AAGUGCCGCCAUCUUUUGAGUGU
C-301425-00	hsa-miR-1292	UGGGAACGGGUUCCGGCAGACGCUG
C-300917-01	hsa-miR-593*	AGGCACCAGCCAGGCAUUGCUCAGC
C-301345-00	hsa-miR-1291	UGGCCCUGACUGAAGACCAGCAGU
C-301061-01	hsa-miR-125b-2*	UCACAAGUCAGGCUCUUGGGAC
C-301347-00	hsa-miR-1293	UGGGUGGUCUGGAGAUUUGUGC
C-301188-01	hsa-let-7d*	CUAUACGACCUGCUGCCUUUCU
C-300757-05	hsa-miR-492	AGGACCUGCGGGACAAGAUUCUU
C-301106-01	hsa-miR-499-3p	AACAUCACAGCAAGUCUGUGCU
C-300842-07	hsa-miR-504	AGACCCUGGUCUGCACUCUAUC
C-301189-01	hsa-miR-488	UUGAAAGGCUAUUUCUUGGUC
C-300726-03	hsa-miR-191*	GCUGCGCUUGGAUUUCGUCCCC
C-301363-00	hsa-miR-1304	UUUGAGGCUACAGUGAGAUGUG
C-301418-00	hsa-miR-1279	UCAUAUUGCUUCUUUCU

C-301255-01	hsa-miR-920	GGGGAGCUGUGGAAGCAGUA
C-301118-01	hsa-miR-550	AGUGCCUGAGGGAGUAAGAGCCC
C-301303-00	hsa-miR-205*	GAUUUCAGUGGAGUGAAGUUC
C-300588-05	hsa-miR-23b	AUCACAUUGCCAGGGAUUACC
C-300756-07	hsa-miR-202	AGAGGUAUAGGGCAUGGGAA
C-301040-01	hsa-miR-187*	GGCUACAACACAGGACCCGGGC
C-301052-01	hsa-miR-132*	ACCGUGGCUUUCGAUUGUUACU
C-301200-01	hsa-miR-135b*	AUGUAGGGCUAAAAGCCAUGGG
C-300696-05	hsa-miR-342-3p	UCUCACACAGAAAUCGCACCCGU
C-301480-00	hsa-miR-2110	UUGGGGAAACGGCCGCUGAGUG
C-301297-00	hsa-let-7a-2*	CUGUACAGCCUCCUAGCUUUCC
C-300992-01	hsa-miR-657	GGCAGGUUCUCACCCUCUCUAGG
C-301047-01	hsa-miR-124*	CGUGUUCACAGCGGACCUUGAU
C-300806-03	hsa-miR-524-5p	CUACAAAGGGAAGCACUUUCUC
C-300627-03	hsa-miR-127-3p	UCGGAUCCGUCUGAGCUUGGCU
C-301023-01	hsa-miR-21*	CAACACCAGUCGAUGGGCUGU
C-301150-01	hsa-miR-29b-1*	GCUGGUUUCAUAUGGUGGUUUAGA
C-300658-03	hsa-miR-99b	CACCCGUAGAACCGACCUUGCG
C-301464-00	hsa-miR-1914*	GGAGGGGUCCCGCACUGGGAGG
C-300921-01	hsa-miR-597	UGUGUCACUCGAUGACCACUGU
C-301032-01	hsa-miR-100*	CAAGCUUGUAUCUAUAGGUAUG
C-301225-01	hsa-miR-891b	UGCAACUUACCUGAGUCAUUGA
C-300934-01	hsa-miR-609	AGGGUGUUUCUCUCAUCUCU
C-300820-05	hsa-miR-516b	AUCUGGAGGUAAGAAGCACUUU
C-300866-03	hsa-miR-542-3p	UGUGACAGAUUGAUAACUGAAA
C-301459-00	hsa-miR-1911	UGAGUACCGCCAUGUCUGUUGGG
C-300637-07	hsa-miR-186	CAAAGAAUUCUCCUUUUGGGCU
C-300523-03	hsa-miR-103	AGCAGCAUUGUACAGGGCUAUGA
C-301323-00	hsa-miR-1182	GAGGGUCUUGGGAGGGAUGUGAC
C-300614-05	hsa-miR-152	UCAGUGCAUGACAGAACUUGG
C-300759-03	hsa-miR-432	UCUUGGAGUAGGUCAUUGGGUGG
C-300535-05	hsa-miR-199a-3p	ACAGUAGUCUGCACAUUGGUUA
C-300751-05	hsa-miR-491-5p	AGUGGGGAACCCUUCCAUGAGG
C-301149-01	hsa-miR-29b-2*	CUGGUUUCACAUGGUGGCUUAG
C-301140-01	hsa-let-7f-2*	CUAUACAGUCUACUGUCUUUCC
C-300670-05	hsa-miR-302c*	UUUAACAUGGGGGUACCUGCUG
C-301372-00	hsa-miR-1245	AAGUGAUCUAAAGGCCUACAU
C-300898-03	hsa-miR-579	UUCAUUUGGUAUAAACCGCGAUU
C-301010-01	hsa-miR-765	UGGAGGAGAAGGAAGGUGAUG
C-301398-00	hsa-miR-1269	CUGGACUGAGCCGUGCUACUGG
C-300558-05	hsa-miR-182*	UGGUUCUAGACUUGCCAACUA

C-301321-00	hsa-miR-1180	UUUCCGGCUCGCGUGGGUGUGU
C-300728-03	hsa-miR-369-5p	AGAUCGACCGUGUUAUAUUCGC
C-301134-01	hsa-miR-654-3p	UAUGUCUGCUGACCAUCACCUU
C-301195-01	hsa-miR-105*	ACGGAUGUUUGAGCAUGUGCUA
C-301373-00	hsa-miR-1246	AAUGGAUUUUUGGAGCAGG
C-300591-05	hsa-miR-122	UGGAGUGUGACAAUGGUGUUUG
C-301144-01	hsa-miR-200b*	CAUCUUACUGGGCAGCAUUGGA
C-300884-01	hsa-miR-566	GGGCGCCUGUGAUCCCAAC
C-301037-01	hsa-miR-7-2*	CAACAAAUCCCAGUCUACCUAA
C-301288-01	hsa-miR-1229	CUCUCACCACUGCCCUCCCACAG
C-300959-01	hsa-miR-632	GUGUCUGCUUCCUGUGGGA
C-301082-01	hsa-miR-330-5p	UCUCUGGGCCUGUGUCUUAGGC
C-300939-01	hsa-miR-614	GAACGCCUGUUCUUGCCAGGUGG
C-300825-05	hsa-miR-518e	AAAGCGCUUCCCUUCAGAGUG
C-300760-03	hsa-miR-432*	CUGGAUGGCUCCUCCAUGUCU
C-300844-07	hsa-miR-513a-5p	UUCACAGGGAGGUGUCAU
C-300893-03	hsa-miR-574-3p	CACGCUCAUGCACACACCCACA
C-301353-00	hsa-miR-548l	AAAAGUAUUUGCGGGUUUUGUC
C-301453-00	hsa-miR-103-as	UCAUAGCCCUGUACAAUGCUGCU
C-301385-00	hsa-miR-1259	AUAUAUGAUGACUUAGCUUUU
C-300512-07	hsa-miR-93	CAAAGUGCUGUUCGUGCAGGUAG
C-301420-00	hsa-miR-1281	UCGCCUCCUCCUCUCCC
C-300920-01	hsa-miR-596	AAGCCUGCCCGGCUCCUCGGG
C-301135-01	hsa-miR-101*	CAGUUAUCACAGUGCUGAUGCU
C-300582-07	hsa-miR-200b	UAAUACUGCCUGGUAAUGAUGA
C-300789-05	hsa-miR-526b	CUCUUGAGGGAAGCACUUUCUGU
C-301178-01	hsa-miR-29a*	ACUGAUUUCUUUUGGUGUUCAG
C-301472-00	hsa-miR-1975	CCCCCACAACCGCGCUUGACUAGCU
C-301335-00	hsa-miR-1208	UCACUGUUCAGACAGGCGGA
C-300679-03	hsa-miR-373*	ACUCAAAAUGGGGGCGCUUUCC
C-300849-07	hsa-miR-509-3p	UGAUUGGUACGUCUGUGGGUAG
C-300607-05	hsa-miR-140-5p	CAGUGGUUUUACCCUAUGGUAG
C-300968-01	hsa-miR-641	AAAGACAUAGGAUAGAGUCACCUC
C-301304-00	hsa-miR-224*	AAAAUGGUGCCCUAGUGACUACA
C-301458-00	hsa-miR-1910	CCAGUCCUGUGCCUGCCGCCU
C-300684-03	hsa-miR-377	AUCACACAAAGGCAACUUUUGU
C-301341-00	hsa-miR-1287	UGCUGGAUCAGUGGUUCGAGUC
C-301199-01	hsa-miR-30c-1*	CUGGGAGAGGGUUGUUUACUCC
C-300715-05	hsa-miR-422a	ACUGGACUUAGGGUCAGAAGGC
C-300734-05	hsa-miR-451	AAACCGUUACCAUUACUGAGUU
C-300564-05	hsa-miR-205	UCCUUCAUUCCACCGGAGUCUG

C-301002-01	hsa-miR-767-5p	UGCACCAUGGUUGUCUGAGCAUG
C-301190-01	hsa-miR-188-3p	CUCCCACAUGCAGGGUUUGCA
C-300970-01	hsa-miR-643	ACUUGUAUGCUAGCUCAGGUAG
C-300712-03	hsa-miR-346	UGUCUGCCCGCAUGCCUGCCUCU
C-301348-00	hsa-miR-1294	UGUGAGGUUGGCAUUGUUGUCU
C-300933-01	hsa-miR-608	AGGGGUGGUGUUGGGACAGCUCCGU
C-301249-01	hsa-miR-374b*	CUUAGCAGGUUGUAUUAUCAUU
C-301154-01	hsa-miR-27b*	AGAGCUUAGCUGAUUGGUGAAC
C-300961-01	hsa-miR-634	AACCAGCACCCCAACUUUGGAC
C-301329-00	hsa-miR-1203	CCCGGAGCCAGGAUGCAGCUC
C-301265-01	hsa-miR-936	ACAGUAGAGGGAGGAAUCGCAG
C-301051-01	hsa-miR-130a*	UUCACAUUGUGCUACUGUCUGC
C-300966-01	hsa-miR-639	AUCGCUGCGGUUGCGAGCGCUGU
C-301266-01	hsa-miR-937	AUCCGCGCUCUGACUCUCUGCC
C-301434-00	hsa-miR-1307	ACUCGGCGUGGCGUCGGUCGUG
C-301217-01	hsa-miR-892a	CACUGUGUCCUUUCUGCGUAG
C-300651-05	hsa-miR-200a	UAACACUGUCUGGUAACGAUGU
C-300794-05	hsa-miR-523	GAACGCGCUUCCCUAUAGAGGGU
C-301393-00	hsa-miR-1265	CAGGAUGUGGUCAAGUGUUGUU
C-301187-01	hsa-miR-18b*	UGCCCUAAAUGCCCCUUCUGGC
C-300678-03	hsa-miR-372	AAAGUGCUGCGACAUUUGAGCGU
C-301176-01	hsa-miR-222*	CUCAGUAGCCAGUGUAGAUCCU
C-301298-00	hsa-miR-103-2*	AGCUUCUUUACAGUGCUGCCUUG
C-301035-01	hsa-miR-30d*	CUUUCAGUCAGAUGUUUGCUGC
C-301157-01	hsa-miR-361-3p	UCCCCCAGGUGUGAUUCUGAUUU
C-301403-00	hsa-miR-548h	AAAAGUAAUCGCGGUUUUUGUC
C-300606-05	hsa-miR-138	AGCUGGUGUUGUGAAUCAGGCCG
C-301122-01	hsa-miR-548a-5p	AAAAGUAAUUGCGAGUUUUACC
C-300915-01	hsa-miR-591	AGACCAUGGGUUCUCAUUGU
C-301337-00	hsa-miR-548j	AAAAGUAAUUGCGGUCUUUGGU
C-301392-00	hsa-miR-548m	CAAAGGUAUUUGUGGUUUUUG
C-301226-01	hsa-miR-220c	ACACAGGGCUGUUGUGAAGACU
C-301346-00	hsa-miR-548k	AAAAGUACUUGCGGAUUUUGCU
C-300984-01	hsa-miR-663	AGGCGGGGCGCCGCGGGACCGC
C-300854-03	hsa-miR-299-5p	UGGUUUACCGUCCCACAUACAU
C-300628-05	hsa-miR-134	UGUGACUGGUUGACCAGAGGGG
C-301182-01	hsa-miR-545*	UCAGUAAAUGUUUAUUAGAUGA
C-300727-05	hsa-miR-200a*	CAUCUUACCGGACAGUGCUGGA
C-301234-01	hsa-miR-875-3p	CCUGGAAACACUGAGGUUGUG
C-301006-01	hsa-miR-769-3p	CUGGGAUCUCCGGGGUCUUGGUU
C-301201-01	hsa-miR-129*	AAGCCCUUACCCCAAAAAGUAU

C-301383-00	hsa-miR-1257	AGUGAAUGAUGGGUUCUGACC
C-301371-00	hsa-miR-1244	AAGUAGUUGGUUUGUAUGAGAUGGUU
C-301057-01	hsa-miR-143*	GGUGCAGUGCUGCAUCUCUGGU
C-300714-07	hsa-miR-196b	UAGGUAGUUUCCUGUUGUUGGG
C-300493-03	hsa-miR-22	AAGCUGCCAGUUGAAGAACUGU
C-300562-03	hsa-miR-203	GUGAAAUGUUUAGGACCACUAG
C-300520-05	hsa-miR-29b	UAGCACCAUUUGAAAUCAGUGUU
C-300909-01	hsa-miR-588	UUGGCCACAAUGGGUUAGAAC
C-300664-05	hsa-miR-362-5p	AAUCCUUGGAACCUAGGUGUGAGU
C-300954-03	hsa-miR-628-3p	UCUAGUAAGAGUGGCAGUCGA
C-300817-03	hsa-miR-517b	UCGUGCAUCCCUUUAGAGUGUU
C-300930-01	hsa-miR-605	UAAAUCCCAUGGUGCCUUCUCCU
C-301027-01	hsa-miR-26a-1*	CCUAUUCUUGGUUACUUGCACG
C-300876-01	hsa-miR-558	UGAGCUGCUGUACCAAAAU
C-300995-01	hsa-miR-660	UACCCAUUGCAUAUCGGAGUUG
C-300937-01	hsa-miR-612	GCUGGGCAGGGCUUCUGAGCUCCUU
C-300647-05	hsa-miR-155	UUAAUGCUAAUCGUGAUAGGGGU
C-301208-01	hsa-miR-219-1-3p	AGAGUUGAGUCUGGACGUCCCG
C-301460-00	hsa-miR-1911*	CACCAGGCAUUGUGGUCUCC
C-300617-05	hsa-miR-191	CAACGGAAUCCCAAAAGCAGCUG
C-301005-01	hsa-miR-454*	ACCCUAUCAAUAUUGUCUCUGC
C-300803-05	hsa-miR-520c-3p	AAAGUGCUUCCUUUUAGAGGGU
C-300624-05	hsa-miR-125a-5p	UCCCUGAGACCCUUUAACCUGUGA
C-301302-00	hsa-miR-449b*	CAGCCACAACUACCCUGCCACU
C-301167-01	hsa-miR-501-3p	AAUGCACCCGGGCAAGGAUUCU
C-301003-01	hsa-miR-767-3p	UCUGCUCAUACCCCAUGGUUUCU
C-300735-07	hsa-miR-452	AACUGUUUGCAGAGGAAACUGA
C-300537-03	hsa-miR-208a	AUAAGACGAGCAAAAAGCUUGU
C-300473-05	hsa-let-7a	UGAGGUAGUAGGUUGUAUAGUU
C-300851-07	hsa-miR-514	AUUGACACUUCUGUGAGUAGA
C-300578-05	hsa-miR-221	AGCUACAUUGUCUGCUGGGUUUC
C-301280-01	hsa-miR-877*	UCCUCUUCUCCCUCCUCCCAG
C-301185-01	hsa-miR-339-3p	UGAGCGCCUCGACGACAGAGCCG
C-300922-01	hsa-miR-598	UACGUCAUCGUUGUCAUCGUCA
C-300554-07	hsa-miR-181b	AACAUUCAUUGCUGUCGGUGGGU
C-301376-00	hsa-miR-1249	ACGCCCUUCCCCCCCUUCUUCA
C-300480-05	hsa-let-7f	UGAGGUAGUAGAUUGUAUAGUU
C-301317-00	hsa-miR-1185	AGAGGAUACCCUUUGUAUGUU
C-300610-03	hsa-miR-142-3p	UGUAGUGUUUCCUACUUUAUGGA
C-300718-07	hsa-miR-425*	AUCGGGAAUGUCGUGUCCGCCC

C-300571-07	hsa-miR-216a	UAAUCUCAGCUGGCAACUGUGA
C-300895-03	hsa-miR-576-5p	AUUCUAAUUUCUCCACGUCUUU
C-300569-07	hsa-miR-214	ACAGCAGGCACAGACAGGCAGU
C-301115-01	hsa-miR-582-3p	UAACUGGUUGAACAACUGAACC
C-301334-00	hsa-miR-1207-3p	UCAGCUGGCCCUCAUUUC
C-300731-03	hsa-miR-329	AACACACCUGGUUAACCUCUUU
C-301034-01	hsa-miR-30c-2*	CUGGGAGAAGGCUGUUUACUCU
C-300486-05	hsa-miR-17*	ACUGCAGUGAAGGCACUUGUAG
C-300498-05	hsa-miR-25	CAUUGCACUUGUCUCGGUCUGA
C-301421-00	hsa-miR-1282	UCGUUUGCCUUUUUCUGCUU
C-301069-01	hsa-miR-195*	CCAAUAUUGGCUGUGCUGCUCC
C-300890-01	hsa-miR-571	UGAGUUGGCCAUCUGAGUGAG
C-300583-05	hsa-let-7g	UGAGGUAGUAGUUUGUACAGUU
C-301476-00	hsa-miR-1979	CUCCCACUGCUUCACUUGACUA
C-300950-01	hsa-miR-624*	UAGUACCAGUACCUUGUGUUCA
C-300546-07	hsa-miR-7	UGGAAGACUAGUGAUUUUGUUGU
C-300681-05	hsa-miR-374a	UUAUAAUACAACCUGAUAAGUG
C-301354-00	hsa-miR-1302	UUGGGACAUACUUAUGCUAAA
C-300953-01	hsa-miR-627	GUGAGUCUCUAAGAAAAGAGGA
C-300695-03	hsa-miR-328	CUGGCCCUCUCUGCCCUUCCGU
C-301436-00	hsa-miR-1322	GAUGAUGCUGCUGAUGCUG
C-301120-01	hsa-miR-590-3p	UAAUUUUAUGUAUAAGCUAGU
C-301410-00	hsa-miR-302f	UAAUUGCUUCCAUGUUU
C-300657-03	hsa-miR-301a	CAGUGCAAUAGUAUUGUCAAAGC
C-301305-00	hsa-miR-196b*	UCGACAGCACGACACUGCCUUC
C-301029-01	hsa-miR-31*	UGCUAUGCCAACAUAUUGCCAU
C-301384-00	hsa-miR-1258	AGUUAGGAUUAGGUCGUGGAA
C-301197-01	hsa-miR-223*	CGUGUAUUUGACAAGCUGAGUU
C-301252-01	hsa-miR-301b	CAGUGCAAUGAUAUUGUCAAAGC
C-301159-01	hsa-miR-106a*	CUGCAAUGUAAGCACUUCUUAC
C-301000-03	hsa-miR-671-5p	AGGAAGCCCUGGAGGGGCUGGAG
C-300635-03	hsa-miR-184	UGGACGGAGAACUGAUAAGGGU
C-301145-01	hsa-miR-34a*	CAAUCAGCAAGUAUACUGCCCU
C-301044-01	hsa-let-7i*	CUGCGCAAGCUACUGCCUUGCU
C-301184-01	hsa-miR-28-3p	CACUAGAUUGUGAGCUCCUGGA
C-300896-01	hsa-miR-577	UAGAUAAAAUAUUGGUACCUG
C-300604-07	hsa-miR-137	UUAUUGCUUAAGAAUACGCGUAG
C-300778-05	hsa-miR-519e	AAGUGCCUCCUUUUAGAGUGUU
C-301011-01	hsa-miR-768-3p	UCACAAUGCUGACACUCAAACUGCUGAC
C-301014-01	hsa-miR-801	GAUUGCUCUGCGUGCGGAAUCGAC
C-301229-01	hsa-miR-892b	CACUGGCUCCUUUCUGGGUAGA

C-300719-07	hsa-miR-18b	UAAGGUGCAUCUAGUGCAGUUAG
C-300502-03	hsa-miR-27a	UUCACAGUGGCUAAGUUCCGC
C-301016-01	hsa-let-7c*	UAGAGUUACACCCUGGGAGUUA
C-300973-01	hsa-miR-646	AAGCAGCUGCCUCUGAGGC
C-300674-05	hsa-miR-376c	AACAUAGAGGAAAUUCCACGU
C-301143-01	hsa-miR-219-2-3p	AGAAUUGUGGCUGGACAUCUGU
C-300644-03	hsa-miR-206	UGGAAUGUAAGGAAGUGUGUGG
C-301291-01	hsa-miR-1234	UCGGCCUGACCACCCACCCCAC
C-300711-05	hsa-miR-345	GCUGACUCCUAGUCCAGGGCUC
C-301019-01	hsa-miR-16-1*	CCAGUAUUAACUGUGCUGCUGA
C-301241-01	hsa-miR-744*	CUGUUGCCACUAACCUCAACCU
C-301374-00	hsa-miR-1247	ACCCGUCCCGUUCGUCCCCGGA
C-301424-00	hsa-miR-1288	UGGACUGCCCUGAUCUGGAGA
C-300626-07	hsa-miR-126	UCGUACCGUGAGUAAUAAUGCG
C-300590-03	hsa-miR-30b	UGUAAACAUCCUACACUCAGCU
C-300773-03	hsa-miR-515-5p	UUCUCCAAAAGAAAGCACUUUCUG
C-300706-05	hsa-miR-338-3p	UCCAGCAUCAGUGAUUUUGUUG
C-301104-01	hsa-miR-516a-5p	UUCUCGAGGAAAGAAGCACUUUC
C-300888-01	hsa-miR-569	AGUUAAUGAAUCCUGGAAAGU
C-301163-01	hsa-miR-221*	ACCUGGCAUACAAUGUAGAUUU
C-300506-03	hsa-miR-30a*	CUUUCAGUCGGAUGUUUGCAGC
C-301388-00	hsa-miR-1261	AUGGAUAAGGCUUUGGCUU
C-301437-00	hsa-miR-720	UCUCGCUGGGGCCUCCA
C-300969-01	hsa-miR-642	GUCCCUCUCCAAAUGUGUCUUG
C-301381-00	hsa-miR-1255a	AGGAUGAGCAAAGAAAGUAGAUU
C-300830-03	hsa-miR-518d-3p	CAAAGCGCUUCCCUUUGGAGC
C-300926-01	hsa-miR-601	UGGUCUAGGAUUGUUGGAGGAG
C-301025-01	hsa-miR-23a*	GGGGUUCCUGGGGAUGGGAUUU
C-301336-00	hsa-miR-548e	AAAAACUGAGACUACUUUUGCA
C-300869-01	hsa-miR-552	AACAGGUGACUGGUUAGACAA
C-300689-03	hsa-miR-380	UAUGUAAUAUGGUCCACAUCUU
C-301450-00	hsa-miR-1537	AAAACCGUCUAGUUACAGUUGU
C-301251-01	hsa-miR-760	CGGCUCUGGGUCUGUGGGGA
C-300912-01	hsa-miR-550*	UGUCUUACUCCCUCAGGCACAU
C-301435-00	hsa-miR-1321	CAGGGAGGUGAAUGUGAU
C-301332-00	hsa-miR-1206	UGUUCAUGUAGAUGUUUAAGC
C-300532-05	hsa-miR-198	GGUCCAGAGGGGAGAUAGGUUC
C-301275-01	hsa-miR-943	CUGACUGUUGCCGUCCUCCAG
C-300787-03	hsa-miR-520a-5p	CUCCAGAGGGAAGUACUUUCU
C-300600-05	hsa-miR-133a	UUUGGUCCCCUUCAACCAGCUG

C-301155-01	hsa-miR-424*	CAAAACGUGAGGCGCUGCUAU
C-301444-00	hsa-miR-1826	AUUGAUCAUCGACACUUCGAACGCAAU
C-300567-03	hsa-miR-212	UAACAGUCUCCAGUCACGGCC
C-301281-01	hsa-miR-1225-5p	GUGGGUACGGCCCAGUGGGGGG
C-301124-01	hsa-miR-616	AGUCAUUGGAGGGUUUGAGCAG
C-300553-05	hsa-miR-181a	AACAUUCAACGCUGUCGGUGAGU
C-301262-01	hsa-miR-933	UGUGCGCAGGGAGACCUCUCCC
C-301477-00	hsa-miR-2052	UGUUUUGAUAACAGUAAUGU
C-301248-01	hsa-miR-543	AAACAUUCGCGGUGCACUUCUU
C-301170-01	hsa-miR-23b*	UGGGUUCCUGGCAUGCUGAUUU
C-300807-03	hsa-miR-524-3p	GAAGGCGCUUCCCUUUGGAGU
C-300891-01	hsa-miR-572	GUCCGCUCGGCGGUGGCCCA
C-300499-05	hsa-miR-26a	UUCAAGUAAUCCAGGAUAGGCU
C-301068-01	hsa-miR-193a-5p	UGGGUCUUUGCGGGCGAGAUGA
C-301447-00	hsa-miR-1469	CUCGGCGCGGGGCGCGGGCUCC
C-301221-01	hsa-miR-450b-5p	UUUUGCAAUAUGUUCCUGAAUA
C-300850-07	hsa-miR-510	UACUCAGGAGAGUGGCAAUCAC
C-301077-01	hsa-miR-26a-2*	CCUAUUCUUGAUUACUUGUUUC
C-301456-00	hsa-miR-1909	CGCAGGGGCCGGGUGCUCACCG
C-301191-01	hsa-miR-186*	GCCCAAAGGUGAAUUUUUUGGG
C-300709-07	hsa-miR-133b	UUUGGUCCCCUUCAACCAGCUA
C-300752-03	hsa-miR-511	GUGUCUUUUGCUCUGCAGUCA
C-300584-05	hsa-let-7i	UGAGGUAGUAGUUUGUGCUGUU
C-300568-05	hsa-miR-181a*	ACCAUCGACCGUUGAUUGUACC
C-300938-01	hsa-miR-613	AGGAAUGUUCCUUCUUUGCC
C-300540-05	hsa-miR-148a	UCAGUGCACUACAGAACUUUGU
C-301263-01	hsa-miR-934	UGUCUACUACUGGAGACACUGG
C-301440-00	hsa-miR-320d	AAAAGCUGGGUUGAGAGGA
C-301133-01	hsa-miR-411*	UAUGUAACACGGUCCACUAACC
C-300860-03	hsa-miR-544	AUUCUGCAUUUUUAGCAAGUUC
C-301274-01	hsa-miR-942	UCUUCUCUGUUUUGGCCAUGUG
C-300932-01	hsa-miR-607	GUUCAAAUCCAGAUCUAUAAC
C-300510-05	hsa-miR-92a	UAUUGCACUUGUCCCGGCCUGU
C-301257-01	hsa-miR-922	GCAGCAGAGAAUAGGACUACGUC
C-300779-03	hsa-miR-520f	AAGUGCUUCCUUUUAGAGGGUU
C-301207-01	hsa-miR-93*	ACUGCUGAGCUAGCACUUCCCG
C-301193-01	hsa-miR-183*	GUGAAUUACCGAAGGGCCAUAA
C-300775-05	hsa-miR-515-3p	GAGUGCCUUCUUUUGGAGCGUU
C-301471-00	hsa-miR-1974	UGGUUGUAGUCCGUGCGAGAAUA
C-301062-01	hsa-miR-127-5p	CUGAAGCUCAGAGGGCUCUGAU
C-300563-05	hsa-miR-204	UUCCCUUUGUCAUCCUAUGCCU

C-300767-03	hsa-miR-512-5p	CACUCAGCCUUGAGGGCACUUUC
C-300772-03	hsa-miR-520e	AAAGUGCUUCCUUUUUGAGGG
C-301224-01	hsa-miR-890	UACUUGGAAAGGCAUCAGUUG
C-300985-01	hsa-miR-449b	AGGCAGUGUAUUGUUAGCUGGC
C-301449-00	hsa-miR-1471	GCCCGCGUGUGGAGCCAGGUGU
C-301039-01	hsa-miR-181c*	AACCAUCGACCGUUGAGUGGAC
C-301033-01	hsa-miR-192*	CUGCCAAUUCCAUAGGUCACAG
C-300838-05	hsa-miR-500*	AUGCACCUGGGCAAGGAUUCUG
C-300958-03	hsa-miR-33b	GUGCAUUGCUGUUGCAUUGC
C-300904-01	hsa-miR-585	UGGGCGUAUCUGUAUGCUA
C-300654-03	hsa-miR-34b*	UAGGCAGUGUCAUUAGCUGAUUG
C-300544-05	hsa-miR-139-5p	UCUACAGUGCACGUGUCUCCAG
C-300882-01	hsa-miR-564	AGGCACGGUGUCAGCAGGC
C-301247-01	hsa-miR-873	GCAGGAACUUGUGAGUCUCCU
C-301307-00	hsa-miR-1264	CAAGUCUUAUUUGAGCACCUGUU
C-301401-00	hsa-miR-1273	GGGCGACAAAGCAAGACUCUUUCUU
C-300889-03	hsa-miR-570	CGAAAACAGCAAUUACCUUUGC
C-301223-01	hsa-miR-874	CUGCCCUGGCCCGAGGGACCGA
C-301004-03	hsa-miR-454	UAGUGCAAUAUUGCUUAUAGGGU
C-301087-01	hsa-miR-148b*	AAGUUCUGUUAUACACUCAGGC
C-300808-03	hsa-miR-517*	CCUCUAGAUGGAAGCACUGUCU
C-300835-05	hsa-miR-519a	AAAGUGCAUCCUUUUAGAGUGU
C-301365-00	hsa-miR-1243	AACUGGAUCAAUUAUAGGAGUG
C-301320-00	hsa-miR-1179	AAGCAUUCUUUCAUUGGUUGG
C-301129-01	hsa-miR-629	UGGGUUUACGUUGGGAGAACU
C-301283-01	hsa-miR-1226*	GUGAGGGCAUGCAGGCCUGGAUGGGG
C-300513-05	hsa-miR-95	UUCAACGGGUAUUUAUUGAGCA
C-301131-01	hsa-miR-548d-5p	AAAAGUAAUUGUGGUUUUUGCC
C-300892-01	hsa-miR-573	CUGAAGUGAUGUGUAACUGAUCAG
C-301114-01	hsa-miR-576-3p	AAGAUGUGGAAAAAUUGGAAUC
C-301060-01	hsa-miR-125a-3p	ACAGGUGAGGUUCUUGGGAGCC
C-300561-05	hsa-miR-199b-5p	CCCAGUGUUUAGACUAUCUGUUC
C-300903-01	hsa-miR-584	UUAUGGUUUGCCUGGGACUGAG
C-300914-01	hsa-miR-590-5p	GAGCUUAUUCAUAAAAGUGCAG
C-300816-05	hsa-miR-520d-3p	AAAGUGCUUCUCUUUGGUGGGU
C-301310-00	hsa-miR-1296	UUAGGGCCCUGGCUCCAUCUCC
C-300483-03	hsa-miR-16	UAGCAGCACGUAAAUAUUGGCG
C-300503-05	hsa-miR-28-5p	AAGGAGCUCACAGUCUAUUGAG
C-300747-03	hsa-miR-487a	AAUCAUACAGGGACAUCCAGUU
C-300685-03	hsa-miR-378*	CUCCUGACUCCAGGUCCUGUGU
C-300559-07	hsa-miR-183	UAUGGCACUGGUAGAAUUCACU

C-300575-05	hsa-miR-219-5p	UGAUUGUCCAAACGCAAUUCU
C-301299-00	hsa-miR-365*	AGGGACUUUCAGGGGCAGCUGU
C-301128-01	hsa-miR-628-5p	AUGCUGACAUAUUUACUAGAGG
C-300945-01	hsa-miR-619	GACCUGGACAUGUUUGUGCCCAGU
C-300630-03	hsa-miR-146a	UGAGAACUGAAUUCCAUGGGUU
C-301352-00	hsa-miR-1300	UUGAGAAGGAGGCUGCUG
C-301058-01	hsa-miR-144*	GGAUAUCAUCAUAUACUGUAAG
C-301107-01	hsa-miR-483-5p	AAGACGGGAGGAAAGAAGGGAG
C-301290-01	hsa-miR-1233	UGAGCCCUGUCCUCCCGCAG
C-301461-00	hsa-miR-1912	UACCCAGAGCAUGCAGUGUGAA
C-301328-00	hsa-miR-1202	GUGCCAGCUGCAGUGGGGGAG
C-301038-01	hsa-miR-10a*	CAAAUUCGUAUCUAGGGGAAUA
C-300925-01	hsa-miR-600	ACUUACAGACAAGAGCCUUGCUC
C-301054-01	hsa-miR-138-2*	GCUAUUUCACGACACCAGGGUU
C-300928-01	hsa-miR-603	CACACACUGCAAUUACUUUUGC
C-300885-01	hsa-miR-567	AGUAUGUUCUUCCAGGACAGAAC
C-300542-05	hsa-miR-30c	UGUAAACAUCCUACACUCUCAGC
C-301395-00	hsa-miR-1266	CCUCAGGGCUGUAGAACAGGGCU
C-301138-01	hsa-miR-218-1*	AUGGUUCCGUCAAGCACCAUGG
C-300708-05	hsa-miR-335	UCAAGAGCAAUAACGAAAAAUGU
C-301313-00	hsa-miR-1301	UUGCAGCUGCCUGGGAGUGACUUC
C-300479-05	hsa-let-7e	UGAGGUAGGAGGUUGUAUAGUU
C-300797-03	hsa-miR-520b	AAAGUGCUUCCUUUUAGAGGG
C-300771-03	hsa-miR-498	UUUCAAGCCAGGGGGCGUUUUUC
C-300589-05	hsa-miR-27b	UUCACAGUGGCUAAGUUCUGC
C-300566-03	hsa-miR-211	UUCCCUUUGUCAUCCUUCGCCU
C-301400-00	hsa-miR-1272	GAUGAUGAUGGCAGCAAAUUCUGAAA
C-300598-03	hsa-miR-130a	CAGUGCAAUGUUAAAAGGGCAU
C-301243-01	hsa-miR-885-5p	UCCAUUACACUACCCUGCCUCU
C-301214-01	hsa-miR-300	UAUACAAGGGCAGACUCUCUCU
C-300694-03	hsa-miR-330-3p	GCAAAGCACACGGCCUGCAGAGA
C-301021-01	hsa-miR-19b-1*	AGUUUUGCAGGUUUGCAUCCAGC
C-301478-00	hsa-miR-2053	GUGUUAAUUAAACCUCUAUUUAC
C-300843-07	hsa-miR-505	CGUCAACACUUGCUGGUUUCCU
C-301455-00	hsa-miR-1908	CGGCGGGGACGGCGAUUGGUC
C-301085-01	hsa-miR-323-5p	AGGUGGUCCGUGGCGCGUUCGC
C-300749-07	hsa-miR-489	GUGACAUCACAUAUACGGCAGC
C-301204-01	hsa-let-7f-1*	CUAUACAAUCUAUUGCCUUCCC
C-300704-03	hsa-miR-324-5p	CGCAUCCCCUAGGGCAUUGGUGU
C-301088-01	hsa-miR-338-5p	AACAAUAUCCUGGUGCUGAGUG
C-301172-01	hsa-miR-455-3p	GCAGUCCAUGGGCAUAUACAC

C-301322-00	hsa-miR-1181	CCGUCGCCGCCACCCGAGCCG
C-301113-01	hsa-miR-574-5p	UGAGUGUGUGUGUGUGAGUGUGU
C-301008-01	hsa-miR-766	ACUCCAGCCCCACAGCCUCAGC
C-301267-01	hsa-miR-938	UGCCCUUAAAGGUGAACCCAGU
C-300545-05	hsa-miR-147	GUGUGUGGAAAUGCUUCUGC
C-301089-01	hsa-miR-423-5p	UGAGGGGCAGAGAGCGAGACUUU
C-301426-00	hsa-miR-1252	AGAAGGAAAUUGAAUUCAUUUA
C-301417-00	hsa-miR-1278	UAGUACUGUGCAUAUCAUCUAU
C-300979-03	hsa-miR-652	AAUGGCGCCACUAGGGUUGUG
C-301306-00	hsa-miR-675*	CUGUAUGCCCUCACCGCUCA
C-300663-05	hsa-miR-361-5p	UUAUCAGAAUCUCCAGGGGUAC
C-301053-01	hsa-miR-135a*	UAUAGGGAUUGGAGCCGUGGCG
C-300632-03	hsa-miR-150	UCUCCCAACCCUUGUACCAGUG
C-300609-05	hsa-miR-142-5p	CAUAAAGUAGAAAGCACUACU
C-301232-01	hsa-miR-889	UUAAUAUCGGACAACCAUUGU
C-300996-01	hsa-miR-421	AUCAACAGACAUUAAUUGGGCGC
C-301227-01	hsa-miR-888*	GACUGACACCUCUUUGGGUGAA
C-301173-01	hsa-miR-10b*	ACAGAUUCGAUUCUAGGGGAAU
C-300653-05	hsa-miR-302a	UAAGUGCUUCCAUGUUUUGGUGA
C-301183-01	hsa-miR-25*	AGGCGGAGACUUGGGCAAUUG
C-301036-01	hsa-miR-139-3p	GGAGACGCGGCCCUGUUGGAGU
C-301091-01	hsa-miR-491-3p	CUUAUGCAAGAUUCCCUUCUAC
C-300900-01	hsa-miR-581	UCUUGUGUUCUCUAGAUCAGU
C-301324-00	hsa-miR-1183	CACUGUAGGUGAUGGUGAGAGUGGGCA
C-301240-01	hsa-miR-190b	UGAUAUGUUUGAUAUUGGGUU
C-300723-03	hsa-miR-449a	UGGCAGUGUAUUGUUAGCUGGU
C-300621-07	hsa-miR-9*	AUAAAGCUAGAUAACCGAAAGU
C-300538-05	hsa-miR-129-5p	CUUUUUGCGGUCUGGGCUUGC

Appendix B: Wounding Tool

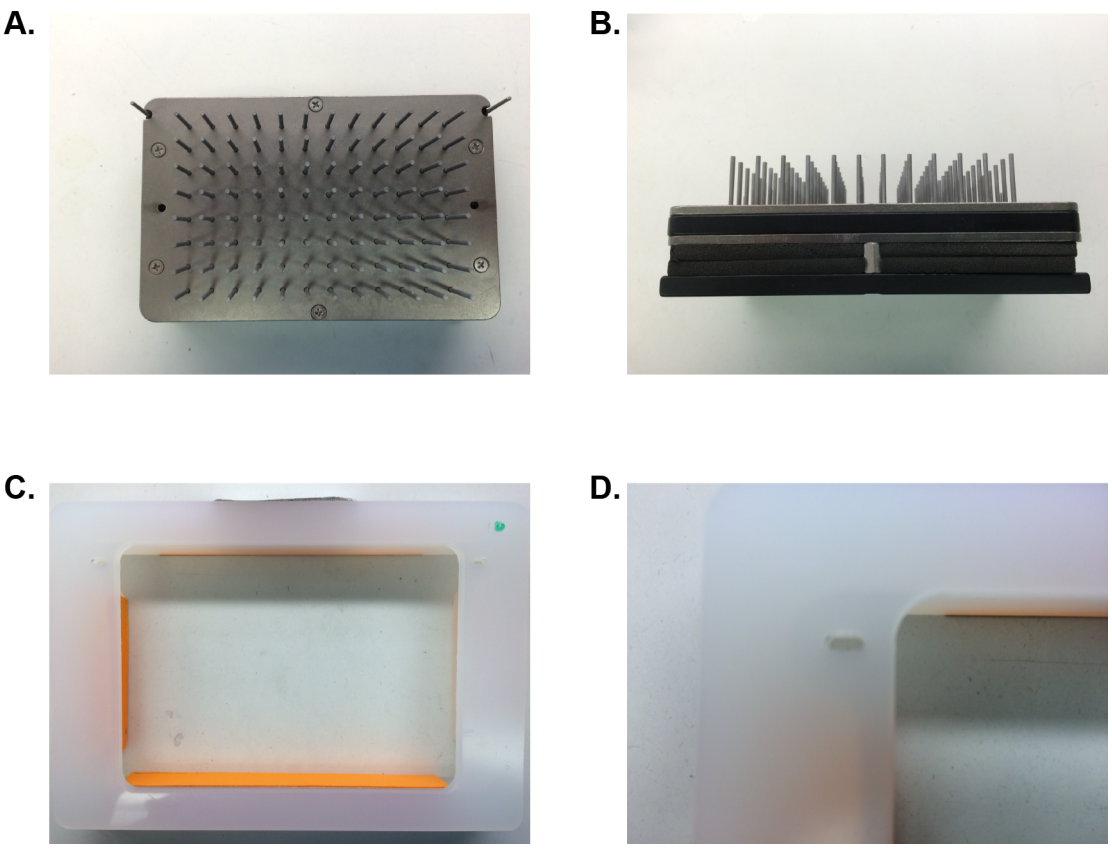

A. Overhead view of wounding tool. **B.** Side view of wounding tool. **C.** Overhead view of wounding template. **D.** Close up view of guiding wounding track.

Appendix C: MiRNAs that enhance wound closure

	Wounding Data				Relative Fluorescence
Mature Sanger ID	**Avg_Activity (%)**	**STDEV**	**Z-score**	**Probability**	**Avg_Activity (%)**
hsa-miR-1276	-123.867	0.058	-4.6415	0.0000	6.299
hsa-miR-516a-5p	-116.300	2.100	-4.3543	0.0000	6.339
hsa-miR-614	-115.433	0.252	-4.3214	0.0000	-7.708
hsa-miR-373*	-112.200	0.200	-4.1987	0.0000	5.629
hsa-miR-626	-109.567	0.058	-4.0988	0.0000	3.203
hsa-miR-26b	-109.400	5.910	-4.0925	0.0000	6.469
hsa-miR-769-3p	-108.233	0.153	-4.0482	0.0000	-24.317
hsa-miR-299-5p	-107.467	0.153	-4.0191	0.0000	-7.258
hsa-miR-566	-103.800	12.743	-3.8799	0.0001	5.068
hsa-miR-558	-103.417	19.776	-3.8654	0.0001	-15.820
hsa-miR-651	-98.507	0.006	-3.6790	0.0001	7.655
hsa-miR-191	-98.467	0.025	-3.6775	0.0001	-35.237
hsa-miR-873	-98.217	12.864	-3.6680	0.0001	4.590
hsa-miR-205	-97.880	0.030	-3.6552	0.0001	-10.357
hsa-miR-431	-95.450	4.581	-3.5630	0.0002	-37.573
hsa-miR-26a	-93.757	0.815	-3.4987	0.0002	5.364
hsa-miR-1226*	-93.713	8.490	-3.4971	0.0002	3.411
hsa-miR-202*	-93.277	0.105	-3.4805	0.0003	-2.169
hsa-miR-29b-1*	-92.783	0.115	-3.4618	0.0003	2.786
hsa-miR-155*	-91.990	0.330	-3.4317	0.0003	-15.823
hsa-miR-499-5p	-91.630	8.408	-3.4180	0.0003	-6.839
hsa-miR-19a*	-91.027	1.824	-3.3951	0.0003	-45.417
hsa-miR-1323	-91.013	15.822	-3.3946	0.0003	-23.113
hsa-miR-523	-87.697	21.045	-3.2687	0.0005	2.704
hsa-miR-592	-84.507	14.609	-3.1477	0.0008	4.481
hsa-miR-609	-80.820	2.257	-3.0078	0.0013	-11.050
hsa-miR-33b	-78.997	7.880	-2.9385	0.0016	1.102
hsa-miR-1225-5p	-76.980	3.005	-2.8620	0.0021	-0.122
hsa-miR-425*	-76.420	13.951	-2.8408	0.0023	-7.091
hsa-miR-23b	-74.577	3.760	-2.7708	0.0028	3.716
hsa-miR-324-5p	-74.323	17.929	-2.7612	0.0029	-6.766
hsa-miR-147b	-73.797	14.257	-2.7412	0.0031	4.527
hsa-miR-576-5p	-72.153	16.737	-2.6788	0.0037	1.586

hsa-miR-1297	-70.960	12.353	-2.6335	0.0042	3.842
hsa-miR-325	-69.570	0.110	-2.5808	0.0049	1.731
hsa-miR-541*	-68.053	11.338	-2.5232	0.0058	-0.351
hsa-miR-658	-67.787	16.196	-2.5131	0.0060	4.506
hsa-miR-1251	-67.150	31.275	-2.4889	0.0064	4.003
hsa-miR-1203	-65.947	34.789	-2.4433	0.0073	2.836
hsa-miR-517*	-65.683	19.560	-2.4333	0.0075	0.817
hsa-miR-590-3p	-65.090	5.543	-2.4107	0.0080	3.535
hsa-miR-130a*	-65.053	2.399	-2.4094	0.0080	5.034
hsa-miR-2052	-64.833	7.049	-2.4010	0.0082	4.341
hsa-miR-1296	-63.147	39.707	-2.3370	0.0097	-1.762
hsa-miR-708*	-62.833	24.896	-2.3251	0.0100	-6.000
hsa-miR-33a	-62.020	21.121	-2.2942	0.0109	-0.886
hsa-miR-335	-61.487	3.095	-2.2740	0.0115	2.164
hsa-miR-487a	-59.000	17.500	-2.1796	0.0146	-4.224
hsa-miR-1302	-58.100	5.365	-2.1454	0.0160	2.853
hsa-miR-513c	-57.640	24.088	-2.1280	0.0167	-3.589
hsa-miR-628-3p	-54.710	32.355	-2.0168	0.0219	-11.963
hsa-miR-1225-3p	-54.490	10.114	-2.0084	0.0223	1.879
hsa-miR-379*	-53.080	13.574	-1.9549	0.0253	2.336

Appendix D: MiRNAs that inhibit wound closure

	Wounding Data				Relative Fluorescence
Mature Sanger ID	Avg_Activity (%)	STDEV	Z-score	Probability	Avg_Activity (%)
hsa-miR-589*	464.467	63.119	17.6878	1.0000	-48.333
hsa-miR-642	463.333	25.498	17.6447	1.0000	-26.023
hsa-miR-215	441.767	71.340	16.8262	1.0000	-41.470
hsa-miR-768-5p	416.233	35.926	15.8571	1.0000	-43.520
hsa-miR-320c	361.067	74.193	13.7634	1.0000	-44.033
hsa-miR-675*	352.600	52.658	13.4420	1.0000	-27.743
hsa-miR-620	344.800	21.882	13.1460	1.0000	-49.217
hsa-miR-1258	342.567	49.554	13.0612	1.0000	-18.650
hsa-miR-323-3p	342.233	54.671	13.0486	1.0000	-31.390
hsa-miR-224	341.567	7.276	13.0233	1.0000	-20.120
hsa-miR-340	336.000	54.224	12.8120	1.0000	-46.540
hsa-miR-132	335.767	78.835	12.8031	1.0000	-30.893
hsa-miR-139-3p	333.567	8.649	12.7196	1.0000	-33.570
hsa-miR-1299	321.867	17.180	12.2756	1.0000	-48.283
hsa-miR-221	320.900	19.846	12.2389	1.0000	-28.223
hsa-miR-222	318.933	45.986	12.1643	1.0000	-21.504
hsa-miR-148a*	311.967	49.911	11.8999	1.0000	-27.793
hsa-miR-675	310.867	46.998	11.8581	1.0000	-48.333
hsa-miR-135a	309.967	9.800	11.8239	1.0000	-16.367
hsa-miR-150*	303.800	35.503	11.5899	1.0000	-5.001
hsa-miR-768-3p	300.200	23.649	11.4533	1.0000	-37.220
hsa-miR-22*	299.567	30.316	11.4292	1.0000	-27.917
hsa-miR-493	296.100	22.997	11.2977	1.0000	-16.323
hsa-let-7c*	294.500	29.842	11.2369	1.0000	-13.130
hsa-miR-31*	293.200	50.740	11.1876	1.0000	-44.967
hsa-miR-582-5p	292.767	23.884	11.1711	1.0000	-10.811
hsa-miR-492	289.667	34.043	11.0535	1.0000	-31.060
hsa-miR-619	289.433	46.058	11.0446	1.0000	-30.527
hsa-miR-216b	287.267	44.673	10.9624	1.0000	-23.853
hsa-miR-1226	287.133	39.795	10.9573	1.0000	-17.623
hsa-miR-18a*	284.733	44.230	10.8663	1.0000	-37.137
hsa-miR-223	283.267	24.364	10.8106	1.0000	-4.802
hsa-miR-1290	283.000	64.540	10.8005	1.0000	-34.570

hsa-miR-320a	282.300	21.473	10.7739	1.0000	-28.463
hsa-miR-505	281.567	43.764	10.7461	1.0000	-13.533
hsa-miR-182	277.000	71.204	10.5727	1.0000	-27.754
hsa-miR-10a*	275.667	46.367	10.5221	1.0000	-25.527
hsa-miR-423-5p	273.500	24.494	10.4399	1.0000	-23.543
hsa-miR-520d-5p	273.200	32.611	10.4285	1.0000	-40.170
hsa-miR-203	271.700	40.628	10.3716	1.0000	-36.530
hsa-miR-488	270.867	30.312	10.3400	1.0000	-29.730
hsa-miR-518c*	270.700	54.241	10.3336	1.0000	-32.177
hsa-miR-655	269.100	38.194	10.2729	1.0000	-14.107
hsa-miR-513a-5p	259.033	23.955	9.8909	1.0000	-17.033
hsa-miR-200b*	258.200	17.064	9.8592	1.0000	-6.301
hsa-miR-200a*	257.867	9.928	9.8466	1.0000	-9.220
hsa-miR-212	257.733	37.604	9.8415	1.0000	-13.040
hsa-miR-500	257.133	66.005	9.8187	1.0000	-38.467
hsa-miR-557	256.567	13.683	9.7972	1.0000	-48.813
hsa-miR-1470	252.433	9.582	9.6404	1.0000	-14.850
hsa-let-7i*	250.633	30.345	9.5720	1.0000	-30.577
hsa-miR-421	250.300	25.301	9.5594	1.0000	-21.217
hsa-miR-128	248.433	13.459	9.4885	1.0000	-10.932
hsa-miR-2054	248.167	59.497	9.4784	1.0000	-8.520
hsa-miR-219-2-3p	248.000	35.784	9.4721	1.0000	-36.933
hsa-miR-938	247.367	63.480	9.4481	1.0000	-33.003
hsa-miR-181d	247.100	34.767	9.4379	1.0000	-24.360
hsa-miR-924	246.833	18.874	9.4278	1.0000	-42.347
hsa-miR-504	245.400	55.353	9.3734	1.0000	-5.798
hsa-miR-99a*	244.867	8.173	9.3532	1.0000	-27.850
hsa-miR-135a*	244.800	50.303	9.3506	1.0000	-44.363
hsa-miR-24-2*	244.767	15.830	9.3494	1.0000	-33.123
hsa-miR-595	243.800	17.621	9.3127	1.0000	-12.573
hsa-miR-101	242.700	59.843	9.2709	1.0000	-11.719
hsa-miR-101*	242.500	34.448	9.2634	1.0000	-27.680
hsa-miR-488*	240.700	37.570	9.1950	1.0000	-9.574
hsa-miR-298	240.533	38.461	9.1887	1.0000	-9.469
hsa-miR-149	238.200	19.948	9.1002	1.0000	-7.671
hsa-miR-876-5p	237.467	9.799	9.0723	1.0000	-12.627
hsa-miR-770-5p	236.300	22.678	9.0280	1.0000	-5.281
hsa-miR-181c	235.800	40.365	9.0091	1.0000	-22.283
hsa-miR-654-3p	234.433	15.267	8.9572	1.0000	-11.120

hsa-miR-188-5p	233.233	32.693	8.9117	1.0000	-3.265
hsa-miR-24-1*	233.133	7.060	8.9079	1.0000	-25.490
hsa-miR-525-3p	232.200	24.145	8.8724	1.0000	-39.853
hsa-miR-99b	232.133	4.933	8.8699	1.0000	-19.080
hsa-miR-617	231.067	36.020	8.8294	1.0000	-43.930
hsa-miR-9	231.033	31.590	8.8282	1.0000	-5.685
hsa-miR-423-3p	230.267	21.759	8.7991	1.0000	-6.076
hsa-miR-146b-5p	229.833	4.212	8.7826	1.0000	-3.974
hsa-miR-142-3p	229.733	75.162	8.7788	1.0000	-14.126
hsa-miR-340*	229.567	15.500	8.7725	1.0000	-11.014
hsa-miR-875-5p	227.933	63.933	8.7105	1.0000	-5.334
hsa-miR-377*	226.067	18.016	8.6397	1.0000	-7.722
hsa-miR-508-3p	225.133	66.903	8.6042	1.0000	-39.823
hsa-miR-1973	224.267	13.091	8.5713	1.0000	-5.445
hsa-miR-802	223.067	30.658	8.5258	1.0000	-15.833
hsa-miR-586	222.333	10.886	8.4980	1.0000	-5.429
hsa-miR-18b	220.833	37.015	8.4410	1.0000	-21.213
hsa-miR-551b	220.700	43.900	8.4360	1.0000	-4.042
hsa-miR-622	220.500	33.409	8.4284	1.0000	-11.495
hsa-miR-1298	218.233	39.845	8.3424	1.0000	-8.943
hsa-miR-371-3p	217.467	15.134	8.3133	1.0000	-30.380
hsa-miR-579	216.267	9.122	8.2677	1.0000	-6.395
hsa-miR-369-5p	215.433	11.890	8.2361	1.0000	-32.643
hsa-miR-1179	215.367	30.471	8.2336	1.0000	-34.593
hsa-miR-589	214.600	18.616	8.2045	1.0000	-20.907
hsa-miR-1977	214.567	8.445	8.2032	1.0000	-21.360
hsa-miR-641	213.500	3.516	8.1627	1.0000	-3.692
hsa-miR-296-5p	213.467	27.306	8.1614	1.0000	-16.017
hsa-miR-518d-5p	213.467	18.551	8.1614	1.0000	-6.084
hsa-miR-331-3p	211.967	38.987	8.1045	1.0000	-3.335
hsa-miR-30a*	210.467	45.916	8.0476	1.0000	-4.360
hsa-miR-532-3p	210.267	26.034	8.0400	1.0000	-30.360
hsa-miR-484	208.533	24.773	7.9742	1.0000	-7.732
hsa-miR-490-5p	208.333	7.550	7.9666	1.0000	-6.999

Appendix E: Gene expression comparison of MDA-MB-231 and MCFDCIS transfected with miR614

Genes in yellow are genes we tested in our mini-screen.

	MDA-MB-231 values		MCFDCIS values	
ILMN_Gene	Log ratio	p-value	Log ratio	p-value
ADD3	-0.7927	0.0008	-1.2571	0.0299
CCDC117	-0.7289	0.0009	-1.2356	0.0151
CNO	-0.9552	0.0018	-1.0876	0.0038
DDX46	-0.8952	0.0075	-1.2764	0.0007
HMGB1	-0.6124	0.0056	-1.0721	0.0137
HNRNPA0	-0.952	0.0078	-1.1369	0.0123
HS.538962	-0.9116	0.0017	-1.5732	0.0096
LBR	-0.9451	0.0067	-1.0367	0.0156
LOC653604	-0.8267	0.0044	-1.0263	0.0017
LRRC26	-0.5925	0.0012	-1.8401	0.0093
MED28	-0.6664	0.0035	-1.0496	0.0054
NKIRAS2	-1.1056	0.0011	-1.091	0.0005
PSMD9	-1.3022	0.024	-1.7129	0.0099
RAD1	-1.0431	0.0017	-1.2723	0.0068
RAD51L3	-1.1575	0.0076	-1.2208	0.0228
RHOT1	-0.8989	0	-1.3951	0.0112
RPL15	-1.0092	0.0063	-1.1577	0.0022
RRBP1	-0.9361	0.0016	-1.2334	0.0026
RRM2	-1.2263	0.008	-1.283	0.0096
SGTA	-1.0809	0.0005	-1.0252	0.0027
SHISA2	-0.6887	0.0022	-1.0815	0.0035
SIRT2	-1.0496	0.006	-1.0307	0.0112
SYT15	-0.667	0.0026	-1.8616	0.0006
TAPT1	-0.8014	0.0093	-1.2048	0.0003
TIMM8A	-1.0819	0.0058	-1.1961	0.002
TMEM2	-1.2435	0.0033	-1.4596	0.0035
TRAK2	-0.6921	0.0005	-1.5925	0.0273
TRAPPC2	-0.929	0.0143	-1.7807	0.0066
ADIPOR1	-1.0565	0.0014	-0.6112	0.0257
C11ORF57	-0.9145	0.0061	-0.7511	0.0012
C2ORF18	-0.8286	0.0107	-0.7417	0.0192
CA2	-1.1593	0.0069	-0.9553	0.0067

CBFB	-0.8339	0.0062	-0.9155	0.0117
CCND1	-0.8808	0.0102	-0.6039	0.032
CSNK1G1	-0.6368	0.0011	-0.8301	0.0439
CYBASC3	-0.8722	0.0082	-0.6719	0.0184
DAZAP1	-0.9801	0.0072	-1.0295	0.0214
DIABLO	-0.5839	0.0059	-0.6788	0.0042
DR1	-0.6786	0.0019	-0.7364	0.0144
ECHDC1	-0.6366	0.0327	-0.6242	0.0278
EFEMP1	-0.6015	0.0123	-1.1708	0.0008
EPRS	-1.183	0.0011	-0.7753	0.025
GNPAT	-1.0334	0.0073	-0.8659	0.006
H3F3B	-0.8651	0.0031	-0.7754	0.0098
HEXA	-1.0229	0.0169	-0.944	0.0286
HMGCL	-0.9607	0.0184	-0.9829	0.0213
HS.40289	-0.7054	0.0031	-0.9633	0.0044
HS.527657	-0.5942	0.0452	-0.9495	0.0345
ING3	-0.8528	0	-1.0705	0.0241
KATNAL1	-1.2907	0.0068	-0.7174	0.0097
LOC339970	-0.6415	0.0132	-0.6805	0.0146
LOC389816	-0.5873	0.0129	-1.7666	0.0005
LOC440093	-0.87	0.0022	-0.6231	0.0183
LOC646836	-0.7597	0.0208	-0.9572	0.0053
LOC653066	-0.8069	0.0469	-1.1284	0.0086
LOC654002	-0.8428	0.039	-0.638	0.0415
LYRM7	-0.6611	0.0301	-1.1471	0.0285
MAP3K4	-0.5844	0.0048	-0.813	0.0078
MARVELD2	-0.6275	0.0244	-0.8375	0.029
MAST3	-0.7799	0.0306	-0.721	0.0428
METTL10	-0.6204	0.0351	-0.756	0.0158
MRPS27	-0.5893	0.0306	-0.7172	0.0114
MST4	-1.0832	0.0138	-0.788	0.0241
NME1	-0.5861	0.0097	-0.8694	0.0272
NOL8	-0.9993	0.0012	-0.7876	0.0284
OVCA2	-0.6941	0.026	-0.6303	0.0416
PDE12	-0.7006	0.013	-0.8874	0.0042
PHGDH	-0.7641	0.007	-0.8146	0.016
RBPJ	-0.5968	0.0117	-0.87	0.0241
REXO4	-0.8501	0.0193	-0.9016	0.0076
RPA2	-0.6359	0.0071	-0.8447	0.0059
SATB2	-0.8165	0.0048	-0.7647	0.0275
SOCS5	-0.8254	0.0083	-0.8125	0.0022

TARS	-0.7979	0.0017	-0.7942	0.0006
TIPIN	-1.3996	0.0007	-1.2218	0.0243
TMEM168	-0.8094	0.0273	-0.6618	0.0165
TPMT	-0.8103	0.0047	-0.7376	0.0247
TRUB2	-1.0905	0.0017	-0.9879	0.0114
UBE2G2	-0.7241	0.0216	-1.2179	0.0111
UBP1	-0.6095	0.001	-0.763	0.0421
VAPA	-0.9758	0.0022	-0.7231	0.0222
VPS36	-0.8301	0.0002	-1.0232	0.0431
ZBED4	-0.6366	0.0141	-0.6929	0.0294

Appendix F: MiRNA expression comparison of MCFDCIS versus HCC1428

	MCFDCIS vs HCC1428		Wounding (Primary screen)		Relative Fluorescence (Primary screen)
miRNA	**Log ratio**	**p-value**	**Avg_Activity (%)**	**Z-score**	**Avg_Activity (%)**
hsa-miR-26b-5p	-1.7572	0.0009	-109.400	-4.0925	6.469
hsa-miR-191-5p	-2.3369	0.0106	-98.467	-3.6775	-35.237
hsa-miR-205-5p	5.3549	0.001	-97.880	-3.6552	-10.357
hsa-miR-26a-5p	-1.5185	0.0241	-93.757	-3.4987	5.364
hsa-miR-23a-3p	2.7725	0.0051	-33.830	-1.2243	1.285
hsa-miR-98	-1.38	0.0404	-32.985	-1.1922	-16.043
hsa-miR-375	-3.6208	0.0039	-28.560	-1.0243	2.373
hsa-miR-934	-1.1715	0.0061	-20.673	-0.7250	-31.917
hsa-miR-151a-3p	-1.9384	0.0102	-12.950	-0.4319	-45.660
hsa-miR-130a-3p	-1.6889	0.0074	-5.798	-0.1604	-0.643
hsa-miR-454-3p	-1.2771	0.0042	24.658	0.9955	-1.490
hsa-miR-652-3p	-1.4394	0.0057	25.205	1.0163	-9.136
hsa-miR-374a-5p	-2.3449	0.0437	30.990	1.2358	0.778
hsa-miR-301a-3p	-2.6873	0	34.900	1.3842	0.018
hsa-miR-27b-3p	-1.5222	0.023	46.363	1.8193	-3.669
hsa-miR-29a-5p	1.2551	0.0044	68.813	2.6713	-3.402
hsa-miR-21-3p	1.2561	0.02	77.383	2.9966	-27.853
hsa-miR-342-3p	-1.2997	0.0388	81.887	3.1675	-2.617
hsa-miR-196a-5p	-1.3722	0.0094	93.190	3.5965	-5.496
hsa-let-7b-5p	1.5732	0.0165	93.853	3.6217	-11.176
hsa-miR-20a-5p	1.3664	0.0212	110.250	4.2440	-1.810
hsa-miR-17-5p	1.0249	0.0049	116.667	4.4875	-1.332
hsa-miR-584-5p	1.7568	0.0151	145.413	5.5786	-55.340
hsa-miR-29a-3p	1.2847	0.0093	153.300	5.8779	-6.869
hsa-miR-100-5p	4.678	0.0008	159.033	6.0955	-6.244
hsa-miR-21-5p	1.3718	0.035	159.567	6.1157	-4.537
hsa-miR-548d-5p	-1.0739	0.007	165.300	6.3333	-3.917

hsa-miR-194-5p	-1.4621	0.0246	170.227	6.5203	-13.216
hsa-miR-30d-5p	-1.1403	0.0017	184.467	7.0608	-10.789
hsa-miR-374b-5p	-2.3493	0.002	185.533	7.1013	-4.535
hsa-miR-365a-3p	-1.278	0.0307	202.700	7.7528	-30.417
hsa-miR-30b-5p	-1.1335	0.0186	203.733	7.7920	-12.087
hsa-miR-339-5p	-1.2762	0.0094	204.200	7.8097	-9.509
hsa-miR-331-3p	-1.795	0.0045	211.967	8.1045	-3.335
hsa-miR-99b-5p	-1.7733	0.015	232.133	8.8699	-19.080
hsa-miR-125b-5p	5.2203	0.0002	234.800	8.9711	-19.567
hsa-miR-34a-5p	1.5463	0.0173	241.367	9.2203	-67.390
hsa-miR-181d	-1.013	0.0217	247.100	9.4379	-24.360
hsa-miR-421	-2.1448	0.0151	250.300	9.5594	-21.217
hsa-miR-203	-2.5266	0.0024	271.700	10.3716	-36.530
hsa-miR-31-3p	1.9412	0.0116	293.200	11.1876	-44.967
hsa-let-7i-5p	-1.3531	0.0457	297.867	11.3647	-52.180
hsa-miR-135a-5p	4.3309	0.0016	309.967	11.8239	-16.367
hsa-miR-222-3p	5.4175	0	318.933	12.1643	-21.504
hsa-miR-221-3p	3.188	0.0177	320.900	12.2389	-28.223
hsa-miR-340-5p	-1.027	0.037	336.000	12.8120	-46.540
hsa-miR-126-3p	-1.5014	0.014	363.633	13.8608	-53.273
hsa-miR-31-5p	2.4471	0.0002	366.067	13.9531	-55.277
hsa-miR-205-3p	2.0722	0.0066	408.567	15.5662	-59.313
hsa-miR-135b-5p	3.3013	0.0036	432.767	16.4846	-50.377
hsa-miR-215	-1.2871	0.0167	441.767	16.8262	-41.470
hsa-miR-22-3p	5.4793	0.0017	443.400	16.8882	-82.927
hsa-miR-7-5p	-2.8564	0.0041	453.967	17.2892	-53.807
hsa-miR-192-5p	-1.7158	0.0129	538.167	20.4849	-55.273
hsa-miR-105-5p	-1.9828	0.0107	563.800	21.4578	-69.223
hsa-miR-195-5p	-2.1149	0.0232	582.100	22.1523	-42.563
hsa-miR-193b-3p	-1.4381	0.0134	646.100	24.5814	-81.413
hsa-miR-28-5p	-2.1953	0.0082	758.700	28.8549	-83.740
hsa-miR-708-5p	1.4446	0.0081	809.800	30.7943	-86.893
hsa-miR-151a-5p	-2.4251	0.0138	N/A		
hsa-miR-374c-5p	-1.9554	0.0036	N/A		
hsa-miR-4288	4.5024	0.0006	N/A		

hsa-miR-4324	1.7673	0.03	N/A		
hsa-miR-4516	-1.2149	0.02	N/A		
hsa-miR-3940-5p	-1.9642	0.0415	N/A		

Appendix G: P63 Regulated Motility Genes

Genes that were 2-fold or more fold change from control; p-value 0.05

Genes UP regulated in motile cells and DOWN regulated upon knockdown of p63	Genes DOWN regualted in motile cells and UP regulated upon knockdown of p63
ABCC4	ABCA1
ALDH3A1	APH1B
ANTXR1	BSPRY
ANXA8L1	C11ORF52
ANXA8L2	C17ORF28
APOBEC3G	CEACAM6
ARHGAP22	CGN
AXL	CLIC3
BBS7	CNFN
BDKRB1	CPEB3
BCL11A	DNASE1
C17ORF81	ELF3
C3ORF54	ENPP5
CASP1	EPS8L1
CD44	ERBB3
CDH13	FAM80A
CKAP4	GALK1
CPNE8	GDPD3
CTGF	HSD3B7
DLK2	KIAA0513
DST	LOC647859
DYRK3	MB
EXTL2	MUC1
FAM189B	NAT1
FAT2	OCEL1
GNG11	PDGFB
GPX8	PKIB
HS.12876	PPM1H
HS.551128	PRR15L
HS.554203	RAB15
IKBIP	RHOV
IRF6	RHPN2

KCTD12	RTN2
LOC653110	SULT1A3
MAMDC2	SYTL4
MFNG	TJP3
MIR205	YPEL3
MTMR15	ZNF750
NEK1	
NFASC	
NFIX	
NKX3-1	
NOTCH1	
PALMD	
PLXNA2	
PM20D2	
POLR3G	
PPFIBP1	
PROCR	
PSTPIP2	
PTPRZ1	
RFC3	
SIM2	
SLC47A1	
SNAI2	
SNCA	
TP63	
TP73L	
TWIST2	
UGT1A6	
VSNL1	

Appendix H: SiRNA and MiRNA sequences

Gene/miRNA	Vendor	Seqeunce (5' to 3')	Oligo/Cat. No.
miR1276	Dharmacon, miRIDIAN	UAAAGAGCCCUGUGGAGACA	C-301408-00-0005
miR203	Dharmacon, miRIDIAN	GUGAAAUGUUUAGGACCACUAG	C-300562-03-0005
miR205-5p	Dharmacon, miRIDIAN	UCCUUCAUUCCACCGGAGUCUG	C-300564-05-0005
miR545-3p	Dharmacon, miRIDIAN	UCAGCAAACAUUUAUUGUGUGC	C-300861-05-0005
miR614	Dharmacon, miRIDIAN	GAACGCCUGUUCUUGCCAGGUGG	C-300939-01-0005
AXL	Dharmacon, On-Target plus	ACAGCGAGAUUUAUGACUA	J-003104-10
AXL	Dharmacon, On-Target plus	GAAGGAGACCCGUUAUGGA	J-003104-13
AXL	Dharmacon, On-Target plus	GACGAAAUCCUCUAUGUCA	J-003104-12
AXL	Dharmacon, On-Target plus	GGUACCGGCUGGCGUAUCA	J-003104-11
Non-Targeting Pool	Dharmacon, On-Target plus	UGGUUUACAUGUCGACUAA, UGGUUUACAUGUUGUGUGA, UGGUUUACAUGUUUUCUGA, UGGUUUACAUGUUUUCCUA	D-001810-10-05
RhoT1	Dharmacon, On-Target plus	CCAGAGAGGGAGACACGAA	J-010365-11
RhoT1	Dharmacon, On-Target plus	GCAAUUAGCAGAGGCGUUA	J-010365-10
RhoT1	Dharmacon, On-Target plus	GCUUAAUCGUAGCUGCAAA	J-010365-12
RhoT1	Dharmacon, On-Target plus	UGUGGAGUGUUCAGCGAAA	J-010365-09

SNAI2 (Slug)	Dharmacon, On-Target plus	ACAGCGAACUGGACACACA	J-017386-07
SNAI2 (Slug)	Dharmacon, On-Target plus	GAAUGUCUCUCCUGCACAA	J-017386-08
SNAI2 (Slug)	Dharmacon, On-Target plus	GCGAUGCCCAGUCUAGAAA	J-017386-06
SNAI2 (Slug)	Dharmacon, On-Target plus	UCUCUCCUCUUUCCGGAUA	J-017386-05
TAPT1	Dharmacon, On-Target plus	CAAAUGUCAAAUAGCGAUA	J-015826-18
TAPT1	Dharmacon, On-Target plus	GAACAAUGCCACCGUGAAU	J-015826-17
TAPT1	Dharmacon, On-Target plus	GCUAAAAGGAUUCGAUGUU	J-015826-20
TAPT1	Dharmacon, On-Target plus	GUGUUUGGGUCGACAGCGA	J-015826-19
TP63	Dharmacon, On-Target plus	CGACAGUCUUGUACAAUUU	J-003330-14
TP63	Dharmacon, On-Target plus	GAUGAACUGUUAUACUUAC	J-003330-15
TP63	Dharmacon, On-Target plus	GCACACAGACAAAUGAAUU	J-003330-13
TP63	Dharmacon, On-Target plus	UCUAUCAGAUUGAGCAUUA	J-003330-12
TP63	Dharmacon, siGENOME	CAAACAAGAUUGAGAUUAG	D-003330-06
TP63	Dharmacon, siGENOME	CAUCAUGUCUGGACUAUUU	D-003330-05
TP63	Dharmacon, siGENOME	CGACAGUCUUGUACAAUUU	D-003330-08
TP63	Dharmacon, siGENOME	GCACACAGACAAAUGAAUU	D-003330-07
TP63	Sigma	CAGUCUUGUACAAUUUCAU	SASI_Hs02_00326866

TP63	Sigma	GCAGCAAGUUUCGGACAGU	SASI_Hs02_00326865
TP63	Sigma	GGAUGAACCGCCGUCCAAU	SASI_Hs02_00326864

Appendix I: List of Antibodies and PCR Primers

IF = immunofluorescence, IF-IHC = immunofluorescence on paraffin sections, ChIP = chromatin immunoprecipitation

Antibody	Vendor	Cat. no.	Protocol
Alexa Fluor 488	Life Technologies	A-11001, A-11034	IF-IHC
Alexa Fluor 546	Life Technologies	A-11010, A-11030	IF-IHC
Alexa Fluor 680	Life Technologies	A-21057	Western blot
Axl	Cell Signal	8661	Western blot
Collagen I	Abcam	ab292	IF
Collagen IV	Millipore	ab756P	IF
E-cadherin	BD Biosciences	610182	IF-IHC
ERK1/2	Cell Signal	4696	Western blot
GAPDH	Calbiochem	CB1001	Western blot
Hoechst	Life Technologies	H1399	IF-IHC
IgG rabbit	Santa Cruz	Sc-2027	ChIP
IR Dye 800CW	Licor	926-32211	Western blot
Laminin-5	Millipore	MAB19562	IF
P63	Cell Signal	4892	Western blot, IF-IHC
P63alpha (H-129)	Santa Cruz	Sc-8344	Western blot, ChIP
Phalloidin	Life Technologies	A-22283	IF
Slug	Cell Signal	9585	Western blot, IF-IHC

Gene	Vendor	Assay Number
miR203a	Life Technologies	000507
miR205	Life Technologies	000509
TP63 (p63)	Life Technologies	Hs_00978343_m1
GAPDH (loading control)	Life Technologies	Hs_02758991_g1

Bibliography

1. Cancer Facts and Figures 2014. American Cancer Society. 2014.

2. Parmar H, Cunha GR. Epithelial–stromal interactions in the mouse and human mammary gland in vivo. Endocrine-Related Cancer. 2004;11(3):437-58. doi: 10.1677/erc.1.00659.

3. Mailleux AA, Overholtzer M, Brugge JS. Lumen formation during mammary epithelial morphogenesis: insights from in vitro and in vivo models. Cell cycle (Georgetown, Tex). 2008;7(1):57-62. Epub 2008/01/17. PubMed PMID: 18196964.

4. Schmelzle T, Mailleux AA, Overholtzer M, Carroll JS, Solimini NL, Lightcap ES, Veiby OP, Brugge JS. Functional role and oncogene-regulated expression of the BH3-only factor Bmf in mammary epithelial anoikis and morphogenesis. Proceedings of the National Academy of Sciences of the United States of America. 2007;104(10):3787-92. Epub 2007/03/16. doi: 10.1073/pnas.0700115104. PubMed PMID: 17360431; PubMed Central PMCID: PMCPmc1820662.

5. Burstein HJ, Polyak K, Wong JS, Lester SC, Kaelin CM. Ductal carcinoma in situ of the breast. The New England journal of medicine. 2004;350(14):1430-41. Epub 2004/04/09. doi: 10.1056/NEJMra031301. PubMed PMID: 15070793.

6. Polyak K, Metzger Filho O. SnapShot: breast cancer. Cancer cell. 2012;22(4):562-.e1. Epub 2012/10/20. doi: 10.1016/j.ccr.2012.06.021. PubMed PMID: 23079664.

7. Chiang AC, Massague J. Molecular basis of metastasis. The New England journal of medicine. 2008;359(26):2814-23. Epub 2008/12/26. doi: 10.1056/NEJMra0805239. PubMed PMID: 19109576; PubMed Central PMCID: PMCPmc4189180.

8. Valastyan S, Weinberg RA. Tumor metastasis: molecular insights and evolving paradigms. Cell. 2011;147(2):275-92. Epub 2011/10/18. doi: 10.1016/j.cell.2011.09.024. PubMed PMID: 22000009; PubMed Central PMCID: PMCPmc3261217.

9. Friedl P, Gilmour D. Collective cell migration in morphogenesis, regeneration and cancer. Nature reviews Molecular cell biology. 2009;10(7):445-57. Epub 2009/06/24. doi: 10.1038/nrm2720. PubMed PMID: 19546857.

10. Friedl P, Locker J, Sahai E, Segall JE. Classifying collective cancer cell invasion. Nature cell biology. 2012;14(8):777-83. Epub 2012/08/03. doi: 10.1038/ncb2548. PubMed PMID: 22854810.

11. Giampieri S, Manning C, Hooper S, Jones L, Hill CS, Sahai E. Localized and reversible TGFbeta signalling switches breast cancer cells from cohesive to single cell motility. Nature cell biology. 2009;11(11):1287-96. Epub 2009/10/20. doi: 10.1038/ncb1973. PubMed PMID: 19838175; PubMed Central PMCID: PMCPmc2773241.

12. Sabeh F, Ota I, Holmbeck K, Birkedal-Hansen H, Soloway P, Balbin M, Lopez-Otin C, Shapiro S, Inada M, Krane S, Allen E, Chung D, Weiss SJ. Tumor cell traffic through the

extracellular matrix is controlled by the membrane-anchored collagenase MT1-MMP. The Journal of cell biology. 2004;167(4):769-81. Epub 2004/11/24. doi: 10.1083/jcb.200408028. PubMed PMID: 15557125; PubMed Central PMCID: PMCPmc2172570.

13. Sabeh F, Shimizu-Hirota R, Weiss SJ. Protease-dependent versus -independent cancer cell invasion programs: three-dimensional amoeboid movement revisited. The Journal of cell biology. 2009;185(1):11-9. Epub 2009/04/01. doi: 10.1083/jcb.200807195. PubMed PMID: 19332889; PubMed Central PMCID: PMCPmc2700505.

14. Gerhardt H, Golding M, Fruttiger M, Ruhrberg C, Lundkvist A, Abramsson A, Jeltsch M, Mitchell C, Alitalo K, Shima D, Betsholtz C. VEGF guides angiogenic sprouting utilizing endothelial tip cell filopodia. The Journal of cell biology. 2003;161(6):1163-77. Epub 2003/06/18. doi: 10.1083/jcb.200302047. PubMed PMID: 12810700; PubMed Central PMCID: PMCPmc2172999.

15. Ewald AJ, Brenot A, Duong M, Chan BS, Werb Z. Collective epithelial migration and cell rearrangements drive mammary branching morphogenesis. Developmental cell. 2008;14(4):570-81. Epub 2008/04/16. doi: 10.1016/j.devcel.2008.03.003. PubMed PMID: 18410732; PubMed Central PMCID: PMCPmc2773823.

16. Finak G, Bertos N, Pepin F, Sadekova S, Souleimanova M, Zhao H, Chen H, Omeroglu G, Meterissian S, Omeroglu A, Hallett M, Park M. Stromal gene expression predicts clinical outcome in breast cancer. Nature medicine. 2008;14(5):518-27. Epub 2008/04/29. doi: 10.1038/nm1764. PubMed PMID: 18438415.

17. Green CE, Liu T, Montel V, Hsiao G, Lester RD, Subramaniam S, Gonias SL, Klemke RL. Chemoattractant signaling between tumor cells and macrophages regulates cancer cell migration, metastasis and neovascularization. PloS one. 2009;4(8):e6713. Epub 2009/08/22. doi: 10.1371/journal.pone.0006713. PubMed PMID: 19696929; PubMed Central PMCID: PMCPmc2725301.

18. Goswami S, Sahai E, Wyckoff JB, Cammer M, Cox D, Pixley FJ, Stanley ER, Segall JE, Condeelis JS. Macrophages promote the invasion of breast carcinoma cells via a colony-stimulating factor-1/epidermal growth factor paracrine loop. Cancer research. 2005;65(12):5278-83. Epub 2005/06/17. doi: 10.1158/0008-5472.can-04-1853. PubMed PMID: 15958574.

19. Eck SM, Cote AL, Winkelman WD, Brinckerhoff CE. CXCR4 and matrix metalloproteinase-1 are elevated in breast carcinoma-associated fibroblasts and in normal mammary fibroblasts exposed to factors secreted by breast cancer cells. Molecular cancer research : MCR. 2009;7(7):1033-44. Epub 2009/07/09. doi: 10.1158/1541-7786.mcr-09-0015. PubMed PMID: 19584257; PubMed Central PMCID: PMCPmc2743167.

20. Kalluri R, Zeisberg M. Fibroblasts in cancer. Nature reviews Cancer. 2006;6(5):392-401. Epub 2006/03/31. doi: 10.1038/nrc1877. PubMed PMID: 16572188.

21. Lewis MP, Lygoe KA, Nystrom ML, Anderson WP, Speight PM, Marshall JF, Thomas GJ. Tumour-derived TGF-beta1 modulates myofibroblast differentiation and promotes HGF/SF-dependent invasion of squamous carcinoma cells. British journal of cancer. 2004;90(4):822-32. Epub 2004/02/19. doi: 10.1038/sj.bjc.6601611. PubMed PMID: 14970860; PubMed Central PMCID: PMCPmc2410183.

22. Thannickal VJ, Lee DY, White ES, Cui Z, Larios JM, Chacon R, Horowitz JC, Day RM, Thomas PE. Myofibroblast differentiation by transforming growth factor-beta1 is dependent on cell adhesion and integrin signaling via focal adhesion kinase. The Journal of biological chemistry. 2003;278(14):12384-9. Epub 2003/01/18. doi: 10.1074/jbc.M208544200. PubMed PMID: 12531888.

23. Orimo A, Gupta PB, Sgroi DC, Arenzana-Seisdedos F, Delaunay T, Naeem R, Carey VJ, Richardson AL, Weinberg RA. Stromal fibroblasts present in invasive human breast carcinomas promote tumor growth and angiogenesis through elevated SDF-1/CXCL12 secretion. Cell. 2005;121(3):335-48. Epub 2005/05/11. doi: 10.1016/j.cell.2005.02.034. PubMed PMID: 15882617.

24. Gaggioli C, Hooper S, Hidalgo-Carcedo C, Grosse R, Marshall JF, Harrington K, Sahai E. Fibroblast-led collective invasion of carcinoma cells with differing roles for RhoGTPases in leading and following cells. Nature cell biology. 2007;9(12):1392-400. Epub 2007/11/27. doi: 10.1038/ncb1658. PubMed PMID: 18037882.

25. Boyd NF, Lockwood GA, Martin LJ, Knight JA, Byng JW, Yaffe MJ, Tritchler DL. Mammographic densities and breast cancer risk. Breast disease. 1998;10(3-4):113-26. Epub 2005/02/03. PubMed PMID: 15687568.

26. Provenzano PP, Inman DR, Eliceiri KW, Knittel JG, Yan L, Rueden CT, White JG, Keely PJ. Collagen density promotes mammary tumor initiation and progression. BMC medicine. 2008;6:11. Epub 2008/04/30. doi: 10.1186/1741-7015-6-11. PubMed PMID: 18442412; PubMed Central PMCID: PMCPmc2386807.

27. Conklin MW, Eickhoff JC, Riching KM, Pehlke CA, Eliceiri KW, Provenzano PP, Friedl A, Keely PJ. Aligned collagen is a prognostic signature for survival in human breast carcinoma. The American journal of pathology. 2011;178(3):1221-32. Epub 2011/03/02. doi: 10.1016/j.ajpath.2010.11.076. PubMed PMID: 21356373; PubMed Central PMCID: PMCPmc3070581.

28. Dang TT, Prechtl AM, Pearson GW. Breast cancer subtype-specific interactions with the microenvironment dictate mechanisms of invasion. Cancer research. 2011;71(21):6857-66. Epub 2011/09/13. doi: 10.1158/0008-5472.can-11-1818. PubMed PMID: 21908556; PubMed Central PMCID: PMCPmc3206184.

29. Vogel W, Gish GD, Alves F, Pawson T. The discoidin domain receptor tyrosine kinases are activated by collagen. Molecular cell. 1997;1(1):13-23. Epub 1998/07/11. PubMed PMID: 9659899.

30. Campbell ID, Humphries MJ. Integrin structure, activation, and interactions. Cold Spring Harbor perspectives in biology. 2011;3(3). Epub 2011/03/23. doi: 10.1101/cshperspect.a004994. PubMed PMID: 21421922; PubMed Central PMCID: PMCPmc3039929.

31. Emsley J, Knight CG, Farndale RW, Barnes MJ, Liddington RC. Structural Basis of Collagen Recognition by Integrin α2β1. Cell. 2000;101(1):47-56. doi: http://dx.doi.org/10.1016/S0092-8674(00)80622-4.

32. Valiathan RR, Marco M, Leitinger B, Kleer CG, Fridman R. Discoidin domain receptor tyrosine kinases: new players in cancer progression. Cancer metastasis reviews. 2012;31(1-2):295-321. Epub 2012/03/01. doi: 10.1007/s10555-012-9346-z. PubMed PMID: 22366781; PubMed Central PMCID: PMCPmc3351584.

33. Kadler KE, Holmes DF, Trotter JA, Chapman JA. Collagen fibril formation. The Biochemical journal. 1996;316 (Pt 1):1-11. Epub 1996/05/15. PubMed PMID: 8645190; PubMed Central PMCID: PMCPmc1217307.

34. Miyahara M, Hayashi K, Berger J, Tanzawa K, Njieha FK, Trelstad RL, Prockop DJ. Formation of collagen fibrils by enzymic cleavage of precursors of type I collagen in vitro. Journal of Biological Chemistry. 1984;259(15):9891-8.

35. Pinnell SR, Martin GR. The cross-linking of collagen and elastin: enzymatic conversion of lysine in peptide linkage to alpha-aminoadipic-delta-semialdehyde (allysine) by an extract from bone. Proceedings of the National Academy of Sciences of the United States of America. 1968;61(2):708-16. Epub 1968/10/01. PubMed PMID: 5246001; PubMed Central PMCID: PMCPmc225217.

36. Trackman PC, Bedell-Hogan D, Tang J, Kagan HM. Post-translational glycosylation and proteolytic processing of a lysyl oxidase precursor. The Journal of biological chemistry. 1992;267(12):8666-71. Epub 1992/04/25. PubMed PMID: 1349020.

37. Levental KR, Yu H, Kass L, Lakins JN, Egeblad M, Erler JT, Fong SF, Csiszar K, Giaccia A, Weninger W, Yamauchi M, Gasser DL, Weaver VM. Matrix crosslinking forces tumor progression by enhancing integrin signaling. Cell. 2009;139(5):891-906. Epub 2009/11/26. doi: 10.1016/j.cell.2009.10.027. PubMed PMID: 19931152; PubMed Central PMCID: PMCPmc2788004.

38. Lee RC, Feinbaum RL, Ambros V. The C. elegans heterochronic gene lin-4 encodes small RNAs with antisense complementarity to lin-14. Cell. 1993;75(5):843-54. doi: http://dx.doi.org/10.1016/0092-8674(93)90529-Y.

39. Wightman B, Ha I, Ruvkun G. Posttranscriptional regulation of the heterochronic gene lin-14 by lin-4 mediates temporal pattern formation in C. elegans. Cell. 1993;75(5):855-62. doi: http://dx.doi.org/10.1016/0092-8674(93)90530-4.

40. Ameres SL, Zamore PD. Diversifying microRNA sequence and function. Nature reviews Molecular cell biology. 2013;14(8):475-88. doi: 10.1038/nrm3611.

41. Carthew RW, Sontheimer EJ. Origins and Mechanisms of miRNAs and siRNAs. Cell. 2009;136(4):642-55. Epub 2009/02/26. doi: 10.1016/j.cell.2009.01.035. PubMed PMID: 19239886; PubMed Central PMCID: PMCPmc2675692.

42. Chi SW, Hannon GJ, Darnell RB. An alternative mode of microRNA target recognition. Nat Struct Mol Biol. 2012;19(3):321-7. doi: http://www.nature.com/nsmb/journal/v19/n3/abs/nsmb.2230.html - supplementary-information.

43. Wang Y, Juranek S, Li H, Sheng G, Tuschl T, Patel DJ. Structure of an argonaute silencing complex with a seed-containing guide DNA and target RNA duplex. Nature. 2008;456(7224):921-6. doi: http://www.nature.com/nature/journal/v456/n7224/suppinfo/nature07666_S1.html.

44. Bartel DP. MicroRNAs: Target Recognition and Regulatory Functions. Cell. 2009;136(2):215-33. doi: http://dx.doi.org/10.1016/j.cell.2009.01.002.

45. Yan LX, Huang XF, Shao Q, Huang MY, Deng L, Wu QL, Zeng YX, Shao JY. MicroRNA miR-21 overexpression in human breast cancer is associated with advanced clinical stage, lymph node metastasis and patient poor prognosis. RNA (New York, NY). 2008;14(11):2348-60. Epub 2008/09/25. doi: 10.1261/rna.1034808. PubMed PMID: 18812439; PubMed Central PMCID: PMCPmc2578865.

46. Yan LX, Wu QN, Zhang Y, Li YY, Liao DZ, Hou JH, Fu J, Zeng MS, Yun JP, Wu QL, Zeng YX, Shao JY. Knockdown of miR-21 in human breast cancer cell lines inhibits proliferation, in vitro migration and in vivo tumor growth. Breast cancer research : BCR. 2011;13(1):R2. Epub 2011/01/12. doi: 10.1186/bcr2803. PubMed PMID: 21219636; PubMed Central PMCID: PMCPmc3109565.

47. Chan JA, Krichevsky AM, Kosik KS. MicroRNA-21 is an antiapoptotic factor in human glioblastoma cells. Cancer research. 2005;65(14):6029-33. Epub 2005/07/19. doi: 10.1158/0008-5472.can-05-0137. PubMed PMID: 16024602.

48. Si ML, Zhu S, Wu H, Lu Z, Wu F, Mo YY. miR-21-mediated tumor growth. Oncogene. 2007;26(19):2799-803. Epub 2006/10/31. doi: 10.1038/sj.onc.1210083. PubMed PMID: 17072344.

49. Zhu S, Wu H, Wu F, Nie D, Sheng S, Mo YY. MicroRNA-21 targets tumor suppressor genes in invasion and metastasis. Cell research. 2008;18(3):350-9. Epub 2008/02/14. doi: 10.1038/cr.2008.24. PubMed PMID: 18270520.

50. Corney DC, Flesken-Nikitin A, Godwin AK, Wang W, Nikitin AY. MicroRNA-34b and MicroRNA-34c are targets of p53 and cooperate in control of cell proliferation and adhesion-independent growth. Cancer research. 2007;67(18):8433-8. Epub 2007/09/08. doi: 10.1158/0008-5472.can-07-1585. PubMed PMID: 17823410.

51. Achari C, Winslow S, Ceder Y, Larsson C. Expression of miR-34c induces G2/M cell cycle arrest in breast cancer cells. BMC cancer. 2014;14:538. Epub 2014/07/30. doi: 10.1186/1471-2407-14-538. PubMed PMID: 25064703; PubMed Central PMCID: PMCPmc4125691.

52. Prat A, Parker JS, Karginova O, Fan C, Livasy C, Herschkowitz JI, He X, Perou CM. Phenotypic and molecular characterization of the claudin-low intrinsic subtype of breast cancer. Breast cancer research : BCR. 2010;12(5):R68. Epub 2010/09/04. doi: 10.1186/bcr2635. PubMed PMID: 20813035; PubMed Central PMCID: PMCPmc3096954.

53. Peppercorn J, Perou CM, Carey LA. Molecular subtypes in breast cancer evaluation and management: divide and conquer. Cancer investigation. 2008;26(1):1-10. Epub 2008/01/09. doi: 10.1080/07357900701784238. PubMed PMID: 18181038.

54. Bauer M, Su G, Casper C, He R, Rehrauer W, Friedl A. Heterogeneity of gene expression in stromal fibroblasts of human breast carcinomas and normal breast. Oncogene. 2010;29(12):1732-40. Epub 2010/01/12. doi: 10.1038/onc.2009.463. PubMed PMID: 20062080; PubMed Central PMCID: PMCPmc2845730.

55. Lazard D, Sastre X, Frid MG, Glukhova MA, Thiery JP, Koteliansky VE. Expression of smooth muscle-specific proteins in myoepithelium and stromal myofibroblasts of normal and malignant human breast tissue. Proceedings of the National Academy of Sciences of the United States of America. 1993;90(3):999-1003. Epub 1993/02/01. PubMed PMID: 8430113; PubMed Central PMCID: PMCPmc45798.

56. Ronnov-Jessen L, Petersen OW, Koteliansky VE, Bissell MJ. The origin of the myofibroblasts in breast cancer. Recapitulation of tumor environment in culture unravels diversity and implicates converted fibroblasts and recruited smooth muscle cells. The Journal of clinical investigation. 1995;95(2):859-73. Epub 1995/02/01. doi: 10.1172/jci117736. PubMed PMID: 7532191; PubMed Central PMCID: PMCPmc295570.

57. Adeyinka A, Nui Y, Cherlet T, Snell L, Watson PH, Murphy LC. Activated mitogen-activated protein kinase expression during human breast tumorigenesis and breast cancer progression. Clinical cancer research : an official journal of the American Association for Cancer Research. 2002;8(6):1747-53. Epub 2002/06/13. PubMed PMID: 12060612.

58. Grill C, Gheyas F, Dayananth P, Jin W, Ding W, Qiu P, Wang L, Doll RJ, English JM. Analysis of the ERK1,2 transcriptome in mammary epithelial cells. The Biochemical journal. 2004;381(Pt 3):635-44. Epub 2004/04/28. doi: 10.1042/bj20031688. PubMed PMID: 15109307; PubMed Central PMCID: PMCPmc1133872.

59. Vial E, Sahai E, Marshall CJ. ERK-MAPK signaling coordinately regulates activity of Rac1 and RhoA for tumor cell motility. Cancer cell. 2003;4(1):67-79. Epub 2003/08/02. PubMed PMID: 12892714.

60. Pearson GW, Hunter T. Real-time imaging reveals that noninvasive mammary epithelial acini can contain motile cells. The Journal of cell biology. 2007;179(7):1555-67. Epub 2008/01/02. doi: 10.1083/jcb.200706099. PubMed PMID: 18166657; PubMed Central PMCID: PMCPmc2373504.

61. Hu M, Yao J, Carroll DK, Weremowicz S, Chen H, Carrasco D, Richardson A, Violette S, Nikolskaya T, Nikolsky Y, Bauerlein EL, Hahn WC, Gelman RS, Allred C, Bissell MJ, Schnitt S, Polyak K. Regulation of in situ to invasive breast carcinoma transition. Cancer cell. 2008;13(5):394-406. Epub 2008/05/06. doi: 10.1016/j.ccr.2008.03.007. PubMed PMID: 18455123; PubMed Central PMCID: PMCPmc3705908.

62. Lin EY, Jones JG, Li P, Zhu L, Whitney KD, Muller WJ, Pollard JW. Progression to malignancy in the polyoma middle T oncoprotein mouse breast cancer model provides a reliable model for human diseases. The American journal of pathology. 2003;163(5):2113-26. Epub 2003/10/28. doi: 10.1016/s0002-9440(10)63568-7. PubMed PMID: 14578209; PubMed Central PMCID: PMCPmc1892434.

63. Camp JT, Elloumi F, Roman-Perez E, Rein J, Stewart DA, Harrell JC, Perou CM, Troester MA. Interactions with fibroblasts are distinct in Basal-like and luminal breast cancers. Molecular cancer research : MCR. 2011;9(1):3-13. Epub 2010/12/07. doi: 10.1158/1541-7786.mcr-10-0372. PubMed PMID: 21131600; PubMed Central PMCID: PMCPmc3045848.

64. Petrovic N, Mandusic V, Stanojevic B, Lukic S, Todorovic L, Roganovic J, Dimitrijevic B. The difference in miR-21 expression levels between invasive and non-invasive breast cancers emphasizes its role in breast cancer invasion. Medical oncology (Northwood, London, England). 2014;31(3):867. Epub 2014/02/04. doi: 10.1007/s12032-014-0867-x. PubMed PMID: 24488617.

65. Mishra S, Deng JJ, Gowda PS, Rao MK, Lin CL, Chen CL, Huang T, Sun LZ. Androgen receptor and microRNA-21 axis downregulates transforming growth factor beta receptor II (TGFBR2) expression in prostate cancer. Oncogene. 2014;33(31):4097-106. doi: 10.1038/onc.2013.374.

66. Lopez JA, Alvarez-Salas LM. Differential effects of miR-34c-3p and miR-34c-5p on SiHa cells proliferation apoptosis, migration and invasion. Biochemical and biophysical research communications. 2011;409(3):513-9. Epub 2011/05/24. doi: 10.1016/j.bbrc.2011.05.036. PubMed PMID: 21600876.

67. Fransson S, Ruusala A, Aspenstrom P. The atypical Rho GTPases Miro-1 and Miro-2 have essential roles in mitochondrial trafficking. Biochemical and biophysical research communications. 2006;344(2):500-10. Epub 2006/04/25. doi: 10.1016/j.bbrc.2006.03.163. PubMed PMID: 16630562.

68. Reis K, Fransson A, Aspenstrom P. The Miro GTPases: at the heart of the mitochondrial transport machinery. FEBS letters. 2009;583(9):1391-8. Epub 2009/04/21. doi: 10.1016/j.febslet.2009.04.015. PubMed PMID: 19376118.

69. Morlino G, Barreiro O, Baixauli F, Robles-Valero J, Gonzalez-Granado JM, Villa-Bellosta R, Cuenca J, Sanchez-Sorzano CO, Veiga E, Martin-Cofreces NB, Sanchez-Madrid F. Miro-1 links mitochondria and microtubule Dynein motors to control lymphocyte migration and polarity. Molecular and cellular biology. 2014;34(8):1412-26. Epub 2014/02/05. doi: 10.1128/mcb.01177-13. PubMed PMID: 24492963; PubMed Central PMCID: PMCPmc3993592.

70. Howell GR, Shindo M, Murray S, Gridley T, Wilson LA, Schimenti JC. Mutation of a ubiquitously expressed mouse transmembrane protein (Tapt1) causes specific skeletal homeotic transformations. Genetics. 2007;175(2):699-707. Epub 2006/12/08. doi: 10.1534/genetics.106.065177. PubMed PMID: 17151244; PubMed Central PMCID: PMCPmc1800629.

71. Casella JF, Flanagan MD, Lin S. Cytochalasin D inhibits actin polymerization and induces depolymerization of actin filaments formed during platelet shape change. Nature. 1981;293(5830):302-5. Epub 1981/09/24. PubMed PMID: 7196996.

72. Aomatsu K, Arao T, Abe K, Kodama A, Sugioka K, Matsumoto K, Kudo K, Kimura H, Fujita Y, Hayashi H, Nagai T, Shimomura Y, Nishio K. Slug is upregulated during wound healing and regulates cellular phenotypes in corneal epithelial cells. Investigative ophthalmology & visual science. 2012;53(2):751-6. Epub 2012/01/17. doi: 10.1167/iovs.11-8222. PubMed PMID: 22247468.

73. Gilles C, Polette M, Zahm JM, Tournier JM, Volders L, Foidart JM, Birembaut P. Vimentin contributes to human mammary epithelial cell migration. Journal of cell science. 1999;112 (Pt 24):4615-25. Epub 1999/11/27. PubMed PMID: 10574710.

74. Nguyen TT, Oh SS, Weaver D, Lewandowska A, Maxfield D, Schuler M-H, Smith NK, Macfarlane J, Saunders G, Palmer CA, Debattisti V, Koshiba T, Pulst S, Feldman EL, Hajnóczky G, Shaw JM. Loss of Miro1-directed mitochondrial movement results in a novel murine model for neuron disease. Proceedings of the National Academy of Sciences. 2014;111(35):E3631-E40. doi: 10.1073/pnas.1402449111.

75. Perez CA, Ott J, Mays DJ, Pietenpol JA. p63 consensus DNA-binding site: identification, analysis and application into a p63MH algorithm. Oncogene. 2007;26(52):7363-70. Epub 2007/06/15. doi: 10.1038/sj.onc.1210561. PubMed PMID: 17563751.

76. Romano RA, Smalley K, Magraw C, Serna VA, Kurita T, Raghavan S, Sinha S. DeltaNp63 knockout mice reveal its indispensable role as a master regulator of epithelial development and differentiation. Development (Cambridge, England). 2012;139(4):772-82. Epub 2012/01/26. doi: 10.1242/dev.071191. PubMed PMID: 22274697; PubMed Central PMCID: PMCPmc3265062.

77. Barbareschi M, Pecciarini L, Cangi MG, Macri E, Rizzo A, Viale G, Doglioni C. p63, a p53 homologue, is a selective nuclear marker of myoepithelial cells of the human breast. The American journal of surgical pathology. 2001;25(8):1054-60. Epub 2001/07/28. PubMed PMID: 11474290.

78. Prater MD, Petit V, Alasdair Russell I, Giraddi RR, Shehata M, Menon S, Schulte R, Kalajzic I, Rath N, Olson MF, Metzger D, Faraldo MM, Deugnier MA, Glukhova MA, Stingl J. Mammary stem cells have myoepithelial cell properties. Nature cell biology. 2014;16(10):942-50. Epub 2014/09/01. doi: 10.1038/ncb3025. PubMed PMID: 25173976; PubMed Central PMCID: PMCPmc4183554.

79. Gu X, Coates PJ, Boldrup L, Nylander K. p63 contributes to cell invasion and migration in squamous cell carcinoma of the head and neck. Cancer letters. 2008;263(1):26-34. Epub 2008/01/16. doi: 10.1016/j.canlet.2007.12.011. PubMed PMID: 18194839.

80. Lo Muzio L, Santarelli A, Caltabiano R, Rubini C, Pieramici T, Trevisiol L, Carinci F, Leonardi R, De Lillo A, Lanzafame S, Bufo P, Piattelli A. p63 overexpression associates with poor prognosis in head and neck squamous cell carcinoma. Human pathology. 2005;36(2):187-94. Epub 2005/03/09. doi: 10.1016/j.humpath.2004.12.003. PubMed PMID: 15754296.

81. Stitt TN, Conn G, Gore M, Lai C, Bruno J, Radziejewski C, Mattsson K, Fisher J, Gies DR, Jones PF, et al. The anticoagulation factor protein S and its relative, Gas6, are ligands for the Tyro 3/Axl family of receptor tyrosine kinases. Cell. 1995;80(4):661-70. Epub 1995/02/24. PubMed PMID: 7867073.

82. Verma A, Warner SL, Vankayalapati H, Bearss DJ, Sharma S. Targeting Axl and Mer kinases in cancer. Molecular cancer therapeutics. 2011;10(10):1763-73. Epub 2011/09/22. doi: 10.1158/1535-7163.mct-11-0116. PubMed PMID: 21933973.

83. Fridell YW, Jin Y, Quilliam LA, Burchert A, McCloskey P, Spizz G, Varnum B, Der C, Liu ET. Differential activation of the Ras/extracellular-signal-regulated protein kinase pathway is responsible for the biological consequences induced by the Axl receptor tyrosine kinase. Molecular and cellular biology. 1996;16(1):135-45.

84. Lu Q, Gore M, Zhang Q, Camenisch T, Boast S, Casagranda F, Lai C, Skinner MK, Klein R, Matsushima GK, Earp HS, Goff SP, Lemke G. Tyro-3 family receptors are essential regulators of mammalian spermatogenesis. Nature. 1999;398(6729):723-8. Epub 1999/05/05. doi: 10.1038/19554. PubMed PMID: 10227296.

85. D'Alfonso TM, Hannah J, Chen Z, Liu Y, Zhou P, Shin SJ. Axl receptor tyrosine kinase expression in breast cancer. Journal of Clinical Pathology. 2014;67(8):690-6. doi: 10.1136/jclinpath-2013-202161.

86. Li Y, Ye X, Tan C, Hongo JA, Zha J, Liu J, Kallop D, Ludlam MJ, Pei L. Axl as a potential therapeutic target in cancer: role of Axl in tumor growth, metastasis and angiogenesis. Oncogene. 2009;28(39):3442-55. Epub 2009/07/28. doi: 10.1038/onc.2009.212. PubMed PMID: 19633687.

87. Holland SJ, Powell MJ, Franci C, Chan EW, Friera AM, Atchison RE, McLaughlin J, Swift SE, Pali ES, Yam G, Wong S, Lasaga J, Shen MR, Yu S, Xu W, Hitoshi Y, Bogenberger J, Nor JE, Payan DG, Lorens JB. Multiple roles for the receptor tyrosine kinase axl in tumor

formation. Cancer research. 2005;65(20):9294-303. Epub 2005/10/19. doi: 10.1158/0008-5472.can-05-0993. PubMed PMID: 16230391.

88. Holland SJ, Pan A, Franci C, Hu Y, Chang B, Li W, Duan M, Torneros A, Yu J, Heckrodt TJ, Zhang J, Ding P, Apatira A, Chua J, Brandt R, Pine P, Goff D, Singh R, Payan DG, Hitoshi Y. R428, a selective small molecule inhibitor of Axl kinase, blocks tumor spread and prolongs survival in models of metastatic breast cancer. Cancer research. 2010;70(4):1544-54. Epub 2010/02/11. doi: 10.1158/0008-5472.can-09-2997. PubMed PMID: 20145120.

89. Bolos V, Peinado H, Perez-Moreno MA, Fraga MF, Esteller M, Cano A. The transcription factor Slug represses E-cadherin expression and induces epithelial to mesenchymal transitions: a comparison with Snail and E47 repressors. Journal of cell science. 2003;116(Pt 3):499-511. Epub 2003/01/01. PubMed PMID: 12508111.

90. Jiang R, Lan Y, Norton CR, Sundberg JP, Gridley T. The slug gene is not essential for mesoderm or neural crest development in mice. Developmental Biology. 1998;198(2):277-85. doi: http://dx.doi.org/10.1016/S0012-1606(98)80005-5.

91. Perez-Mancera PA, Gonzalez-Herrero I, Maclean K, Turner AM, Yip MY, Sanchez-Martin M, Garcia JL, Robledo C, Flores T, Gutierrez-Adan A, Pintado B, Sanchez-Garcia I. SLUG (SNAI2) overexpression in embryonic development. Cytogenetic and genome research. 2006;114(1):24-9. Epub 2006/05/24. doi: 10.1159/000091924. PubMed PMID: 16717446.

92. Yang C, Chen H, Tan G, Gao W, Cheng L, Jiang X, Yu L, Tan Y. FOXM1 promotes the epithelial to mesenchymal transition by stimulating the transcription of Slug in human breast cancer. Cancer letters. 2013;340(1):104-12. doi: http://dx.doi.org/10.1016/j.canlet.2013.07.004.

93. Hajra KM, Chen DY, Fearon ER. The SLUG zinc-finger protein represses E-cadherin in breast cancer. Cancer research. 2002;62(6):1613-8. Epub 2002/03/26. PubMed PMID: 11912130.

94. Desgrosellier Jay S, Lesperance J, Seguin L, Gozo M, Kato S, Franovic A, Yebra M, Shattil Sanford J, Cheresh David A. Integrin αvβ3 Drives Slug Activation and Stemness in the Pregnant and Neoplastic Mammary Gland. Developmental cell. 2014;30(3):295-308. doi: http://dx.doi.org/10.1016/j.devcel.2014.06.005.

95. Ramsey MR, Wilson C, Ory B, Rothenberg SM, Faquin W, Mills AA, Ellisen LW. FGFR2 signaling underlies p63 oncogenic function in squamous cell carcinoma. The Journal of clinical investigation. 2013;123(8):3525-38. Epub 2013/07/23. doi: 10.1172/jci68899. PubMed PMID: 23867503; PubMed Central PMCID: PMCPmc3726171.

96. Lena AM, Shalom-Feuerstein R, Rivetti di Val Cervo P, Aberdam D, Knight RA, Melino G, Candi E. miR-203 represses 'stemness' by repressing DeltaNp63. Cell death and differentiation. 2008;15(7):1187-95. Epub 2008/05/17. doi: 10.1038/cdd.2008.69. PubMed PMID: 18483491.

97. DeCastro AJ, Dunphy KA, Hutchinson J, Balboni AL, Cherukuri P, Jerry DJ, DiRenzo J. MiR203 mediates subversion of stem cell properties during mammary epithelial differentiation via repression of [Delta]NP63[alpha] and promotes mesenchymal-to-epithelial transition. Cell

Death Dis. 2013;4:e514. doi:
http://www.nature.com/cddis/journal/v4/n2/suppinfo/cddis201337s1.html.

98. Westfall MD, Pietenpol JA. p63: Molecular complexity in development and cancer. Carcinogenesis. 2004;25(6):857-64. Epub 2004/03/23. doi: 10.1093/carcin/bgh148. PubMed PMID: 15033906.

99. Tran MN, Choi W, Wszolek MF, Navai N, Lee IL, Nitti G, Wen S, Flores ER, Siefker-Radtke A, Czerniak B, Dinney C, Barton M, McConkey DJ. The p63 protein isoform DeltaNp63alpha inhibits epithelial-mesenchymal transition in human bladder cancer cells: role of MIR-205. The Journal of biological chemistry. 2013;288(5):3275-88. Epub 2012/12/15. doi: 10.1074/jbc.M112.408104. PubMed PMID: 23239884; PubMed Central PMCID: PMCPmc3561548.

100. Cheung Kevin J, Gabrielson E, Werb Z, Ewald Andrew J. Collective Invasion in Breast Cancer Requires a Conserved Basal Epithelial Program. Cell.155(7):1639-51. doi: 10.1016/j.cell.2013.11.029.

101. Osada M, Park HL, Nagakawa Y, Yamashita K, Fomenkov A, Kim MS, Wu G, Nomoto S, Trink B, Sidransky D. Differential recognition of response elements determines target gene specificity for p53 and p63. Molecular and cellular biology. 2005;25(14):6077-89. Epub 2005/07/01. doi: 10.1128/mcb.25.14.6077-6089.2005. PubMed PMID: 15988020; PubMed Central PMCID: PMCPmc1168821.

102. Zarnegar BJ, Webster DE, Lopez-Pajares V, Vander Stoep Hunt B, Qu K, Yan KJ, Berk DR, Sen GL, Khavari PA. Genomic profiling of a human organotypic model of AEC syndrome reveals ZNF750 as an essential downstream target of mutant TP63. American journal of human genetics. 2012;91(3):435-43. Epub 2012/08/28. doi: 10.1016/j.ajhg.2012.07.007. PubMed PMID: 22922031; PubMed Central PMCID: PMCPmc3511987.

103. Kouwenhoven EN, van Heeringen SJ, Tena JJ, Oti M, Dutilh BE, Alonso ME, de la Calle-Mustienes E, Smeenk L, Rinne T, Parsaulian L, Bolat E, Jurgelenaite R, Huynen MA, Hoischen A, Veltman JA, Brunner HG, Roscioli T, Oates E, Wilson M, Manzanares M, Gomez-Skarmeta JL, Stunnenberg HG, Lohrum M, van Bokhoven H, Zhou H. Genome-wide profiling of p63 DNA-binding sites identifies an element that regulates gene expression during limb development in the 7q21 SHFM1 locus. PLoS genetics. 2010;6(8):e1001065. Epub 2010/09/03. doi: 10.1371/journal.pgen.1001065. PubMed PMID: 20808887; PubMed Central PMCID: PMCPmc2924305.

104. Nieto MA. The snail superfamily of zinc-finger transcription factors. Nature reviews Molecular cell biology. 2002;3(3):155-66. Epub 2002/05/08. doi: 10.1038/nrm757. PubMed PMID: 11994736.

105. Vuoriluoto K, Haugen H, Kiviluoto S, Mpindi JP, Nevo J, Gjerdrum C, Tiron C, Lorens JB, Ivaska J. Vimentin regulates EMT induction by Slug and oncogenic H-Ras and migration by

governing Axl expression in breast cancer. Oncogene. 2011;30(12):1436-48. Epub 2010/11/09. doi: 10.1038/onc.2010.509. PubMed PMID: 21057535.

106. Desai SP, Bhatia SN, Toner M, Irimia D. Mitochondrial localization and the persistent migration of epithelial cancer cells. Biophysical journal. 2013;104(9):2077-88. Epub 2013/05/15. doi: 10.1016/j.bpj.2013.03.025. PubMed PMID: 23663851; PubMed Central PMCID: PMCPmc3647149.

107. Wu H, Zhu S, Mo Y-Y. Suppression of cell growth and invasion by miR-205 in breast cancer. Cell research. 2009;19(4):439-48.